THE ROLE OF GALANIN IN PERINEURAL INVASION OF HEAD AND NECK CANCER

by

Christina Springstead Scanlon

A dissertation submitted in partial fulfillment
of the requirements for the degree of
Doctor of Philosophy
(Oral Health Sciences)
in the University of Michigan
2014

Doctoral Committee:

Professor Nisha J. D'Silva, Chair
Assistant Professor Rogerio Castilho
Professor Renny T. Franceschi
Associate Professor Yuji Mishina
Professor John Andrew Williams

DEDICATION

In deepest gratitude I dedicate this thesis to the glory of God and to my loving and supportive family.

ACKNOWLEDGEMENTS

I would like to express my gratitude to all of the people who have made this dissertation possible:

Dr. Nisha J. D'Silva, my dissertation committee chair. Thank you for your mentorship, friendship and advocacy over the past 6 years. You are a wonderful role model and your passion for science is inspirational.

My committee members Dr. Rogerio Castilho, Dr. Renny T. Franceschi, Dr. Yuji Mishina and Dr. John Andrew Williams. Thank you for generously giving your time and talent in serving on my committee. I deeply appreciate your valuable feedback and suggestions as this project developed.

My precandidate advisor and first rotation advisor, Dr. Yvonne Kapila. Thank you for patiently mentoring me as I first approached benchtop science, and for your assistance and encouragement as I co-authored my first publications.

Dean Laurie McCauley, my second rotation advisor. Thank you for your mentorship and introduction to in vivo studies.

The Oral Health Science (OHS) Program – Associate Dean Charlotte Mistretta and acting OHS program director Dr. Jan Hu, current and past OHS supportive staff Patricia Schultz,

Manette London, Kimberly Smith and Charlene Erikson, and fellow OHS graduate students. Thank you for your friendship, encouragement and skillful support over the years.

My undergraduate honors thesis advisor Dr. Geoffrey Gerstner. Thank you for introducing me to the world of research and for encouraging me to pursue a career in science.

Dean Emeritus Peter Polverini. Thank you for your dedication to the OHS program and for your enthusiasm for science.

Lab members Dr. Elizabeth Van Tubergen, Dr. Rajat Banerjee, Nickole Russo, Min Liu, Ronald Inglehart and Amirtha Hariharan. Thank you for your teamwork, friendship and support through the years.

Administrators Kailash Thaker, Diane Lafferty, Anna Taylor, Kendra Renner and Janet Riggs. Thank you for your technical support in assisting with preparing budgets and submitting grant paperwork.

I am deeply grateful for the many funding sources that have made this work possible, including National Institute of Health funding through the Tissue Engineering at Michigan F32 training grant and NRSA F30 fellowship, Rackham Graduate School travel grants, candidate research grant and childcare subsidy funding, OHS block grants, Kellogg

Scholarship from the School of Dentistry, the Critical Difference grant from the Center for Education of Women and funding from my mentor, Dr. D'Silva.

Thank you to the University of Michigan School of Dentistry DDS faculty, especially Dr. Marilyn Woolfolk, Dr. Renee Duff, Dr. Phil Richards and Dr. Ronald Heys.

Thank you to the Community Dental Center, and especially to Dr. Bonita Neighbors and Dr. Anne Bibik for their mentorship and for allowing me to participate in their wonderful community practice.

A special thank you to the many collaborators in this research, including Drs. Sara and Jim Corson, Dr. Irfan Asangani, Dr. Charlotte Mistretta, Dr. Arul Chinnaiyan, Dr. Stephan Fisher and Linda Gates for their assistance with perineural invasion studies. Thank you to Leng-Chun Chen, Sakib F. Elahi, Dr. Shiuhyang Kuo, Dr. Stephen Feinberg and Dr. Mary-Ann Mycek for their collaboration with the organotypic studies.

Thank you to Chris Jung and Kenneth Reiger for their artistic assistance and John Westman for his technical support in preparation of histological specimens. Thank you to the Dr. Robert Bradley and Dr. Charlotte Mistretta laboratories for providing animal tissues for experiments.

Thank you most of all to my wonderful family, including my dear husband Justin Scanlon and our wonderful children Owen, Ian and Aiden. Justin provided emergency computer technical support on many occasions and proofread manuscripts. He also contributed

more than his share of housework and childcare frequently to allow me to complete these studies. My family has been unbelievably patient and supportive, especially when the work was intense and the hours were long. Thank you to my extended family and especially to my parents, who have provided emotional and material support through many years of extended education. I am so grateful.

TABLE OF CONTENTS

LIST OF TABLES

TABLE

LIST OF FIGURES

LIST OF APPENDICES

APPENDIX

ABSTRACT

Head and neck squamous cell carcinoma (HNSCC) is the sixth most common cancer worldwide and has a dismal 50% survival rate. Treatment for HNSCC is expensive and aggressive; surviving patients are left with significant physical impairment and emotional burden. Despite limited therapeutic options and poor survival, no novel effective therapy has been developed in 50 years. Perineural invasion (PNI) is a prognostic factor of poor survival in multiple cancers, including HNSCC, prostate and pancreatic cancers. If PNI is detected in HNSCC, the survival rate drops to 20%. Despite this alarming statistic, PNI is one of the least studied cancer phenotypes. Long-thought to be a passive process, new evidence demonstrates that PNI is an active process where tumor cells must degrade multiple layers of perineural sheath to spread. PNI leads to sensory disturbances including numbness, formication and cancer-associated pain. The nerve-tumor crosstalk necessary to promote PNI is understudied due to the lack of appropriate models that allow observation of nerve-tumor interactions. Due to this deficit in investigations no anti-PNI therapies are available. In this study, we present a novel in vivo model of PNI to characterize interactions between nerves and tumors. This model uses the chicken chorioallantoic membrane in vivo platform with a grafted human HNSCC cell line adjacent to an implanted rat dorsal root ganglion. Mechanistic studies indicate that the neuropeptide galanin (GAL) mediates nerve-tumor crosstalk via activation of galanin receptor 2 (GALR2), a G-protein coupled receptor. Nerves initiate PNI via release

of GAL, which induces GALR2 on cancer cells. Through a novel signaling mechanism of tumor progression, activated GALR2 induces nuclear factor of activated T-cells, cytoplasmic, calcineurin-dependent 2 (NFATc2)-mediated transcription of GAL and cyclooxygenase-2 (COX2) in cancer. Prostaglandin E2, a conversion product of COX2, promotes invasion of cancer cells and in a feedback loop, GAL promotes tumor neuritogenesis. Clinical data show that expression of proteins involved in this cascade are correlated with poor survival. Importantly, the GALR2 inhibitor M871 blocks PNI in the CAM in vivo model. This study provides evidence of the dynamic interaction between nerve and cancer cells that facilitates PNI.

CHAPTER I

Introduction

Part I: The Role of Invasion in Head and Neck Cancer Progression

Head and neck squamous cell carcinoma (HNSCC) is the sixth most common cancer in the world (1). In the United States, HNSCC accounts for more deaths each year than cervical cancer, melanoma, or Hodgkin's lymphoma and costs more than 2 billion dollars to treat (2, 3). Since patients with HNSCC often present with late stage tumors, the 5-year survival rate is only 50%, which is poorer than breast cancer or melanoma (4). Poor survival can be attributed to the high frequency of local recurrences, second primary tumors and distant metastases (1). Understanding the process by which tumor cells destroy the basement membrane, invade and metastasize is essential in controlling recurrence of HNSCC. Moreover, understanding these mechanisms of invasion and targeting key molecular factors facilitating this process will advance HNSCC treatment strategies and improve survival.

The basement membrane is the first and most robust structural barrier to invasion (5). In normal and pre-cancerous mucosa, the basement membrane separates surface stratified squamous epithelium from the underlying connective tissue. Destruction of the basement membrane and invasion of genetically and phenotypically altered cells into the

underlying stroma are required for progression of epithelial dysplasia (pre-cancer) to HNSCC (**Figure I.1**). Epithelial dysplasia exhibits less organization than normal oral epithelium (pre-cancer) due to accumulation of genetically altered cells above the basement membrane. After destruction of the basement membrane, tumor cells invade locally or metastasize to distant sites. Tumor spread contributes to the lethality of the disease.

A process contributing to invasion that has recently become a research-intensive area is epithelial-mesenchymal transition (EMT). **Appendix A** summarizes the molecular biology findings of EMT in HNSCC, and **Appendix B** summarizes our findings of a novel biomarker, cadherin-11, that may play a role in EMT in HSNCC. It is possible that blocking EMT may be an important future treatment strategy to control tumor spread and improve survival for HNSCC patients.

Perineural Invasion: an Understudied Route of Tumor Spread

Although repeatedly shown to be a critical metric of prognosis in many cancer types, perineural invasion (PNI), which is a subset of invasion, is undervalued and understudied. PNI is the pathologic invasion of cancer cells into the perineural space of nerves and is a mode of tumor metastasis that is independent of vascular or lymph node involvement (6). PNI is prominently associated with HNSCC, cutaneous, rectal, biliary tract, pancreatic, stomach and colon cancers (7). PNI is associated with sensory changes including paresthesia, pain and formication, or the feeling of insects crawling under the skin (8). PNI was identified in case reports in the medical literature by the mid-1800's,

including a clear description of cancer of the lip spreading to the brain (9). By the 1950's it was recognized that cancers with PNI were particularly prone to recurrence and resistance to chemotherapy (10). PNI has received little research attention, in part due to the long-held misconception that PNI is a passive process by which tumor cells within the perineural sheath simply spread along the path of least resistance, and for that reason PNI has sometimes been referred to as neurotropic carcinomatous spread or perineural spread (7). Recent evidence suggests that PNI is much more likely an active process involving mutual tropism of the tumor and nerve.

Part II: Diagnostic and Research Challenge Associated with PNI

There are several reasons why the major mechanisms that initiate and sustain PNI remain unknown. Although determined to be an independent prognostic factor in several cancers, PNI is underappreciated compared to some more widely accepted prognostic factors such as lymph node involvement. Therefore, there is a lack of consistent staining for nerves in histopathological examination of specimens, leading to frequently missed diagnoses. The lack of consistency of PNI detection and reporting methods has made retrospective clinical studies challenging to conduct and interpret. Due to wide variations in neurotropism and anatomical features of various cancer types, specific and evidence-based PNI reporting guidelines should be determined for each cancer type. Importantly, a precise definition of PNI and how to report and interpret the extent of neuronal involvement has not been developed for most cancers.

The histological appearance of nerves makes PNI a difficult diagnosis from hematoxylin and eosin staining. In normal peripheral nerve anatomy, nerve fibers or axons and associated Schwann cells are surrounded by collagen fibers and fibroblasts that form a tube called the endoneurium, and bundles of nerves are termed fascicles, which are surrounded by a dense fibrous network called the perineurium (11). Cells of the perineurium are concentrically arranged around nerve fascicles and have an elongated shape and spindle-shaped nuclei. The perineural space lies between the fascicles and the perineurium. When nerves in tissue specimens are cut tangentially, nerve fibers appear long and wavy usually with an elliptical or oval shape. If nerves are cut in cross section, the nerve axons appear as small spheres with round nuclei. Due to processing artifacts the perineurium may appear exaggerated or not intact in both tangential or cross sections. Given the very complex microanatomy of peripheral nerves, histopathologic detection of PNI is very challenging, particularly with subtle microscopic presentations (12). PNI may be missed at tumor margins and in tangential sections of nerves. Additionally, PNI is more likely to be reported in larger nerves than in smaller nerves (12). PNI in small nerves at the margins of tumors is thought to play a large part in local tumor recurrence, while invasion of larger nerves may play a bigger role in distant tumor spread. PNI may also be missed because small nerves may be masked by tumor islands and inflammation (7).

In addition to histopathologic, or “incidental” detection of PNI, PNI can be determined clinically from pain, paresthesia or motor dysfunction reported by patients (13). PNI can result in relentless pain and sensory disturbances including formication; clinical symptoms of PNI are correlated with very poor outcome (14). PNI may be detected

through imaging modalities such as MRI, and metastases may be mapped intracranially (15). On MRI, PNI may appear as neural enhancement or thickening. PNI usually occurs toward the CNS (retrograde), but can also occur in the anterograde direction. Because of the likelihood of skip lesions, it is important to view the entire course of a nerve with imaging (13).

PNI of head and neck cancers have been reported to spread along peripheral nerves as far as 15 cm from a primary tumor (16). Since surgery remains a key component of cancer therapy, it is essential to appreciate the complications that arise from attempting to track and eliminate PNI. Anatomically, PNI of HNSCC usually occurs along the trigeminal and facial nerves, but has also been reported along the sixth cranial nerve (17) and greater auricular nerve (18). Innervation of multiple facial structures and extensive branching and interconnection of these nerves provides conduits for widespread tumor metastases (13). For example, connections exist between the trigeminal and facial nerves, such as at the greater superficial petrosal nerve which branches from the facial nerve and passes through the pterygopalantine fossa and there joins branches of the maxillary branch of the trigeminal. It may be at connections such as these that tumor cells traveling along nerves scatter to locations of the head and neck that are very difficult to predict or resect.

Due to the extensive branching and possibilities of interconnections between nerves of the head and neck, along with the possibility of distant tumor spread and retrograde and anterograde movement of tumor along the nerves, it becomes extremely complicated to attempt to anatomically trace the path of PNI of a tumor. Unfortunately this tracing is essential to eliminate recurrence using surgical or radiation therapy, which are

the current major treatments for HNSCC. This challenge may explain the high incidence of locoregional recurrence that has been noted in HNSCC (1); current treatment strategies have not effectively improved survival in about 50 years. Locoregional recurrence may be in part because clinicians are missing tumors that have undergone complicated local and regional spread along nerves (6), which may be underappreciated, underreported and undertreated. Since imaging technologies are not sensitive enough to adequately track PNI through the extensive nerve system, the best way to address this problem may be to generate specific anti-PNI therapies that target tumor cells that have spread along nerves.

Part III: Understanding Biomarkers and Mechanisms to Direct Future Anti-PNI Therapies

PNI is understudied in part due to the scarcity of appropriate research models. Almost all investigations of PNI are retrospective studies that compare PNI status and outcome. Due to inconsistencies in reporting and detecting PNI, it is nearly impossible to draw meaningful conclusions from the bulk of these studies, and therefore clinicians are calling for more research that will lead to improved management of tumors with PNI.

Only a few clinical studies evaluated PNI molecularly and mechanistically. **Table I.1** lists several studies that have involved investigation of specific biomarkers with immunohistochemistry or in-situ-hybridization in different cancers with PNI. In addition to immunostaining of tumor specimens, clinical investigators have also used some molecular biology methods to investigate potential biomarkers of PNI, including gene

expression profiling of whole tumors (19) or laser capture microscopy with direct sequencing (20).

Some researchers have shown that neuronal signaling pathways may drive PNI by facilitating nerve-tumor crosstalk. A few molecular targets that have been studied include the neuronal cell adhesion molecules L1-CAM (21) and NCAM (22-24), and growth factor/receptor pairs NGF/TRK-A and NGF/TRK-B (25-29). Our laboratory has identified the neuropeptide/receptor pair galanin (GAL)/galanin receptor 2 (GALR2) as having an oncogenic role in HNSCC (30). Although evidence supports that GAL/GALR2 promotes tumor growth, the role of this neurotrophin/receptor pair has not been investigated in invasion or more specifically, PNI. The studies presented in the subsequent chapters will investigate the role of GAL/GALR2 in tumor progression.

Basic Science Methodology for PNI Investigation

The importance of studying PNI is recognized but challenges with in vitro and in vivo models have seriously hampered studies of PNI mechanisms. Early attempts at understanding the molecular mechanisms emphasized that modeling PNI in the laboratory is very challenging. These basic science investigations of PNI reflect the confusion seen in clinical studies.

Of the rudimentary attempts at re-creating PNI in vitro or in vivo, few models are able to simultaneously capture the interaction of the tumor and nerve. There is clinical and in vitro evidence that PNI involves reciprocal interaction between cancer cells and nerves; nerves respond to factors secreted by cancer cells. These factors are also

important in physiologic processes during development and response to injury. **Table I.2** summarizes existing laboratory methodologies that model PNI. Most in vitro assays are simply modifications of traditional cancer assays and do not demonstrate the complexity of neuronal interactions with cancer. Most in vivo models have involved direct injection of cancer cells into nerves, thereby bypassing the initial steps in the invasive process. Due to these deficiencies, the emphasis of research has been on the role of the tumor in initiating and sustaining PNI, while little attention has been given to the active role of nerves in this process.

Part IV: Problem Statement

Deficiencies in clinical detection, reporting and researching PNI have resulted in a gap of understanding of this deadly pathologic process. Lack of understanding of PNI has hindered the development of targeted therapy. When PNI is detected, clinicians often opt for aggressive adjuvant therapies for lesions that may be treated more effectively and conservatively with a therapy that targets PNI. Therefore, research aimed at understanding PNI will lead to novel therapies and improved treatment protocols to address this dangerous phenotype of HNSCC. Ultimately, improved understanding of the molecular biology of PNI, including markers of perineural involvement in profiling tumors, will assist clinicians and scientists in developing personalized medicine strategies to treat patients.

Current management of neurotropic cancers such as HNSCC is insufficient. Due to complicated invasion patterns, HNSCC with PNI cannot be managed with surgery and

radiation alone. Therefore, it is essential to develop anti-PNI therapeutics in order to kill cancer cells protected from existing treatments by invasion along the nerves with subsequent loco-regional recurrence. The shortfalls of current PNI models critically limit research advances in this area. Our *hypothesis* is that the GAL/GALR2 signaling mechanism promotes PNI; however more advanced models are necessary to test the relevance of this interaction. Therefore, the *aims* of this dissertation are: 1) to develop novel models of PNI and 2) to use these models to mechanistically investigate the role of GAL/GALR2 in PNI.

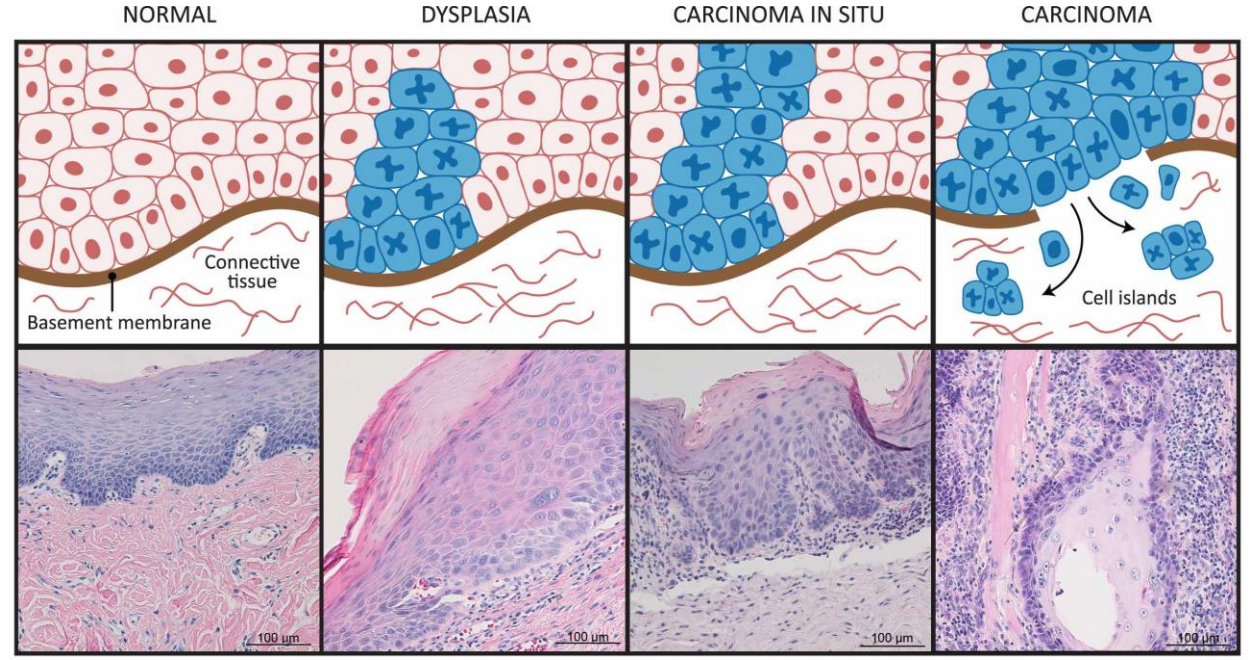

Figure I.1: HNSCC progression. Normal epithelium consists of cells with low mitotic activity separated from the connective tissue with an intact basement membrane. In epithelial dysplasia and carcinoma-in-situ (full thickness epithelial dysplasia), abnormal epithelial cells appear above the basement membrane. In HNSCC, the basement membrane is disrupted by tumor cells, which invade the connective tissue.

Protein Type	Biomarker	Cancer Type and Reference(s)
Antigen	LEU7	Adenoid Cystic (31)
Actin-Binding	DSTN	Pancreatic (32)
Neuronal Cell Adhesion	L1-CAM NCAM	Prostate (21) Bile Duct (22) Gallbladder (23) Squamous Cell (24)
Cell Surface Receptor	FAS	Pancreatic (33)
Cytokine	TGF-β1	Prostate (34)
	CXCL4/CXCL12	Prostate (35)
Cytoplasmic	BYSL	Prostate (36)
	CTTN	Laryngeal (37)
	MUC1/SIGLEC4	Pancreatic (38)
Golgi Membrane	MT	Prostate (39)
Growth Factor/Receptor	NGF/TRK-A/B	HNSCC (25) Basal and Squamous Cell (26) Pancreatic (27-29)
Kinase	RET/GFR1α	Bile Duct (40)
Lens	CRYαβ	Squamous Cell (41)
microRNA	mir-224	Prostate (39)
Microtubule associated	MAPRE2	Pancreatic (42)
Motor	KIF14	Pancreatic (43)
Neurotrophic	GDNF	Bile Duct (40) Pancreatic (44)
Protease	MMP2	Prostate (35)
	MMP9	Pancreatic (44) Prostate (35)
Proteoglycan	SDC2	Pancreatic (45)
	GPC1	Pancreatic (44)
Receptor	CXADR	Prostate (39)
Rho-Associated	ARHGDIB	Pancreatic (43)
Scaffolding	CAV-1	Prostate (34)
Transcription Factor	c-MYC	Pancreatic (33)
	NF-κB	Prostate (46)

Table I.1: Biomarkers of PNI confirmed with immunohistochemistry.

In vitro assays	Neural Monolayer Adhesion	(47, 48)
	Boyden Chamber	(40, 49-52)
	Immunoblot or proteomic analysis of cell lines with high or low PNI	(51, 53)
	Neuroplasticity	(51, 54, 55)
	Dorsal Root Ganglion or Myenteric Plexus Co-Culture with cancer cells	(51, 52, 54, 56-61)
	Genetic profiling of nerve-invasive clones	(43)
	Live Cell Imaging	(54)
In vivo assays	Mouse xenograft models	(51, 53, 62)
	Sciatic nerve injection	(52, 59-61)
	Murine model with human nerve plexus graft	(63)
	Genetic profiling of high/low PNI groups	(63-65)
	In vivo imaging	(60)

Table I.2: Laboratory models of PNI.

CHAPTER II

Models of HNSCC Progression

Portions of Chapter II are adapted from previously published manuscripts (66, 67).

Part I: Models of Invasion

The tumorigenic phenotypes or hallmarks of cancer include invasion and metastasis, proliferation, survival, angiogenesis, and stemness (68). Invasion is required for multiple steps in HNSCC progression including initiation, local spread and metastasis. During transformation of a precancerous lesion to HNSCC, cells invade from the surface epithelium, the tissue of origin of HNSCC, into the underlying connective tissue. Invading cells destroy the basement membrane that separates the epithelium from the connective tissue. Destruction of the basement membrane and invasion are essential for development of HNSCC. Thus, the basement membrane is the first, most robust structural barrier to invasion (5). Cancer cell proliferation and survival promote tumor growth. Angiogenesis facilitates tumor growth and spread, and stemness promotes tumor recurrence. Given the importance of these phenotypes in tumor progression, a robust cancer model should recapitulate these phenotypes.

Many models have been developed in the last few decades to evaluate the oncogenic phenotypes of HNSCC. However, most of these models are in vitro systems that work with monolayer cultures, making these assays difficult to translate into clinical application.

Furthermore, these models do not recapitulate the basement membrane or the connective tissue. Due to the importance of invasion in tumor progression, we recently developed an in vitro three-dimensional (3D) model for human HNSCC as described in **Appendix C** (69, 70), that recapitulates stratification of the surface epithelium, destruction of the basement membrane and invasion of tumor islands into the connective tissue. This oral cancer equivalent model is excellent for studying several of the local effects of invasion. However, the model does not simulate the systemic impact of invasion (e.g. metastasis) as may be observed in an in vivo murine model. Several murine models are used to study HNSCC. Sub-cutaneous injection models of tumor cells into immunocompromised mice are useful to study tumor size (71). The floor-of-the-mouth tumor models have the advantage of placing tumor cells into the oral tumor microenvironment and can lead to metastases (72). However, both models require injection of tumor cells below the basement membrane and do not replicate invasion. The mouse oral carcinogenesis model involves inducing tumors in mice through exposure to carcinogens in the water supply such as 4-nitroquinoline-1 oxide, which mimics the impact of tobacco exposure (73). This model is very useful to study both dysplasia and squamous cell carcinoma, but genetic studies are limited since the tumors produced are of mouse, not human origin.

Unfortunately, most murine models of human HNSCC are inadequate because tumor cells are injected directly into the connective tissue thereby bypassing the basement membrane of the surface epithelium, the first barrier to invasion. Given the importance of invasion in tumor progression, we developed an in vivo model of human HNSCC progression utilizing the chicken embryo. The embryonic chicken is among the

most well-characterized and useful in vivo biological systems (74). The chorioallantoic membrane (CAM) assay is an emerging model of tumor progression using the embryonic chicken. The CAM is a very vascular structure that surrounds the chick embryo. It allows for exchange of dissolved O_2 and CO_2, similar to the function of the placenta of a developing mammal. The CAM is comprised of an upper chorionic epithelium, intervening mesenchyme, and lower allantoic epithelium. The chorionic epithelium is structurally similar to human epithelium (66) and is separated from the underlying connective tissue by basement membrane comprised of collagen IV, similar to that observed in human oral mucosa.

In the CAM assay, a small opening is made in the shell of a fertilized egg, allowing a tumor cell graft to be seeded directly on the chorionic epithelium. Grafted tumor cells invade through the basement membrane of the chorionic epithelium and into vascular structures in the underlying mesenchyme, thereby metastasizing to distant structures and organs including the liver of the developing chicken and the lower CAM (66).

Figure II.1 provides an overview of the CAM model of HNSCC and identifies where HNSCC tumors grow, invade and metastasize within the chick egg. HNSCC cells are seeded on the upper CAM and destroy the basement membrane of the surface epithelium to invade the connective tissue and blood vessels via which they metastasize to the lower CAM and liver. **Figure II.2** provides an overview of the procedure, and outlines the endpoint assays including tumor growth, invasion, angiogenesis and metastasis.

The CAM HNSCC in vivo model was validated by investigating the role of EZH2 (enhancer of zeste homolog 2) in HNSCC growth, angiogenesis, invasion and metastasis

(**Appendix D**). Using this model, we recently showed that EZH2, a histone methyltransferase, promotes progression of HNSCC by inducing multiple cancer phenotypes, likely via methylation of multiple tumor suppressor genes (71, 75).

The first tumor grafts on the CAM were successfully performed in 1913 using rat sarcoma tissue, establishing that the CAM is an appropriate recipient site for xenografts (76). This discovery led to the development of multiple carcinogenesis assays using the CAM, which have become prominent methods to assess tumor angiogenesis, progression and metastasis (77, 78). Although the basic technique of grafting tumors onto the CAM has changed very little, powerful technological advances allow scientists to use the CAM for assays of increasing complexity. These advances have led to renewed attention in this established model, particularly in the past decade (**Figure II.3**). Since 2010, nearly 100 cancer-related publications using the CAM model have appeared annually in peer-reviewed journals listed on PubMed.

Our laboratory recently reported the use of the CAM model to simultaneously study multiple aspects of HNSCC tumor progression, including tumor growth, invasion, metastasis and angiogenesis (66). Although the CAM model has been used to study oral epithelial dysplasia (precancer), peri-tumor lymphatic vessel density, and to test drugs for HNSCC, it had not been characterized as a comprehensive model for HNSCC progression until our recent study. The study and related phenotypes are summarized in **Table II.1**. The CAM model of HNSCC has several benefits over murine in vivo models. The CAM closely replicates the tissue complexity of oral mucosa, i.e. the basement membrane separating the epithelium from the connective tissue, and therefore is an excellent model for HNSCC progression. Most murine models of HNSCC require

subcutaneous or submucosal injection of cancer cells. Because the injected cells artificially bypass the basement membrane, injection-based murine models cannot replicate destruction of the basement membrane with subsequent invasion. This important phenotype is an essential step for transformation of a premalignant lesion into HNSCC (79). However, in the CAM model of HNSCC, tumor cells must degrade the basement membrane of the chorionic epithelium to invade, closely replicating progression of precancerous lesions to HNSCC. Given that some recent work emphasizes the impact on invasion of structures and channels found in true extracellular matrix, the CAM model is attractive to study invasion in vivo (80, 81).

Many technological advances are giving a fresh perspective on the value of CAM tumors. It is now possible to use stop-motion video-microscopy to continuously monitor a target's activity over a period of days (82). Unlike traditional murine models, the CAM model is able to exploit the promise of these new techniques. While both murine and CAM models provide in vivo results, tumors on the CAM are more readily observed and quantified. For similar reasons, the CAM model also offers easier study of angiogenesis.

Another advantage of the CAM model is the short duration (maximum 1 week) required to assess even late events in tumor progression, such as metastasis. This may take several weeks to months to assess in murine models (83). This long duration increases the cost and time required for investigations. The cost per mouse limits the number of mice that can be used for each experiment. The CAM model provides an opportunity to perform large in vivo experiments at a fraction of the cost of murine-based models of HNSCC. The cost effectiveness and easy accessibility of the CAM system enhance the appeal of this in vivo model, particularly when funding resources are limited.

Importantly, the rapid turnaround of results in the CAM model allows in vivo studies with transiently transfected HNSCC cells, which cannot be performed in murine models. For example, the impact of an siRNA on downregulation of a protein lasts 7-10 days for rapidly dividing cells (84). This timeframe is insufficient for tumor studies in mice, which take weeks to months. In contrast, in the CAM the entire sequence of tumor progression including proliferation, invasion and metastasis can be observed in this time frame.

Another advantage of the CAM-HNSCC model is the late development of the immune system in the chick embryo (83). Due to the lack of an immune system in the early chicken embryo, the CAM system readily accepts many types of xenografts. Few cells are needed for xenograft experiments, and metastasis can be quantified very accurately through PCR-based methods (85). The CAM model of tumor progression has some limitations. Perhaps the most significant limitation is that the mouse is currently accepted as the gold standard for in vivo biological studies. Moreover, technical dexterity, and specific equipment/ materials are necessary to set up the CAM protocol. This is also true of some murine HNSCC models such as the tongue and floor-of-mouth models (72).

The chick embryo becomes fully immunocompetent by day 18 (83). The developing immune system of the embryonic chicken limits the duration of a study with human tumor cells and the lack of an immune system prevents the investigation of tumor-host immune system interactions. However, investigations of human HNSCC in mouse also require the use of immunodeficient mice. The larger sample sizes used for CAM experiments yield a wealth of data for multiple phenotypes requiring extensive time for analysis.

Overall, the scientific benefits of the CAM model make it an attractive option to all cancer biologists. The practical advantages of the CAM model over rodent models make it a cost-effective, accessible option to scientists in developing institutions. For these reasons, and because the CAM brings the study of these processes into a uniform setting where interactions can be examined, the popularity of the CAM model will continue to increase.

Part II: Advancing the CAM Model to Become a Model of PNI

The significance of the primed neural niche in the tumor microenvironment has been alluded to in histopathological observation and 3-dimensional (3D) reconstruction of tumors from labeled tissue sections (86). However, the speculated mechanisms of PNI have underplayed the role of neurons in tumor-nerve interactions, since previous in vitro models could not capture the dynamic involvement of neural tissue (7). Most in vivo studies of PNI focus on tumor spread and inhibition of motor function, and depend upon direct injection of tumor cells into sciatic nerves (87). Injection models are useful to show destructive tumor progression and pain resulting from tumor cells within nerves. In a different approach, surgically implanted orthotopic tumor grafts were used to characterize the importance of β-adrenergic receptors in promoting PNI and progression of prostate cancer, thus suggesting a more prominent role of neuritogenesis in tumor progression (88). However, in bypassing the invasive process using surgically implanted tumors, these previous models do not truly replicate PNI.

The prevailing view is that cancer cells are the drivers of tumor-neuronal interactions, in part because limitations of previous in vivo models made it impossible to fully appreciate the role of nerves in these interactions (7). Given the shortcomings of previous in vivo PNI models, we developed a new PNI model on the CAM in vivo platform, rooted in work from the research team of Nobel Laureates Rita Levi-Montalcini and Stanley Cohen, and Victor Hamburger that demonstrates the ability of chicken embryos to sustain tissue grafts (89, 90). In this model, a mammalian dorsal root ganglion (DRG) is isolated and grafted onto the surface epithelium of the upper CAM. After the DRG becomes incorporated into the epithelium of the CAM, HNSCC cells are grafted near the DRG and allowed to interact with the nerve before the entire in vivo system is harvested and analyzed. Importantly, the system allows full visual observation of either the DRG or the tumor in vivo by fluorescent labeling.

In the early development of the CAM-PNI model, both mouse and rat DRG were tested for optimal incorporation into the CAM. We first performed a time course experiment with mouse DRG to determine the optimal number of days necessary for the graft procedure. We found that the mouse DRG becomes fully incorporated by day 3 (**Figure II.4A** and **Figure II.4B**). We also performed optimization using rat DRG (isolation technique shown in **Figure II.4C**) and found that rat DRG had even more reliable incorporation into the CAM epithelium than mouse DRG by day 3 (**Figure II.4D**). Therefore, rat DRG were selected for future model optimization.

Following optimization of the DRG grafting technique, we further adapted the model to study PNI in vivo. The CAM-PNI model was inspired by an in vitro assay of co-culturing DRG with prostate cells in Matrigel™ (57). When using HNSCC cells in co-

culture with rat DRG, we found that they exhibited robust invasion toward nerves in vitro (**Figure II.5A**). When a rat DRG was grafted adjacent to HNSCC tumor cells on the CAM, both were supported by the in vivo system (**Figure II.5B**) and within 2 days, HNSCC invasion into the nerve was observed (**Figure II.5C** and **Figure II.5D**).

Our CAM-PNI in vivo model addresses the deficits of previous models by demonstrating neuronal outgrowth into the peri-tumoral niche. Importantly, tumors in the CAM-PNI system are not surgically implanted, thereby maintaining the invasive process necessary for PNI. The system is also useful in studying therapy to disrupt PNI. In the future, the model could be used to evaluate response to treatment by measuring the responses of the tumor and the nerve, either of which may promote tumor recurrence.

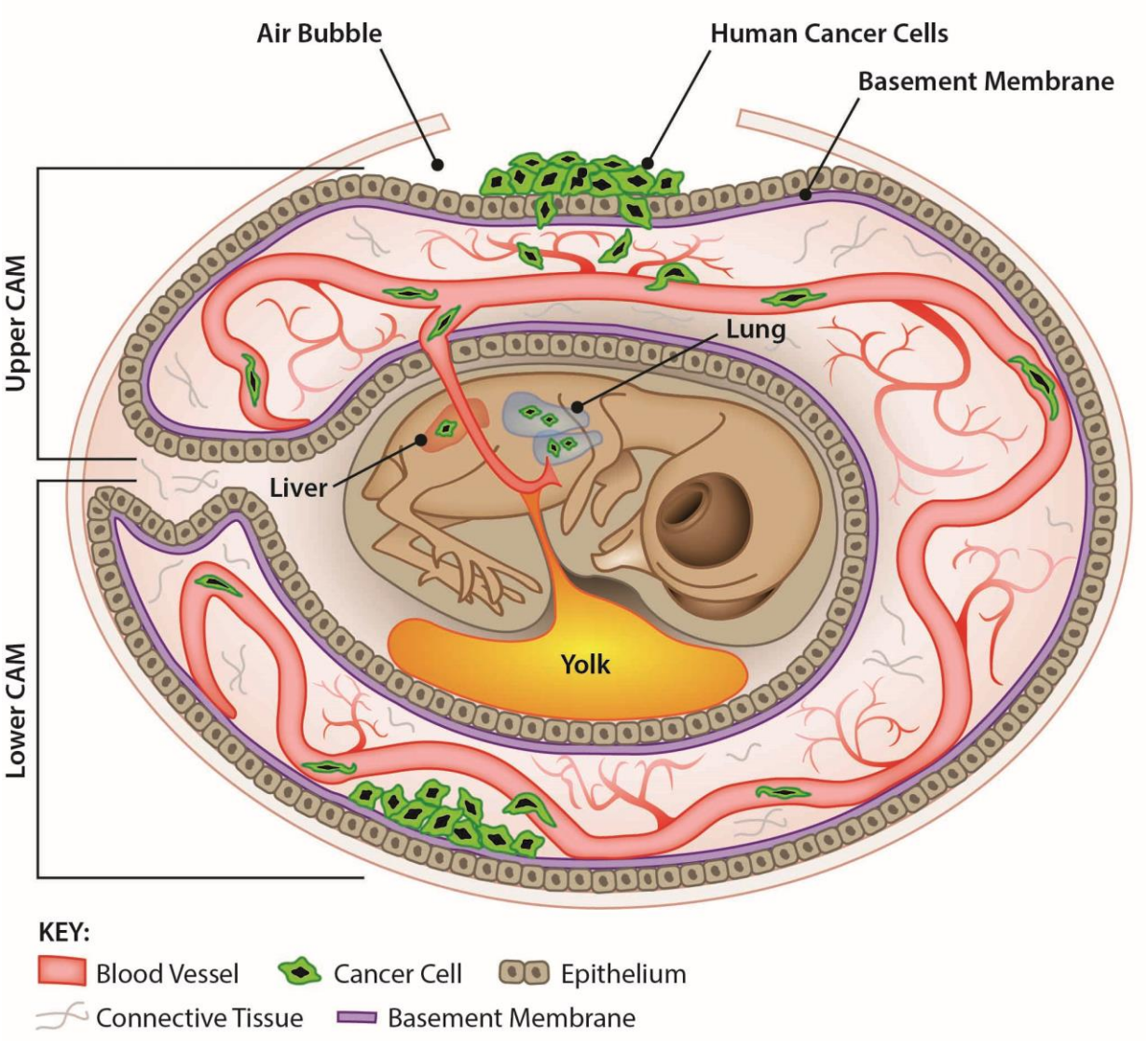

Figure II.1: Overview of the CAM model of tumor progression. Fluorescently labeled cancer cells are seeded on the upper CAM of the chick embryo. The cancer cells invade the epithelium and basement membrane of the upper CAM and move through connective tissue into the vasculature. Cancer cells can metastasize to the lower CAM or liver and lung of the developing chicken.

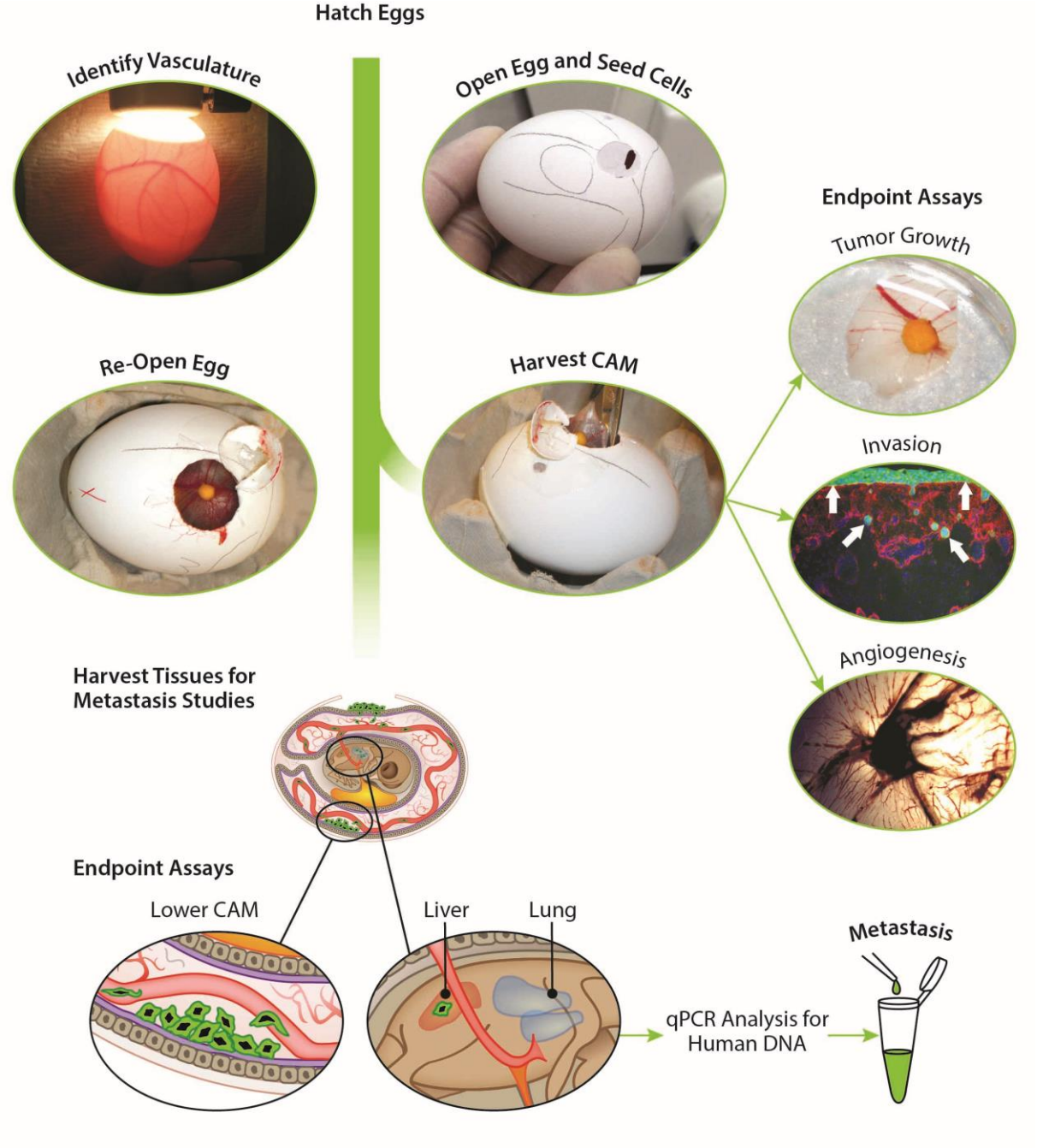

Figure II.2: Experimental procedure and timeline of the CAM assay. Fertilized chicken eggs are incubated at day 0. On day 8, the developing vasculature is identified and a window is opened on the egg to seed human cancer cells. On day 11, the egg can be re-opened to harvest the upper CAM containing the tumor in order to assess tumor growth, invasion and angiogenesis. For metastasis studies, the egg is opened at day 16 to collect the lower CAM and liver of the developing chicken. qPCR analysis of the collected tissues provides an estimation of the number of human cancer cells that have invaded to the collected organs.

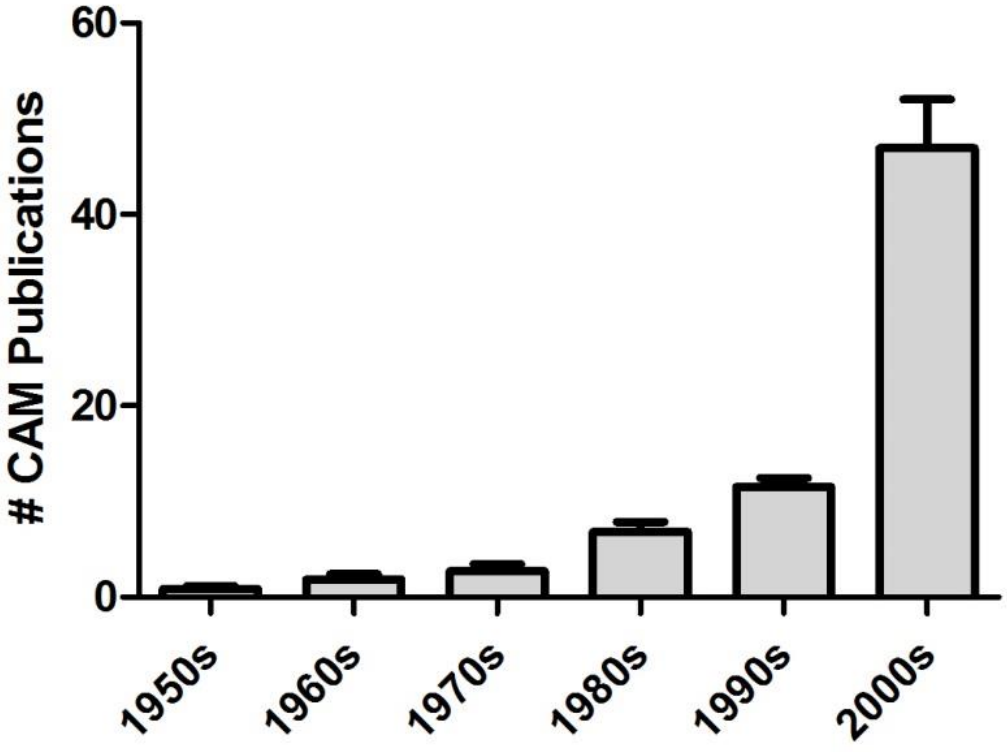

Figure II.3: The CAM emerges as a standard model of carcinogenesis. "Chorioallantoic membrane" and "cancer" were entered as search terms on PubMed (http://www.ncbi.nlm.nih.gov/pubmed/), and the results were sorted by date of addition to PubMed database. The number of articles per decade was quantified, and Student's *t*-test was used to analyze the difference in the number of publications using the CAM method between decades. Between the 1970s and 1980s and beyond there is a statistically significant increase in the number of articles, and the largest increase occurred between the 1990s and 2000s ($P < 0.05$). Given this trend, it is likely that an increasing number of cancer researchers will employ the CAM model.

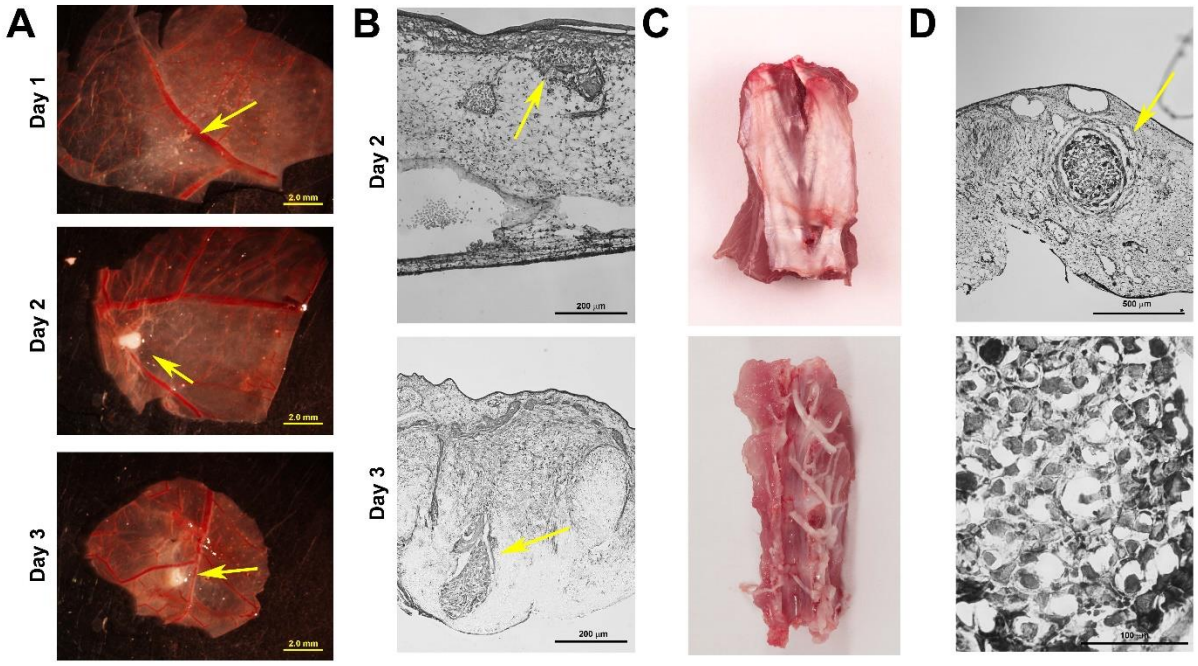

Figure II.4: Optimization of nerve grafting on the CAM. **A.** Stereo microscope images show grafting of a mouse nerve on the CAM (arrows identify nerves). No integration of the nerve was observed after the first day, however by the second day there was partial integration, and complete integration of the nerve into the CAM by the third day after grafting. **B.** Histological images of the grafted nerve are shown for day 2 (partial integration) and day 3 (full integration). **C.** The procedure for opening a rat spinal column to collect DRG is shown. **D.** Full integration of a rat nerve at 3 days post grafting is shown (arrow highlights nerve).

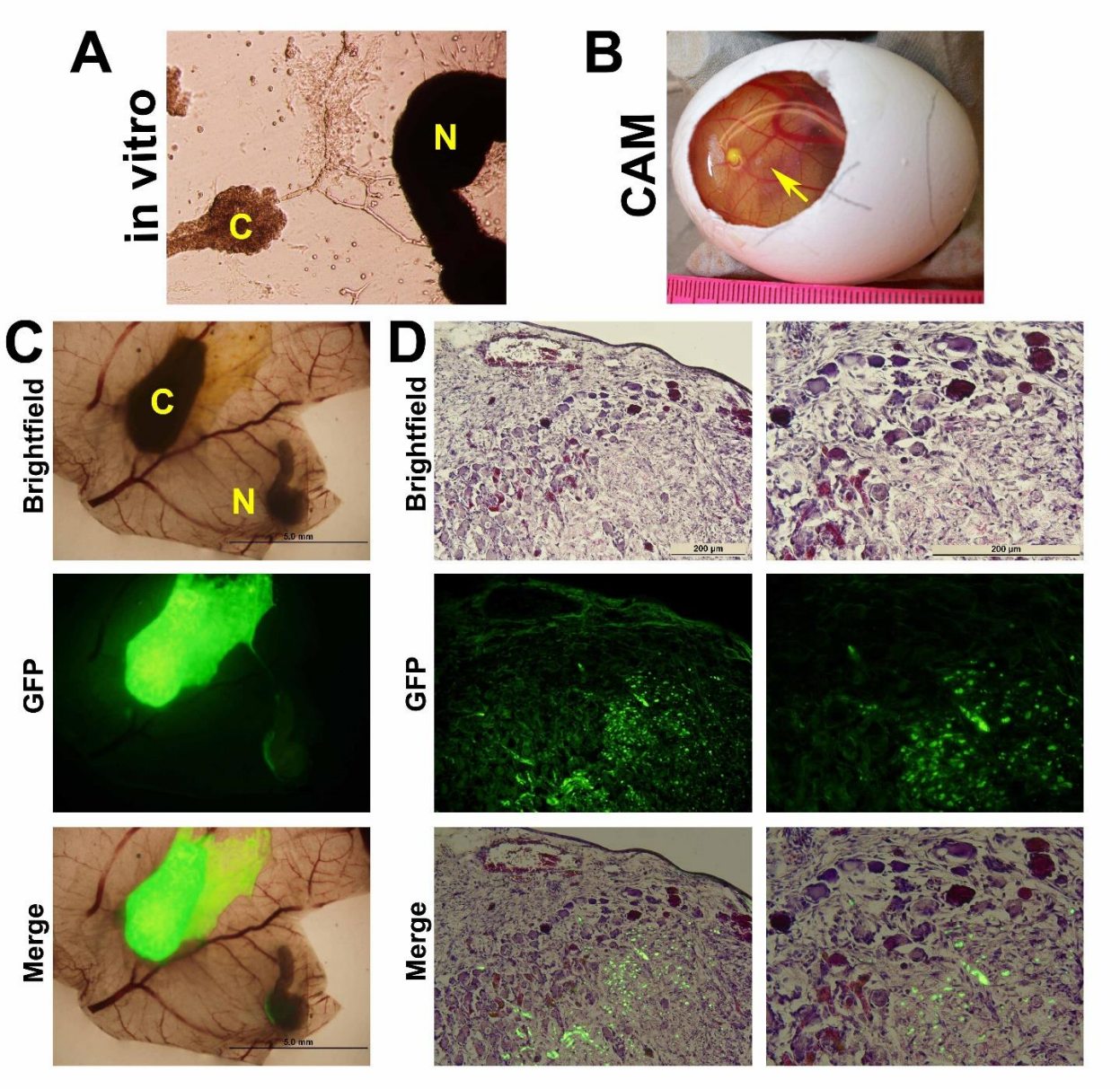

Figure II.5: Optimization of the CAM-PNI model. A. HNSCC cells exhibit PNI when co-cultured with a rat DRG in vitro. **B.** The co-culture approach is adapted to an in vivo system by co-grafting a rat DRG and HNSCC tumor cells onto a CAM (arrow highlights the nerve on the CAM). **C.** The upper CAM tissue is collected, and PNI is observed. **D.** Histologic images of PNI from the CAM co-grafting technique (20x and respective 40x images are shown). In images, “C” labels cancer and “N” labels nerves. Tumor cells, labelled with DIO, fluoresce green.

HNSCC Cancer Phenotype Studied	Reference(s)
Angiogenesis	(66, 91-97)
Biomarker Expression	(66, 92, 93)
Drug Testing	(92-95, 98-101)
Dysplasia Study	(102)
Invasion	(66, 92, 96, 103-105)
Lymphatic Vessel Density	(106)
Metastasis	(99-101, 103, 107)
Tumor Growth	(66, 92, 93, 96, 108)

Table II.1: The use of the CAM model in HNSCC research. The terms “chorioallantoic” and “head and neck cancer” were used to identify articles listed on Pubmed that use the CAM model to study HNSCC. The articles from the resulting search are organized according to the phenotype investigated using the CAM model system.

CHAPTER III

Galanin Modulates the Neural Niche to Favor Perineural Invasion in Head and Neck Cancer

Chapter III is adapted from a manuscript that is under review for publication (109).

INTRODUCTION

PNI predicts poor survival in head and neck squamous cell carcinoma (HNSCC), pancreatic, stomach and colon cancers (7). PNI is associated with pain and tumor spread, independent of lymph or vascular involvement (6). Previously assumed to be a passive process by which cancer spreads along the path of least resistance, recent evidence suggests PNI is an active process whereby tumor cells must degrade several layers of perineural sheath prior to metastasis (110).

PNI is observed in up to 80% of HNSCC cases and correlates with tumor recurrence and spread (110, 111). HNSCC can spread along nerves into the brain or into sensory or motor nerves, and is associated with loss of function, pain, numbness and formication, i.e. the feeling of insects crawling under the skin (111). HNSCC with PNI is treated aggressively but the prognosis remains poor. Unfortunately, there is no targeted treatment for PNI since the molecular mechanisms are largely unknown. Therefore, dissecting the mechanism of PNI is a critical area of research since this would facilitate

the development of novel therapeutics targeting PNI. Specific treatment of PNI would enhance patient survival and quality-of-life.

Although it has been suggested that the altered neural microenvironment adjacent to tumors contributes to cancer progression, the limitations of existing in vivo models of PNI have hindered elucidation of nerve-tumor interactions (7). To overcome this obstacle, we developed an in vivo model of PNI to characterize mechanisms of nerve-tumor interactions. We show that the neuropeptide galanin (GAL) initiates nerve-tumor crosstalk via the activation of the G protein-coupled receptor galanin receptor 2 (GALR2) on cancer cells. Our data reveal that activated GALR2 induces nuclear factor of activated T-cells, cytoplasmic, calcineurin-dependent 2 (NFATC2)-mediated transcription of cyclooxygenase-2 (COX2) and GAL. COX2 enzymatically facilitates prostaglandin E2 (PGE_2) production, promoting tumor progression. In a feedback mechanism, GAL released by cancer induces neuritogenesis and facilitates PNI. These studies demonstrate that the nerve initiates PNI via GAL, providing a potential treatment target. Moreover, the novel approaches presented here provide a starting point to investigate the roles of other neurotrophic proteins in PNI.

METHODS

Cell Culture. HNSCC cell lines UM-SCC-1 (from Thomas Carey, University of Michigan) and OSCC3 (from Peter Polverini, University of Michigan) were genotyped to confirm cell types at the University of Michigan DNA Sequencing Core prior to all studies. HNSCC cells and the neuroblastoma cell line SH-SY5Y (from Stephen K. Fisher, University of Michigan) were cultured in Dulbecco's Modified Eagle Medium (DMEM, Gibco®, 11965-

092) supplemented with 10% fetal bovine serum (FBS, Gibco®, 16000-044) and 1% PenStrep (Gibco®, 15140-122). UM-SCC-1 and OSCC3 cells were transfected with pcDNA™3.1 (Invitrogen™, V790-20) and pcDNA™3.1-GALR2 (Missouri S&T cDNA Resource Center, GALR200000). Geneticin (Gibco®, 10131-027, 50 µg/mL) was used to select and maintain stable colonies. UM-SCC-1 and OSCC3 cells transfected with pcDNA™3.1-GALR2 were infected with control non-targeting small interfering RNA (siRNA, Dharmacon, D-001810-10-05) or siRNA targeting NFATC2 (Dharmacon, L-003606-00) and COX2 (Dharmacon, LQ-004557-00-0002, siRNA sequences available in **Table III.1**). For stable NFATC2 knockdown, UM-SCC-1 and OSCC3 cells overexpressing GALR2 (UM-SCC-1-GALR2 and OSCC3-GALR2, respectively) were transduced with shRNA lentiviral particles (Thermo Scientific, shRNA sequences available in **Table III.1**). Stable colonies were selected using Puromycin (Santa Cruz Biotechnology, sc-108071B, 10 µg/mL for UM-SCC-1 cells and 25 µg/mL for OSCC3 cells).

Chromatin Immunoprecipitation (ChIP). The EZ-Magna ChIP A/G kit (EMD Millipore) was used to perform ChIP as described (71). The sequences of the *Ptgs2* (COX2) and *Gal* (GAL) primers used are provided in **Table III.2**. The *Gal* primers were designed by walking the promoter region of GAL and contain an AP-1 binding site. The *Ptgs2* primers were reported previously and contain AP-1 binding sites (112, 113). The UM-SCC-1-pcDNA and UM-SCC-1-GALR2 cells were grown to 60% confluence and cross-linked using 1% formaldehyde for 10 minutes, and then quenched with 0.125M glycine at room temperature for 5 minutes. The cells were lysed and also sonicated in order to fragment

the chromatin to 500 base pairs, then incubated overnight with antibodies and protein A or G magnetic beads. Crosslink reversal was achieved by incubating the chromatin for 2 hours at 62°C and then the DNA was isolated. qPCR was used to analyse purified DNA to determine relative fold enrichment compared to input DNA. The ChIP antibodies used were anti-NFATC2 antibody (Santa Cruz Biotechnology, sc-7296) and control rabbit IgG (Dako, X0936) was used to normalize NFATC2-specific binding to background nonspecific binding.

Data Analysis. GraphPad Prism (GraphPad software) was used for statistics. A Student's *t*-test was performed with a *P*-value of <0.05 determined to be statistically significant.

DRG Organ Culture. Rat dorsal root ganglia (DRG) and human HNSCC cells were co-cultured in Matrigel™ Basement Membrane Matrix (BD Biosciences, 356234), similar to a described method (57). DRG were dissected from postnatal day 30 Sprague Dawley rats within 1 hour of being euthanized and placed in 15 µL of 4.6 mg/mL Matrigel™. HNSCC cells (2 x 10^4) were seeded in an adjacent droplet of Matrigel™, and cultures were immobilized by warming to 37°C and culturing in DMEM (DMEM, Gibco®, 11965-092) supplemented with 10% FBS (Gibco®, 16000-044) and 1% PenStrep (Gibco®, 15140-122). Cultures were maintained at 37°C with 5% CO_2 for 2 days to observe cancer cell and neurite interactions. GALR2 inhibitor M871 or DMSO control was used at 100 nM in culture. GAL antibody and rabbit serum IgG were used at 3 ng/mL. Neurite extension and cancer cell movement were imaged after 48 hours and quantified using ImageJ

software (W.S. Rasband, NIH, Bethesda, MD; http://imagej.nih.gov/ij/). Cultures were made in quadruplicate and repeated in triplicate.

Efforts to Reduce Bias. Protocols were developed to eliminate investigator bias in quantifying samples. Quantification was routinely performed by 2 individuals, 1 of whom was blinded to the hypothesized outcome. Whenever possible, objective quantification methods, such as microplate readings and computer-based quantification of images were selected.

Enzyme-Linked Immunoadsorbent Assay for PGE_2. CM from HNSCC cell lines UM-SCC-1 and OSCC3 was collected and processed as described (114). The total number of cells was quantified with a Countess® Cell Counter (Invitrogen™, C10227). PGE_2 was quantified as a surrogate for COX2 using a competitive ELISA (R&D Systems®, KGE004B) in 3 independent experiments per cell line.

HNSCC-Neural Cell Interaction Assay. UM-SCC-1-pcDNA or UM-SCC-1-GALR2 ($1x10^4$) cells were labeled with DiO, a dialkylcarbocyanine derivative, and suspended with $1x10^4$ SH-SY5Y neuroblastoma cells that had been labeled with CellTracker Red CMPTX (Life Technologies, C34552) on 8-chambered cover-slips in blank DMEM in triplicate. After 24 hours, the cells were fixed, mounted and imaged at 60x magnification. Colocalization was quantified by counting the number of green HNSCC cells in contact with red SH-SY5Y cells and dividing by the total number of HNSCC cells per high powered field. Differentiation was quantified by counting the number of SH-SY5Y

cells with neurite extensions and dividing by the total number of SH-SY5Y cells present per high powered field.

Human subjects. Paraffin-embedded human HNSCC tissues were used for immunohistochemistry analysis. The University of Michigan Institutional Review Board approved the protocol prior to any human tissue use. All human tissues were de-identified prior to the study; therefore the University of Michigan Institutional Review Board determined that the research qualified for Category 4 Exemption status (Exemption Number 1999-0341).

Immunoblot. Cells were lysed with 1% NP40 protein lysis buffer. The following primary antibodies were used: anti-GAL (EMD Millipore, MAB374), anti-GALR2 (Alpha Diagnostics, GALR21-A), anti-actin (BD Scientific, 612656), anti-NFATc2 (Cell Signaling Technologies®, 5861), anti-COX2 (Cell Signaling Technologies®, 12282) and anti-HNRNP (Santa Cruz Biotechnology, sc-15386). Biotinylated anti-mouse and anti-rabbit secondary antibodies were used (Jackson ImmunoResearch Laboratories, 115-006-075 and 711-006-152). The visualization of immunoreactive proteins was performed with the SuperSignal West Pico Chemiluminescent system (Pierce, 34080).

Invasion Assay. Cell invasion was quantified 24-48 hours after siRNA transfection using Transwell inserts (Corning, 3422) and the modified Boyden chamber assay coated with Matrigel™ (BD Biosciences, 354230). Inserts that were not coated with Matrigel™ were used as a migration control, and invasion was normalized to migration according to the

manufacturer's instructions by dividing the total number of cells that invaded through Matrigel™ by the total number of cells that invaded through the control insert. Five nanomolar GAL (Sigma-Aldrich®, G8041) or conditioned medium (CM) collected from rat DRG cultured in control medium for 48 hours was used as a chemoattractant in the bottom chamber of the assay. CM from rat DRG was incubated with 1:1000 anti-GAL antibody (EMD Millipore, AB5905) or rabbit IgG (Dako, X0936) for 1 hour at room temperature. Conjugated-GAL and unbound antibody or IgG were removed by centrifugation with an Amicon Ultra 50K centrifugal filter (EMD Millipore, UFC805024) for 10 minutes at 4000 rpm.

***Immunohistochemistry and Immunofluorescence*.** Human and mouse tumors were stained with anti-COX2 rabbit monoclonal antibody (Cell Signaling Technology®, 12282), anti-S100 rabbit polyclonal antibody (Dako, Z0311, used to identify nerves on paraffin-embedded tissue), cytokeratin AE1/AE3 mouse monoclonal antibody (Pan cytokeratins, EMD Millipore, IHCR2025-6, used to identify tumor cells on paraffin-embedded tissue), and anti-GAL rabbit serum antibody (EMD Millipore, AB5909). Mouse IgG (Dako, X0931) or rabbit IgG (Dako, X0936) was used at the same concentrations as the primary antibodies as negative controls. Biotinylated goat anti-mouse and anti-rabbit secondary antibodies were used (Biocare Medical, GM601H and GR608H). Hemotoxylin and eosin staining were performed to assess tumor morphology. Immunofluorescence on frozen CAM sections was performed using human collagen IV antibody followed by incubation with DAPI. Immunofluorescent labelling of neurites was performed as follows: nerve explants were blocked with normal goat serum and incubated with anti-neurofilament (NF-

M 160kD chain primary antibody (Zymed Laboratories®, 13-0700) in 0.3% triton X-100, followed by incubation with fluorescent anti-mouse secondary antibody (Jackson ImmunoResearch, 115-006-075). Imaging of representative fields was performed using an Olympus BX-51 microscope.

Inclusion and Exclusion Criteria*.* In most in vivo and in vitro experiments, a normal distribution of samples was obtained. However, significant outliers were excluded from analyses if the values fell outside of a normal distribution.

In vivo models. The University of Michigan University Committee on Use and Care of Animals approved all animal experiments.

> ***Mouse:*** Paraffin-embedded tissues from a previous animal experiment were used for these studies. As described (30), $1x10^5$ OSCC3 cells stably expressing pcDNA-GALR2 or control vector were suspended in Matrigel™ and injected on the backs of 4-6-week-old athymic mice (n=5, Ncr nu/nu strain, NCI, Frederick), so each mouse had an injection of each control and GALR2-overexpressing tumor cells. Animals were euthanized after 14 days. Out of the 5 animals injected, 3 palpable tumors were obtained from each group, so subsequent analyses were performed with n=3 samples for each control and GALR2 overexpressing tumors. Each tumor generated was used for immunohistochemistry, PNI analysis and nerve quantification. Because previously collected samples were used, no power calculation was performed prior to analysis.

CAM Model: Twenty-four fertilized Lohmann White Leghorn eggs were obtained from the Michigan State University Department of Animal Sciences Poultry Farm for each experiment. After incubations, the eggs were randomly distributed into treatment groups of 6-8 eggs each, and tumor cells were seeded as described (66). Eggs that became contaminated during the experiment were excluded from analysis; additionally, CAMs that yielded tumors outside a normal distribution (significant outliers) were excluded due to likely seeding errors.

In Vivo PNI Assay. DRG were dissected from rats within 1 hour of euthanasia and labeled using CellTracker Red CMTPX (Invitrogen™, C34552). DRG were seeded on the CAM with fluorescently-labeled HNSCC cells. The CAM was harvested after 48 hour and tumor spread and neurite outgrowth were imaged using a Leica Stereo microscope and quantified using ImageJ.

Neurite Outgrowth Quantification Assay. The Neurite Outgrowth Assay Plus kit (EMD Millipore, NS220) was used according to the manufacturer's instructions. CM collected from human HNSCC cells was incubated with anti-GAL IgG (EMD Millipore, AB5909) or control rabbit IgG (Dako, X0936) for 1 hour at room temperature. Conjugated GAL and unbound IgG was removed by centrifugation with an Amicon Ultra 50K centrifugal filter (EMD Millipore, UFC805024). The CM was then used as a chemoattractant in the bottom chamber of the assay. SH-SY5Y human neuroblastoma cells were cultured in DMEM (DMEM, Gibco®, 11965-092) overnight and then $1x10^4$ cells were seeded in the top chamber of the assay. After 48 hours, neurites were imaged at 10x and stained using the

stain in the Neurite Outgrowth Assay Plus kit, and retained proprietary AXIS kit dye was solubilized and quantified using a SpectraMax Pro 5 microplate reader (Molecular Devices).

Oncomine™ Analyses. The Oncomine™ database (Compendia Bioscience™) was used to collect clinical data used in meta-analyses. For comparison across 16 HNSCC datasets, a list of neuropeptides was generated based on extensive signalling roles within and outside the neuronal system (110, 115). Because PNI status is not included in the available Oncomine™ datasets, survival was used as a surrogate indicator of potential PNI status since PNI is correlated with poor survival (6). Each neuropeptide was evaluated for expression in cancer versus normal tissue and also for 3-year survival versus 3-year death. The studies were dichotomized to 0 and significant studies at the 5% level were assigned a value of 1.0 while insignificant studies were assigned a value of 0. The set was then subjected to a one-sample *t*-test against a 0.05 expected value. A similar meta-analysis was completed for COX2 expression in cancer versus normal across 16 HNSCC datasets. Datasets used and their references are listed in **Table III.3**.

Proliferation Assay. Human HNSCC cells ($1x10^4$) were seeded in triplicate in a 24-well plate. The total number of live cells was quantified every 24 hours using trypan blue (Invitrogen™, T10282) and a Countess® Cell Counter (Invitrogen™, C10227).

Randomization. An effort was made to randomize samples whenever possible in in vivo and in vitro experiments. Chicken embryos were randomized into treatment and control

groups. Additionally, rat nerves were randomly selected for explant experiments. Mice were not randomized since each mouse received the same 2 injections (one of control cells and one with GALR2-overexpressing cells).

Sample Size Calculations. For CAM experiments, at least a 2-fold difference in tumor size, invasion and metastasis was predicted. Therefore with α of 0.05, power at 0.8 and coefficient of variation at 0.5 (low due to very consistent tumor seeding and incubation of all samples), at least 3 CAMs (eggs) per group was determined to be the minimal sample size. We used 6 CAMs (eggs) per group in each experiment. For in vitro experiments, it was similarly predicted that there would be at least a 2-fold difference in parameters studied with low variance, so with the same equation described above, we determined that using 3 replicates per in vitro experiment was appropriate. In vitro experiments were also repeated in triplicate.

RESULTS

GALR2 Promotes Tumor Progression

Oncomine™ was used to identify neurotrophic factors involved in tumor progression. Meta-analyses were conducted to compare the expression of neurotrophins and neuropeptides in HNSCC and normal samples (**Table III.4**). GAL and brain-derived neurotrophic factor were significantly overexpressed in HNSCC. Importantly, GAL expression correlated with poor clinical outcome in 38 analyses of clinical samples from multiple cancers (**Figure III.1A**) and with positive lymph node status and recurrence in HNSCC (**Figure III.1B**).

The neuropeptide GAL is a ligand for 3 G protein-coupled receptors: GALR1, GALR2 and GALR3. GALR2 is pro-proliferative (30) and is overexpressed in HNSCC due to a frequent chromosomal translocation (116). Previously, we showed that GALR2 induces tumor growth in vivo (30). Using sections from these murine tumors, we found that PNI occurs in GALR2-overexpressing tumors but is absent in controls (**Figure III.2A**). Additionally, more nerves were present adjacent to GALR2-overexpressing murine tumors (**Figure III.2B**), suggesting that GALR2 induces neuritogenesis. Using DNA copy number, we found that high GAL predicted death at 3-years (**Figure III.2C**). In human HNSCC biopsy specimens (demographic data available in **Table III.5**), GAL was expressed in cancer adjacent to nerves (**Figure III.2D**).

Invasion is essential for regional spread and metastasis. Since HNSCC tumors expressing high levels of GAL are correlated with lymph node metastases and recurrence (**Figure III.1B**), we hypothesized that GAL may promote invasion via GALR2. To investigate this possibility in 2 independent HNSCC cell lines, we used the Boyden chamber assay with GAL as the chemoattractant. Invasion was greater in cells overexpressing GALR2 compared to controls (**Figure III.3A** and **Figure III.4A**). Using 2 cell lines in the chick embryo CAM model of HNSCC, GALR2 promoted aggressive tumor growth and invasion in vivo. Tumors overexpressing GALR2 were larger (n=6 for each group, **Figure III.3B** and **Figure III.4B**) and more invasive (**Figure III.3C** and **Figure III.4C**; n=6 for each group) than controls, and destroyed the CAM basement membrane (**Figure III.3D** and **Figure III.4D**). Additionally, UM-SCC-1-GALR2 tumors metastasized more frequently to the lower CAM and liver of the embryos than the corresponding control tumors (**Figure III.3E**; n=3 for each group).

GALR2 Induces PNI

Since the murine studies described above showed strong correlation between GALR2 and PNI, we investigated the impact of GALR2 on PNI with additional models of neural-tumor interactions. UM-SCC-1-GALR2 co-culture with SH-SY5Y human neuroblastoma cells led to neuritogenesis and co-mingling of the cells, which were significantly increased compared to control (empty vector) cells (**Figure III.5A**). Since SH-SY5Y is a neural tumor cell line, we also investigated GALR2-mediated interactions between normal neural tissue and HNSCC using rat dorsal root ganglia (DRG) explants co-cultured with HNSCC cells. Both HNSCC-GALR2 cell lines tested were more invasive toward DRG and induced more neuritogenesis than control cells (**Figure III.5B** and **Figure III.6A**).

The role of the nerve in tumor progression is relatively unknown due to the lack of appropriate in vivo models to characterize nerve-tumor interactions. To address this deficiency, we developed an in vivo model of PNI that demonstrates tumor neuritogenesis. Briefly, a rat DRG was grafted onto the CAM and incorporated into the connective tissue. Subsequently, human HNSCC cells were introduced adjacent to the DRG. The grafted DRG was nourished by the developing vasculature of the CAM that replicates the pro-angiogeneic microenvironment observed in carcinogenesis. Tumor-nerve interactions were observed and quantified. Tumor cell movement and neurite length were higher with HNSCC tumors overexpressing GALR2 than control tumors in both cell lines (**Figure III.5C** and **Figure III.6B**).

To verify that GALR2 promotes neuritogenesis, we disrupted GAL-mediated GALR2 induction. When DRG-UM-SCC-1-GALR2 co-cultures were treated with M871 (a peptide

antagonist against GALR2) or anti-GAL antibody, cancer cell invasion and neuritogenesis were inhibited in vitro (**Figure III.5D**). In the CAM-DRG in vivo PNI model system, M871 disrupted tumor growth and PNI (**Figure III.5E**). These findings establish the importance of GAL-GALR2 in nerve-tumor interactions.

GAL from Nerve Initiates Nerve-Tumor Crosstalk

GAL is secreted by both nerves and cancer cells (114, 117), suggesting that nerve-tumor crosstalk may be initiated by the nerve or cancer. To rule out the possibility that the autocrine stimulation of GALR2 by HNSCC-derived GAL is solely responsible for driving PNI, we explored the role of neural-derived GAL in promoting invasion. In order to investigate this, conditioned medium (CM) from cultured rat DRG was incubated with anti-GAL or control IgG to deplete GAL (**Figure III.7A**). Subsequently, the CM was used for in vitro invasion assays. UM-SCC-1-GALR2 cell invasion was reduced when GAL was depleted compared to CM without depletion (**Figure III.7A**). These findings show that neuronally-derived GAL induces the invasion of HNSCC. HNSCC cells did still invade when provided CM with GAL removed, possibly because there is some residual GAL not removed by the antibody or because other neutrally-derived proteins also affect tumor cell migration. The amount of residual GAL in the CM could be confirmed by ELISA.

GAL from nerves induces invasion of HNSCC cells (**Figure III.7A**) but does not induce neurite formation in the same time frame. Since HNSCC also secrete GAL, we investigated whether in a feedback loop, GAL released by HNSCC cells induced neurite formation. SH-SY5Y cells projected more neurites when incubated with CM from OSCC3-GALR2 cells compared to CM from control cells (**Figure III.6C**). In an investigation using

DRG explants, CM from both HNSCC-GALR2 cell lines tested induced more neuritogenesis than control CM (**Figure III.6D** and **Figure III.7B**). Additionally, CM from UM-SCC-1-GALR2 cells was used as a chemoattractant to induce SH-SY5Y neuritogenesis through a porous membrane. When GAL was depleted in the CM from HNSCC cells using the strategy shown in **Figure III.7A**, fewer neurite projections were induced by the CM (**Figure III.7C**). Taken together, these findings support the hypothesis that GAL secreted from DRG and cancer induces invasion and neuritogenesis, respectively.

GALR2 Mediates Invasion in HNSCC via NFATC2-Induced COX2 Secretion

GALR2 activation induces ERK and calcium signalling in cancer and neurons (118), leading to their increased proliferation and survival (114, 119). In an independent study, increased intracellular calcium and ERK activation leads to the induction and nuclear translocation of NFATC2, a transcription factor that induces transcription of pro-inflammatory cytokines (120). Since GALR2 induces ERK-mediated proliferation (30) we investigated its role in activation of NFATC2. NFATC2 expression was higher in multiple human HNSCC cell lines compared to normal human oral keratinocytes (**Figure III.8A**, upper blot). In 2 independent HNSCC-GALR2 cell lines, GAL led to nuclear translocation of NFATC2 (**Figure III.8A**, lower blot and **Figure III.9A**). After testing a panel of 4 individual siRNAs, si8 was selected due to its superior efficiency in downregulating NFATC2 (**Figure III.9B**). In functional assays, NFATC2 downregulation disrupted proliferation (**Figure III.8B** and **Figure III.9C**) and invasion (**Figure III.8C** and **Figure III.9D**). The in vitro findings were validated in vivo using shRNA lentiviral particles to

induce the stable downregulation of NFATC2 (**Figure III.9E**, shNFATC2-2 selected). NFATC2 downregulation also decreased HNSCC growth (**Figure III.8D**) and invasion (**Figure III.8E**) on the CAM. Histology revealed that the basement membrane of the surface epithelium was disrupted by multiple invasive tumor islands, whereas siNFATC2 prevented invasion of the basement membrane (**Figure III.8F**). Moreover, NFATC2 knockdown disrupted neural-tumor interactions in vitro and reduced HNSCC invasion into DRG (**Figure III.8G** and **Figure III.9F**).

COX2 facilitates the formation of PGE_2, a secreted protein important in tumor progression. Since NFATC2 induces pro-inflammatory mediators such as COX2 in lymphocytes and cancer (121), the promoter regions of *Gal* (GAL) and *Ptgs2* (COX2) were interrogated and found to have NFATC2 binding sites. Using chromatin immunoprecipitation, we validated that NFATC2 binds the promoter regions of *Ptgs2* and *Gal*; binding was higher in UM-SCC-1-GALR2 cells than controls (**Figure III.8H**). Moreover, NFATC2 downregulation reduced COX2 expression (**Figure III.9G**) and PGE_2 secretion in both HNSCC-GALR2 cell lines (**Figure III.8I** and **Figure III.9H**, values normalized to rabbit IgG control). Taken together, GALR2 induces PGE_2 secretion via NFATC2-mediated transcription of COX2. The amount of shRNA-mediated suppression of NFATC2 is greater than the total suppression of COX2, likely because we are directly targeting NFATc2 using shRNA, however multiple factors, including other NFAT proteins, are likely involved in regulating COX2.

In a meta-analysis of multiple HNSCC datasets, COX2 is upregulated in cancer compared to normal (**Figure III.10A**). COX2 is highly expressed adjacent to nerves in most human HNSCC clinical tissue specimens with PNI (**Figure III.11A**). In mice, 80% of

HNSCC-GALR2 tumors expressed COX2 at the invasive front, whereas COX2 was not detected in control tumors (**Figure III.11B**). Immunoblot and ELISA analyses demonstrate that HNSCC-GALR2 cells express more COX2 and secrete more PGE_2 than controls (**Figure III.10B** and **Figure III.11C**). HNSCC-GALR2 cells with siRNA-mediated COX2 knockdown (**Figure III.10C**, si6 and si8 selected) demonstrated reduced invasion compared to controls (**Figure III.10D** and **Figure III.11D**).

COX2 Downregulation Disrupts PNI, but not Tumor Neuritogenesis

COX2 is correlated with PNI in pancreatic cancer (122). Given the importance of GALR2-mediated COX2 expression in invasion (**Figure III.3**), the role of COX2 in mediating PNI was investigated. The downregulation of COX2 reduced HNSCC cell invasion toward DRG in vitro (**Figure III.10E** and **Figure III.11E**). Importantly in vivo, siCOX2 inhibited the invasion of HNSCC towards DRG (**Figure III.11F**, left graph) but did not significantly impact neurite growth toward the tumor (**Figure III.11F**, right graph). Together, these studies indicate that COX2 knockdown in HNSCC disrupts HNSCC cell invasion towards neurons but does not inhibit tumor neuritogenesis.

DISCUSSION

In this focused PNI study, nerve-derived GAL initiates crosstalk between nerves and cancer cells by activating GALR2 in tumors. In turn, activated GALR2 in HNSCC induces NFATC2-mediated secretion of pro-inflammatory mediators and neuropeptides from tumor cells, leading to invasion towards nerves and neuritogenesis (**Figure III.12**).

GALR2-mediated PGE_2 secretion is required for invasion of HNSCC. Moreover, GALR2-mediated GAL secretion induces neuritogenesis towards the tumor, thereby completing a feedback loop. Targeting GALR2 or GAL disrupts neural-tumor crosstalk, and blocks PNI and neuritogenesis. Thus, our findings establish that reciprocal communication between nerves and cancer cells occurs during PNI.

The dynamic interaction between nerves and cancer cells is underexplored. It is likely that PNI requires specific biological interactions between HNSCC and nerves since HNSCC exhibits a tendency towards neural invasion whereas some other head and neck cancers (e.g. low grade mucoepidermoid carcinoma) do not invade nerves (6). Cancer cells establish connections with nerves (neural-neoplastic synapse), and are induced by neural factors (123) that impact metastasis (124). Nerve-tumor interactions are implicated by clinical studies, for example studies showing correlation between PNI and expression of nerve growth factor and its receptor, TrkA (25), semaphorin 4D (51) and laminin-5 (125). Understanding nerve-cancer crosstalk will support the development of targeted therapy for PNI.

Human GAL is a 30-amino acid neuropeptide that regulates memory (126) and has neurotrophic and neuroprotective roles (127). Aside from well-characterized roles of GAL in nocioception and regeneration (128-130), GAL is also implicated in non-neuronal contexts. For example, GAL is highly expressed in keratinocytes where it may play immune and proliferative functions (130), and has abundant binding sites around dermal arteries, artiorioles and sweat glands where it may be involved in thermoregulation and the immune response (131). GAL has an emerging mitogenic role in cancer (126). For example, mice overexpressing GAL develop pituitary tumors (132). GAL induces 3 G

protein-coupled receptors, GALR1, GALR2 and GALR3. While GALR2 and GALR3 are pro-proliferative and promote survival (133), GALR1 is a tumor suppressor (114). In HNSCC, GAL is anti-proliferative via GALR1, and promotes aggressive tumor growth and survival via GALR2 as shown by our previous loss of function studies (30, 114). GALR1 is frequently deleted or silenced in HNSCC (134, 135), effectively increasing the oncogenic activity of GALR2 due to removal of the tumor suppressive activity of GALR1. GAL and GALR2 have actions in the neuronal system and in cancer, but possible roles in regulating crosstalk between nerves and cancer were previously not investigated.

Peripheral nerves release molecules that mediate pain and regeneration (136, 137). GAL is typically expressed at low levels in peripheral nerves but increases following injury (138) and inflammation (139). The CAM model replicates the injury/wound healing microenvironment by allowing neovascularization, thereby sustaining the grafted DRG and supporting neoneuritogenesis. GAL mediates regeneration and survival of inflamed nerves (140). In fact, GAL and GALR2 (but not GALR1) are upregulated in lumbar and facial motor neurons after injury (141). Consistent with these studies, we show that the GALR2-mediated release of GAL from HNSCC induces neuritogenesis. HNSCC is commonly associated with a prominent inflammatory response which may induce nerves (142). In a clinical context, encroachment on nerves by an invading tumor, or transectioning the nerve while removing a tumor or during a surgical biopsy, may stimulate GAL release by nerves, thereby initiating or enhancing nerve-tumor interactions. Thus, using a transected nerve on the CAM-PNI model simulates an injured or inflamed nerve that is primed to release neuropeptides, resulting in PNI and neuritogenesis.

The significance of the primed neural niche in the tumor microenvironment has been alluded to through histopathological observation and 3D reconstruction of tumors from labeled tissue sections (86). However, the mechanisms of PNI are relatively unknown because previously developed in vitro models do not capture the impact of the dynamic involvement of the nerve in neural-tumor interactions (7). Most in vivo studies of PNI focus on tumor spread and inhibition of motor function, and depend upon direct tumor injection into sciatic nerves (87). The sciatic nerve injection model is useful to demonstrate destructive tumour progression and pain resulting from tumor cells within nerves. However, in bypassing the invasive process and the proliferative or inductive roles of the nerve, these previous models do not truly replicate PNI. In a different approach, surgically implanted orthotopic tumor grafts in mice were used to characterize the importance of β-adrenergic receptors in promoting PNI and prostate cancer progression (88).

The CAM-DRG in vivo model used in our study addresses the deficits of previous in vivo models by demonstrating neuronal outgrowth into the peri-tumoral niche. The system is also useful in studying therapy to disrupt PNI. The model can be used to evaluate response to treatment by measuring the response of the tumor and the nerve, which both could promote tumor recurrence. PNI was disrupted chemically with the GALR2 antagonist M871 or with an antibody to GAL. The GAL depletion method (**Figure III.7A**) allowed us to dissect the specific contributions that nerve-derived GAL contributes to invasion and HNSCC-derived GAL contributes to neoneuritogenesis, confirming that these processes involve reciprocal interaction between nerves and HNSCC and not just the autocrine activation of GAL by the nerve or tumor cells. These studies support that therapies targeting GAL and GALR2 should be evaluated as the first potential anti-PNI

therapies. Further investigations with this model will elucidate the role of various stromal tissues in promoting epithelial-mesenchymal transition, an important phenotype in many cancers (79, 143, 144).

An alternative model could have used xenografted tumors in GAL or GALR2 knockout mice; however developmental deficits in the neural tissue of these mice make this option unfavorable. The nerve is atrophic in GAL-knockout mice (145). In GALR2 knockout mice, there is a 20% reduction in neurons in the DRG (146), so changes observed in HNSCC may not represent alterations in GAL secretion or GALR2 signalling but rather an impact on the nerve itself. Since the knockdown of neuronal proteins such as GAL or GALR2 causes deficits in mice (145, 147), it was necessary to develop a model to evaluate the impact of these proteins on PNI using normal DRG.

NFATC2 is emerging as a key regulator of multiple cancer-promoting phenotypes (120). GALR2 and NFATC2 have been independently shown to be important in cancer (116, 148), but their mechanism of action is poorly understood. In HNSCC, GALR2 activates ERK (30) and in adrenal pheochromocytoma cells, GALR2 upregulates intracellular calcium (149). Both these effectors stimulate calcineurin, which regulates NFATC2. However, prior to this study the role of GALR2 signalling in NFATC2-mediated PGE_2 secretion was not established.

A diagnosis of PNI has long been informative to clinicians in treatment planning, but the molecular fingerprint and mechanism need to be developed. PNI requires invasion of tumor cells through layers of collagen and basement membrane, including the epineurium, perineurium and endoneurium, to gain access to axons (7). Factors secreted by nerves bind to receptors on cancer cells to facilitate cancer invasion into nerves.

Precision medicine is a promising treatment planning strategy that relies upon molecular profiling to determine the optimal treatment strategy for each patient. It is critical to identify and understand mediators of neural-tumor interactions to include them in these molecular profiles. Our study identifies GALR2 as a biomarker and potential treatment target of PNI, which may have an implication for future development of personalized therapy.

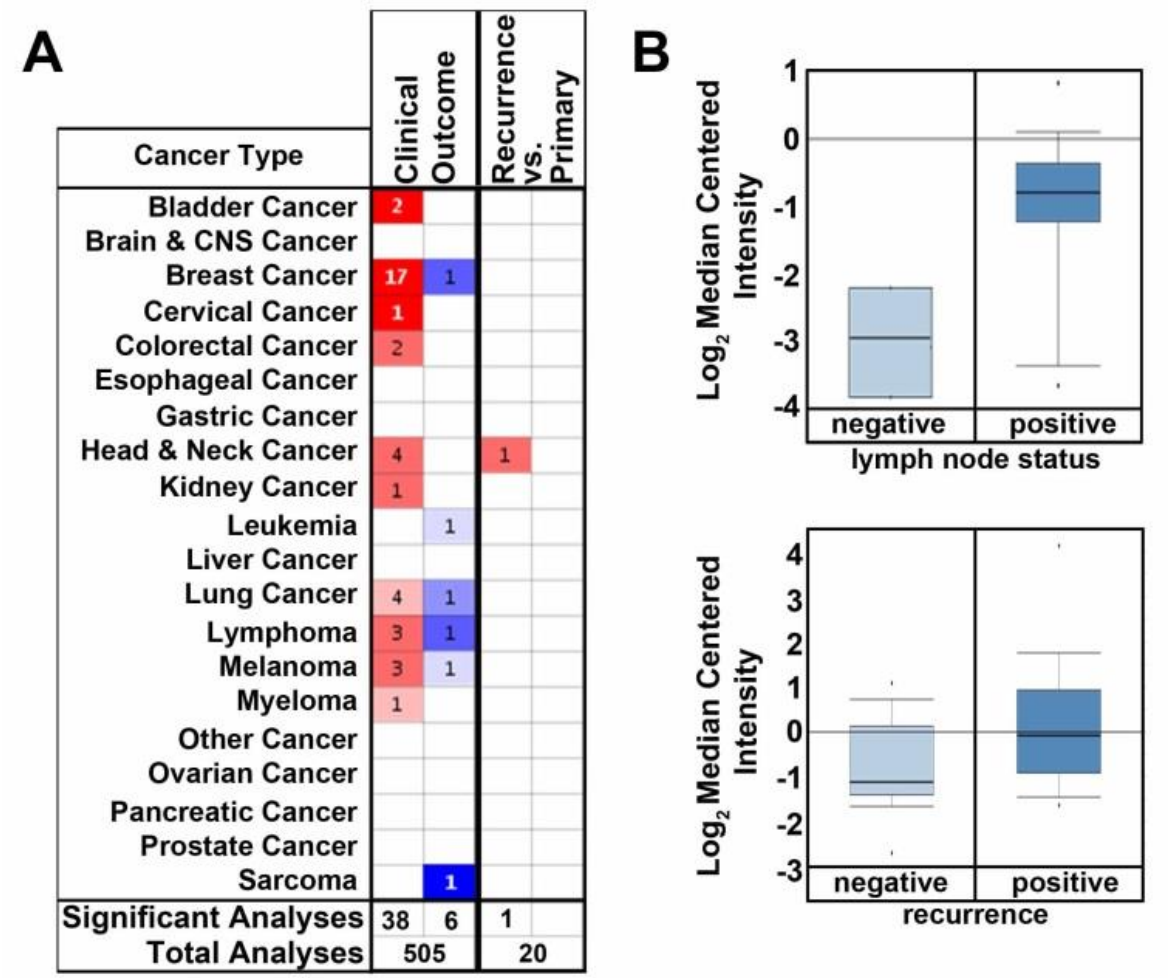

Figure III.1: GAL predicts clinical outcome in multiple cancer types. A. GAL overexpression was correlated with poor clinical outcome in 38 studies across multiple cancer types in the Oncomine™ database and in recurrent tumors versus primary tumors for HNSCC. **B.** GAL overexpression is significantly correlated with positive lymph node status (top graph, from The Cancer Genome Atlas, National Cancer Institute) and recurrence (bottom graph, from the Ginos Head-Neck dataset) of HNSCC.

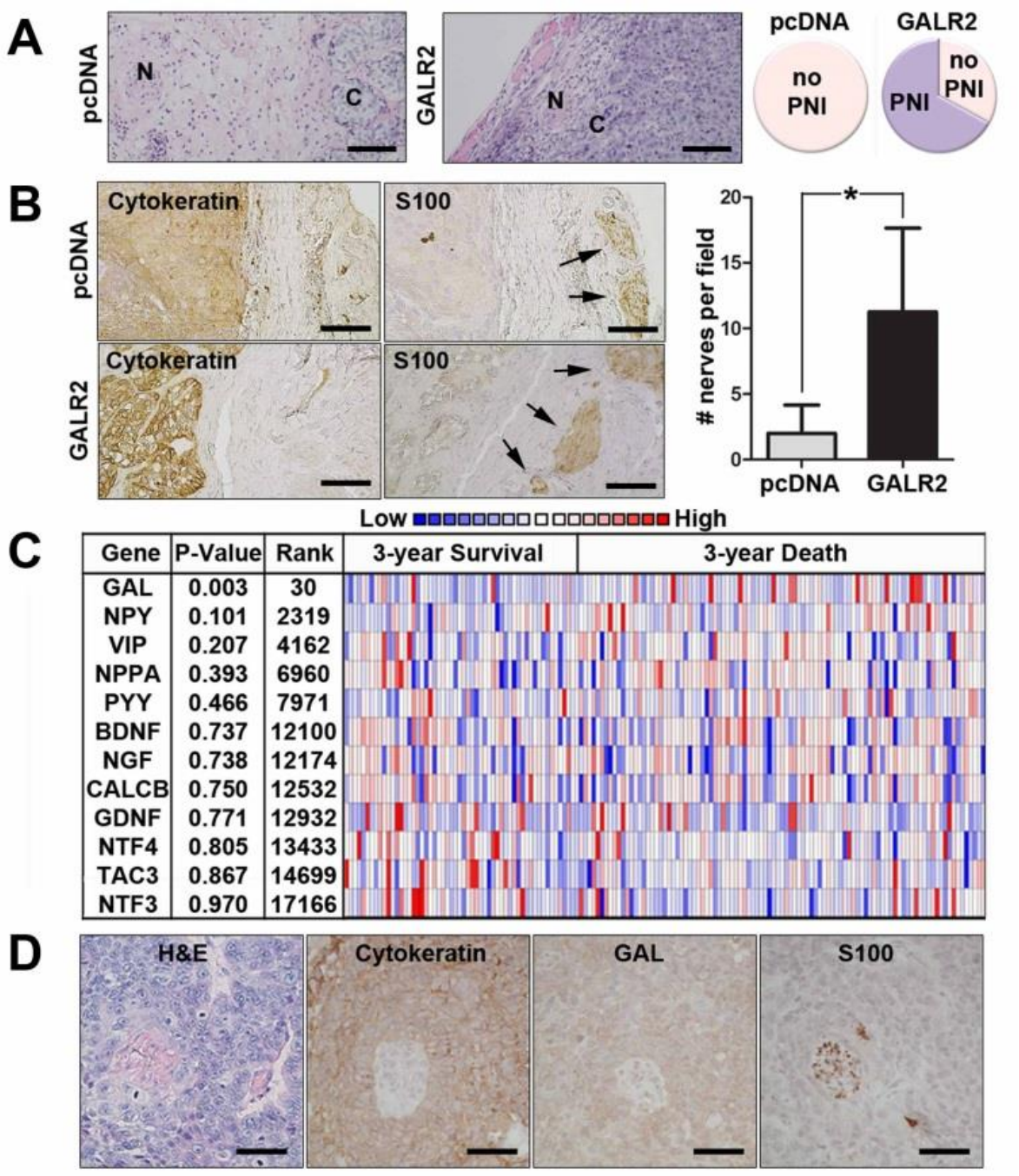

Figure III.2: GAL correlates with poor survival and neuronal involvement. A. Murine tumors with high GALR2, but not control tumors, exhibit PNI (n=3 for both, bar=100μm). **B.** GALR2-expressing murine tumors had more nerves adjacent to the tumors than controls (n=3 for both, arrows identify nerves, bar=50μm). **C.** The Cancer Genome Atlas shows that of several neuronal proteins, only GAL expression significantly correlates with poor survival (P=0.003, 30th most significant). **D.** Human HNSCC adjacent to nerves expresses GAL (Cytokeratin labels tumor and S100 labels nerves, bar=50μm). *$P < 0.05$ (1-sided t-test); data represented by mean + SD.

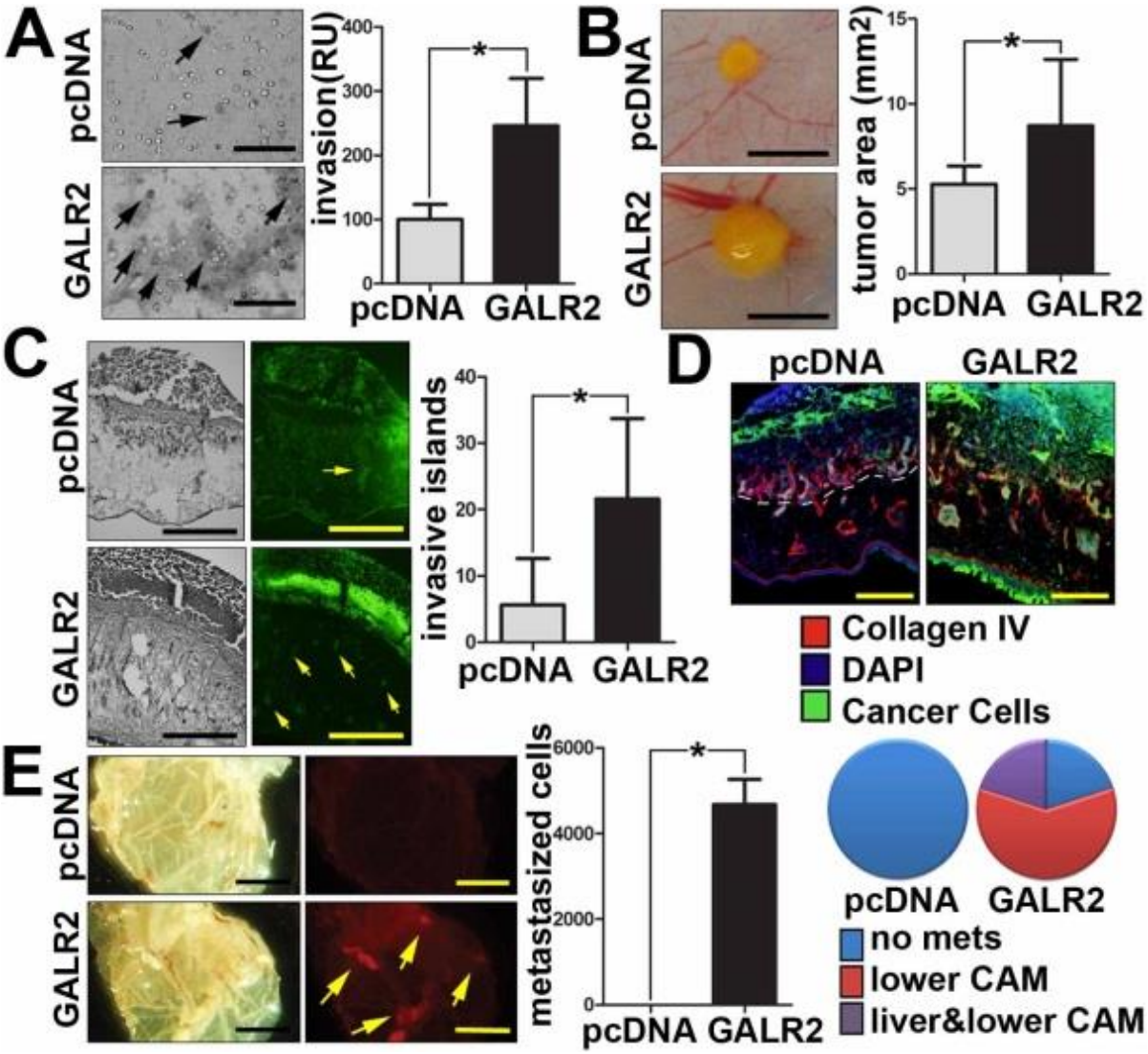

Figure III.3: GALR2 promotes tumor invasion and metastasis (UM-SCC-1). A. UM-SCC-1-GALR2 cells are more invasive than controls when stimulated with GAL (arrows label invasive cells, bar=100µm). UM-SCC-1-GALR2 CAM tumors were larger (**B,** bar=500µm), more invasive (**C,** cancer is green and labeled by arrows, bar=200µm), and more destructive of the basement membrane than controls (**D,** collagen IV and dashed lines label basement membrane, bar=100µm). Metastases from the upper CAM to the lower CAM were observed (**E,** cancer is labeled red and shown with arrows, bar=200µm). Metastases to the lower CAM and liver were also quantified with qPCR for UM-SCC-1-GALR2 and control tumors. There were no metastases to the lower CAM or liver in the pcDNA; in the GALR2 group 4 eggs had metastases to the lower CAM and 1 had a metastasis to the lower CAM and liver (n=6 eggs for both groups). For CAM experiments, n=6 for both groups. In vitro data are representative of 3 independent experiments run with 3 samples. *$P < 0.05$ (1-sided *t*-test); data represented by mean + SD.

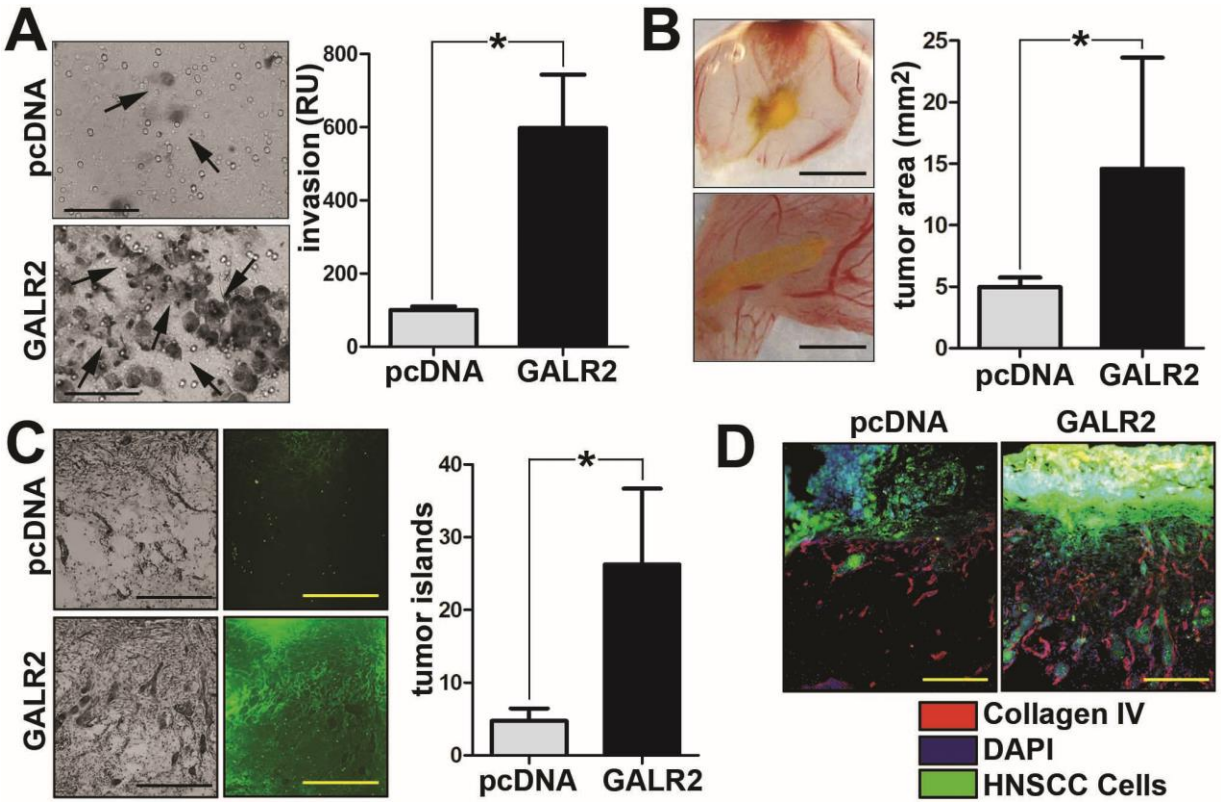

Figure III.4: GALR2 promotes tumor invasion and metastasis (OSCC3). A. OSCC3-GALR2 cells are more invasive than control cells (OSCC3-pcDNA) when stimulated with GAL in the lower chamber of a Boyden chamber assay (bar=100µm). When seeded on a CAM, OSCC3-GALR2 tumors were larger (**B,** bar=500µm), more invasive (**C,** cancer cells are labeled green, bar=200µm), and more destructive of the basement membrane (**D,** labeled with collagen IV, bar=100µm) than control tumors. For CAM experiments, n=6 for both groups. In vitro data are representative of 3 independent experiments run with 3 samples. *$P < 0.05$ (1-sided *t*-test); data are represented by the mean + SD.

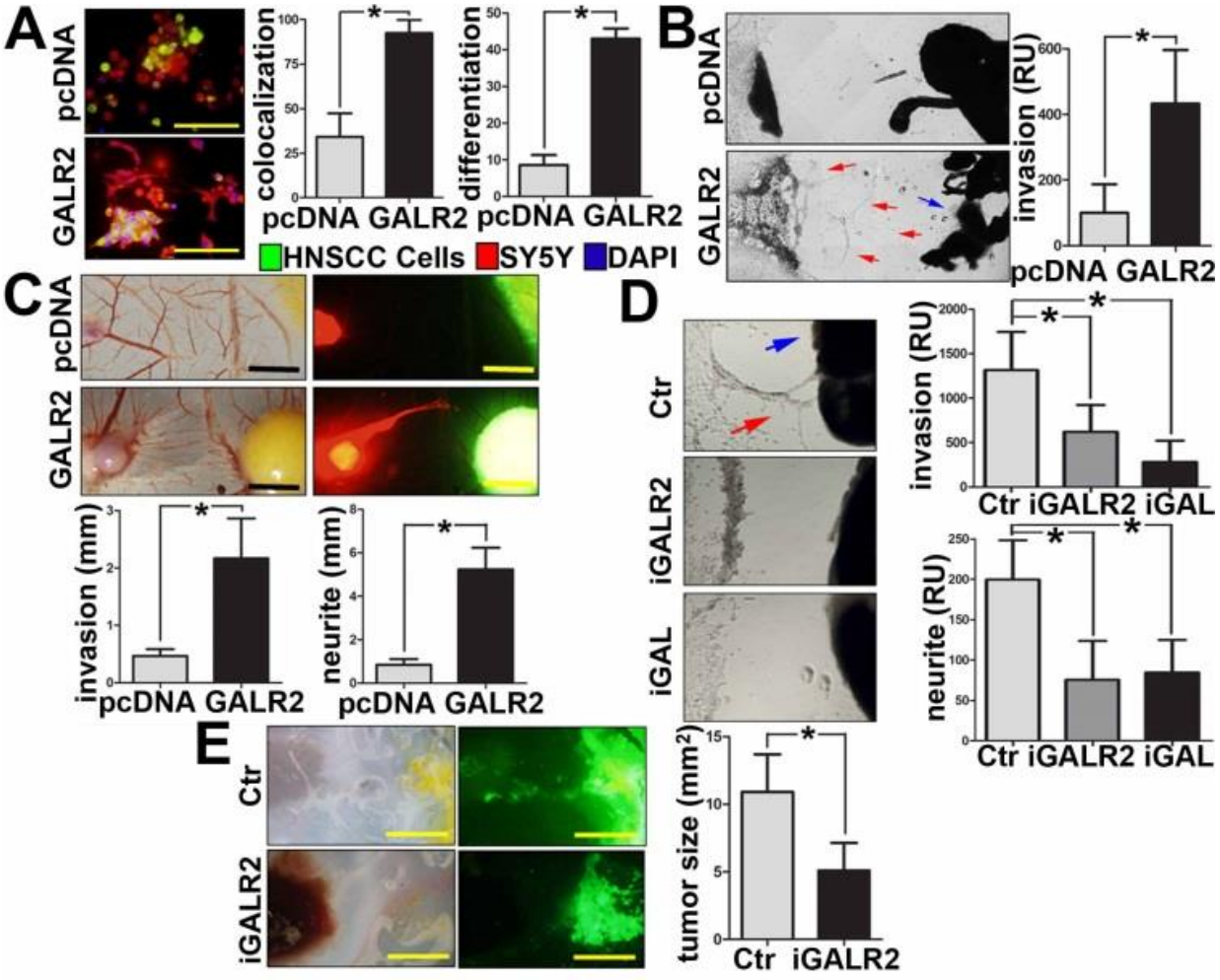

Figure III.5: GALR2 promotes PNI (UM-SCC-1). A. UM-SCC-1 cells (green) overexpressing GALR2 co-mingle with SH-SY5Y neuroblastoma cells (red) and induce more neuritogenesis than controls (bar=100µm). **B.** UM-SSC-1-GALR2 cells are more invasive (red arrows) toward DRG than control cells and induce neurite outgrowth (blue arrow). **C.** UM-SCC-1-GALR2 CAM tumors (green) are more invasive and induce DRG outgrowth (red, bar=5mm) compared to control tumors. **D.** UM-SCC-1-GALR2 cell invasion (red arrow) and neurite outgrowth (blue arrow) are attenuated with either M871 (GALR2 peptide antagonist, iGR2) or anti-GAL antibody (iGAL). **E.** M871 (designated iGR2) blocks PNI and downregulates tumor size of UM-SCC-1-GALR2 CAM tumors (bar=2mm). Length was quantified in images with ImageJ and expressed in mm or relative units (RU). For CAM experiments, n=6 for each group. In vitro and DRG explant data are representative of 3 independent experiments run with 3 samples. *$P < 0.05$ (1-sided *t*-test); data represented by mean + SD.

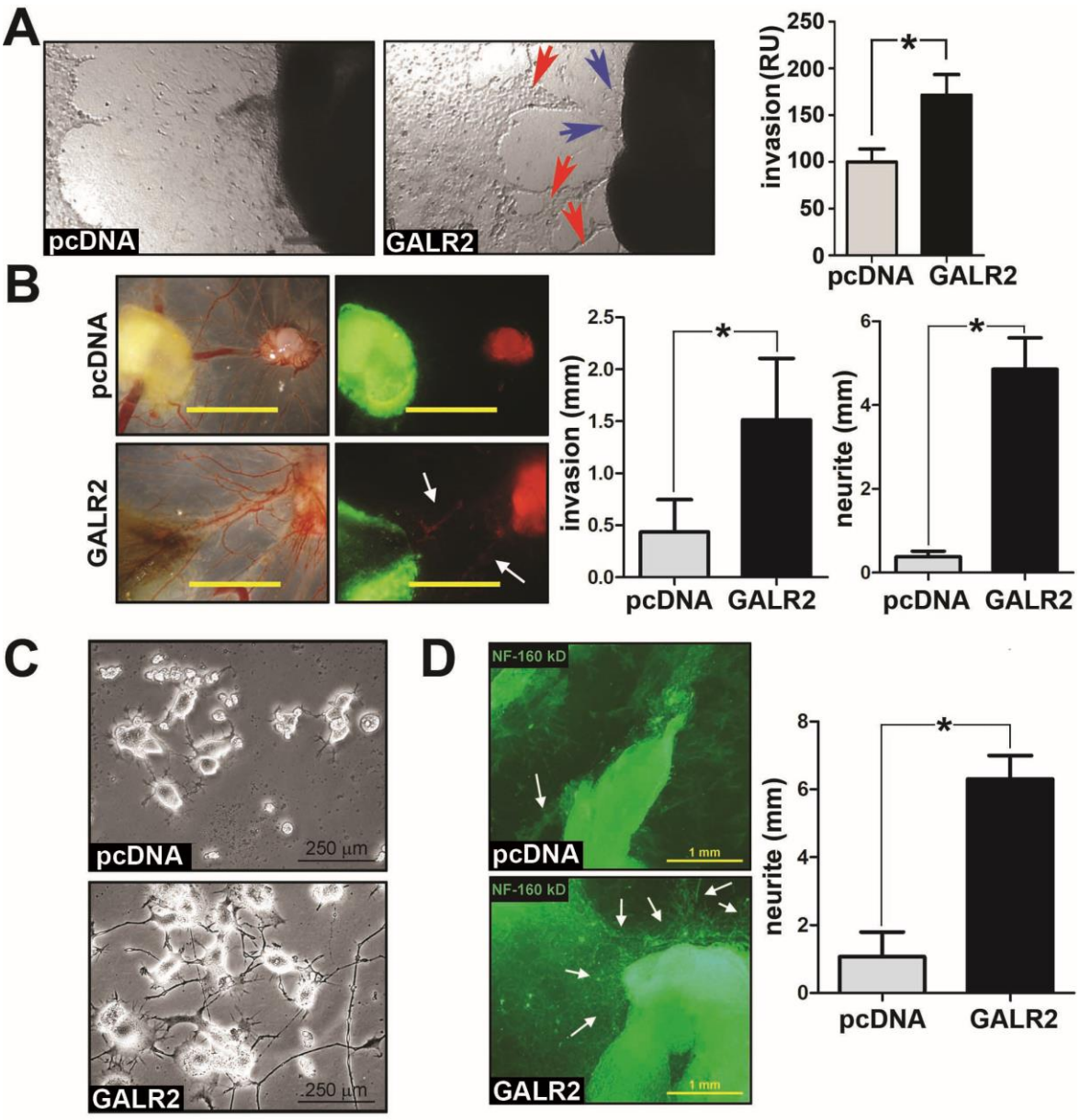

Figure III.6: GALR2 promotes PNI (OSCC3). A. OSCC3-GALR2 cells are more invasive toward nerves than control cells (red arrows) and induce neurite outgrowth (blue arrows). **B.** On the CAM, OSCC3-GALR2 tumors (green) are more invasive and induce outgrowth of nerves (red, identified with arrows, bar=5mm). **C.** SH-SY5Y neuroblastoma cells treated with CM from OSCC3-GALR2 cells differentiated and produce more neurite outgrowth compared to control cells. **D.** Nerves treated with CM from OSCC3-GALR2 cells generated more neurite outgrowth than nerves treated with CM from control cells. For CAM experiments, n=6 for each group, and in vitro and nerve explant data are representative of 3 independent experiments run with 3 samples. *$P < 0.05$ (1-sided *t*-test); data are represented by the mean + SD.

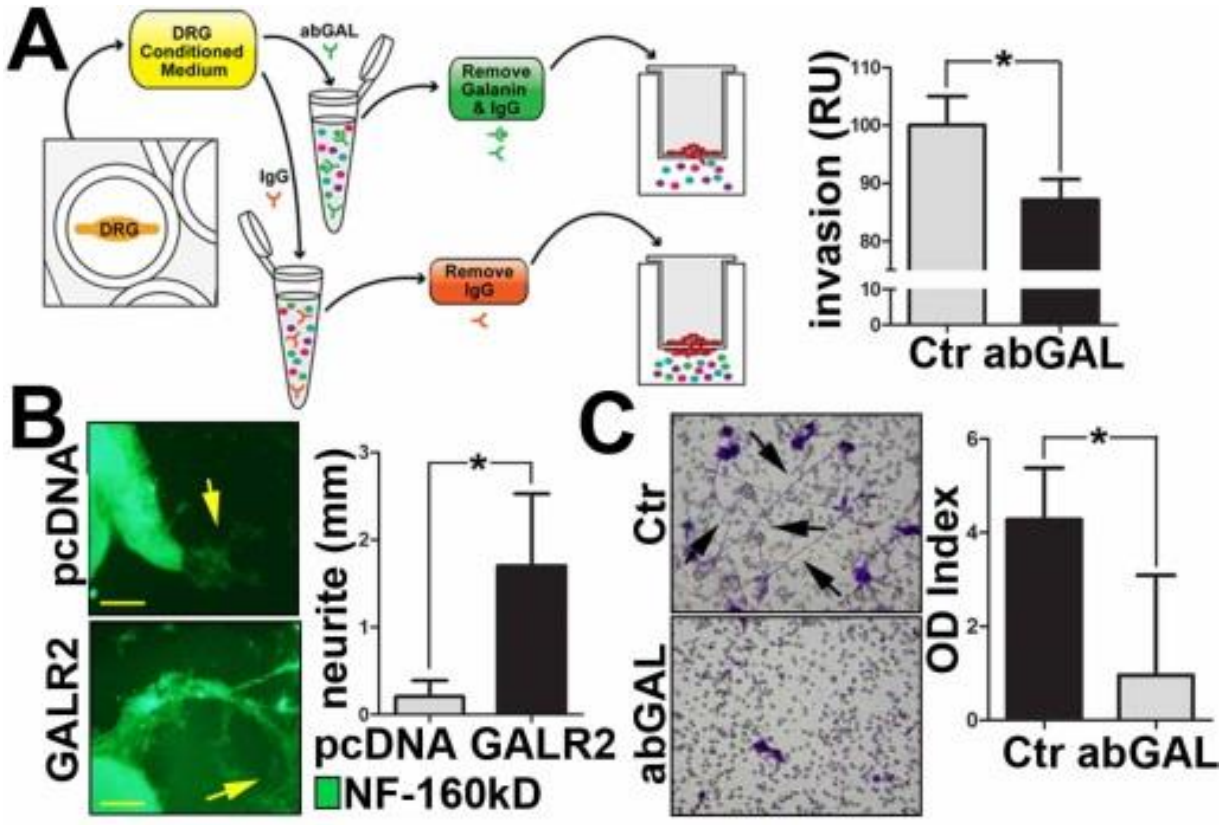

Figure III.7: GAL from both the DRG and tumor promote PNI. A. The strategy to remove GAL from CM is shown. When CM from DRG is depleted of GAL, it is a less effective chemoattractant for UM-SCC-1-GALR2 cells, consequently less invasion is observed. **B.** DRG explants treated with CM from UM-SCC-1-GALR2 cells have more neuritogenesis (arrows) than DRG treated with control CM (bar=1mm). **C.** SH-SY5Y neuroblastoma cells extend more neurites (arrows) when treated with CM from UM-SCC-1-GALR2 cells than when GAL was removed using the strategy shown (**A**). For all studies n=3 per group; *$P < 0.05$ (1-sided *t*-test); data represented by mean + SD.

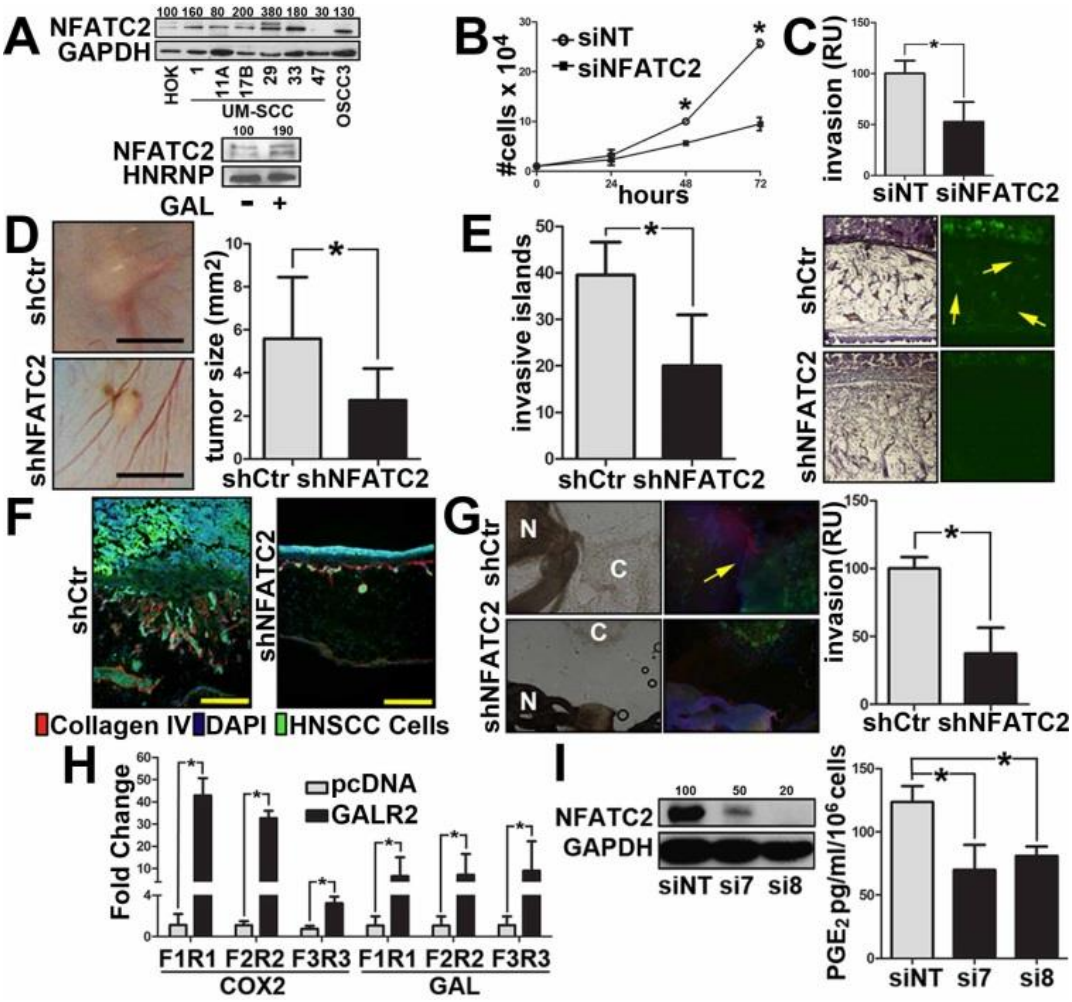

Figure III.8: GALR2 promotes tumor progression and PNI via NFATC2 (UM-SCC-1). (**A,** upper blot) Multiple HNSCC cell lines express more NFATC2 than normal human oral keratinocytes (HOK); (**A,** lower blot) GAL treatment (5nM) induces nuclear translocation of NFATC2 in UM-SCC-1-GALR2 cells. UM-SCC-1-GALR2 cells show reduced proliferation (**B**) and invasion (**C**) when NFATC2 is downregulated with small interfering RNA (siRNA, nontargeting siRNA designated siNT was used for control). UM-SCC-1-GALR2 CAM tumors with constitutive knockdown of NFATC2 using small hairpin RNA (shRNA, control scrambled shRNA is designated "shCtrl" and shRNA targeting NFATC2 is designated "shNFATC2") are (**D**) smaller (bar=5mm), (**E**) less invasive (arrows show invasive islands), and (**F**) less disruptive of the basement membrane (labeled with collagen IV, bar=200µm). (**G**) UM-SCC-1-GALR2 cells with NFATC2 knockdown exhibit less PNI than controls (cancer cells labeled "C" fluoresce green and nerves labeled "N" fluoresce red, arrow identifies neurite growth). **H**. NFATC2 binds more to promoter regions of PTGS2 (COX2) and GAL (GAL) in UM-SCC-1-GALR2 cells compared to control cells. **I**. When NFATC2 is downregulated with siRNA in UM-SCC-1-GALR2 cells, PGE_2 secretion decreases. For CAM experiments, n=6 for both; in vitro and DRG explant data are representative of 3 independent experiments run with 3 samples. *$P < 0.05$ (1-sided *t*-test); data represented by mean + SD.

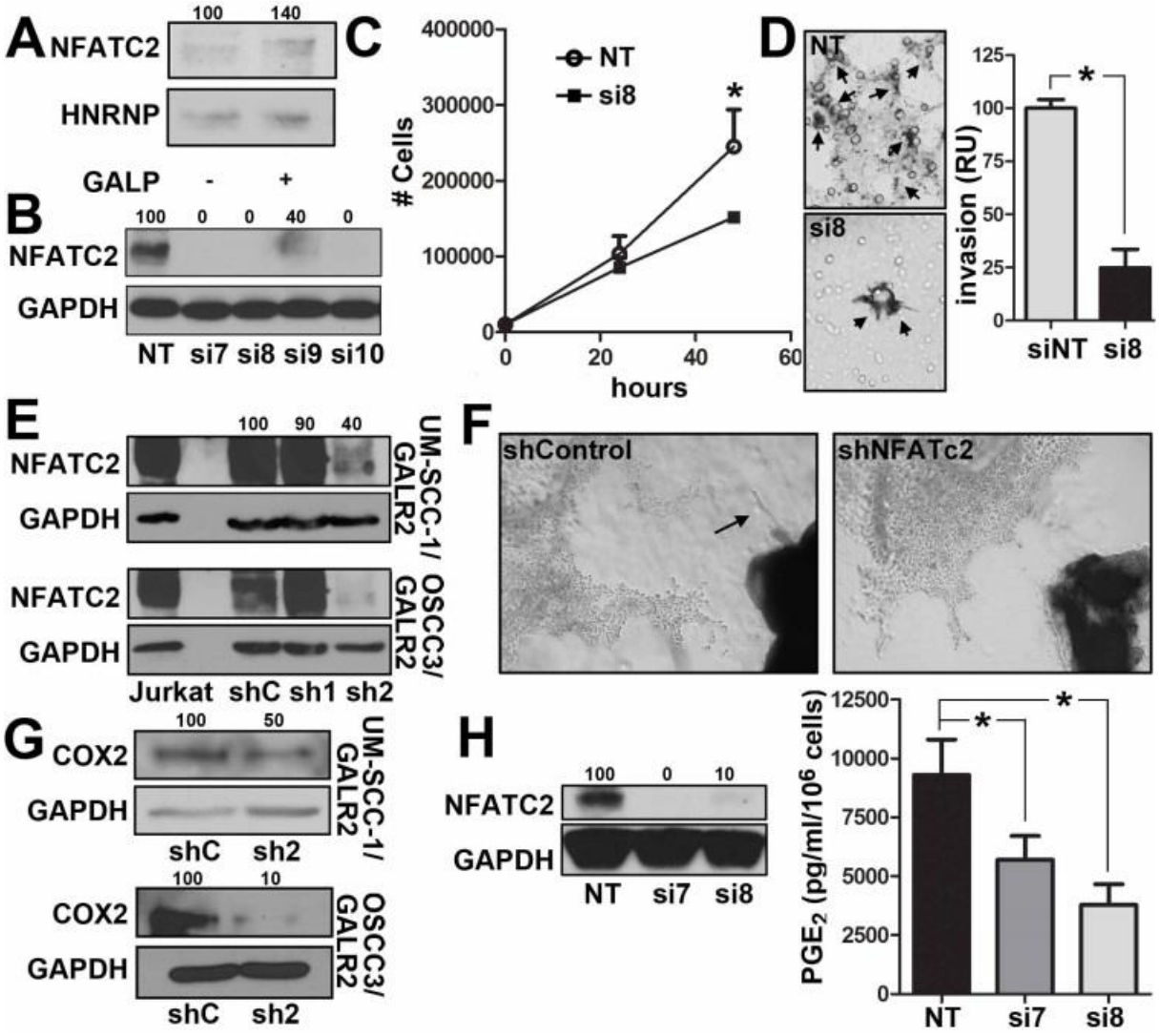

Figure III.9: GALR2 promotes tumor progression and PNI via NFATC2 (OSCC3). A. GAL treatment induces nuclear translocation of NFATC2 in OSCC3-GALR2 cells. **B.** Four individual siRNAs were tested for efficiency in downregulating NFATC2; si7 and si8 were selected for functional studies. OSCC3-GALR2 cells exhibit reduced (**C**) proliferation and (**D**) invasion when NFATC2 is downregulated with siRNA. **E.** shRNA were tested to use for constitutive downregulation of NFATC2 in UM-SCC-1-GALR2 and OSCC3-GALR2 cells; sh2 was selected. Jurkat cell lysate is a positive control for NFATC2 expression. **F.** OSCC3-GALR2 cells with NFATC2 knockdown exhibit less PNI in vitro than control cells (arrow identifies neurite outgrowth in control group). **G.** COX2 expression is decreased in UM-SCC-1-GALR2 and OSCC3-GALR2 cells with constitutive knockdown of NFATC2. **H.** When NFATC2 is downregulated with siRNA in OSCC3-GALR2 cells, PGE_2 secretion decreases. For CAM experiments, n=6 for both groups. In vitro and DRG explant data are representative of 3 independent experiments run with 3 samples. *$P < 0.05$ (1-sided *t*-test); data are represented by the mean + SD.

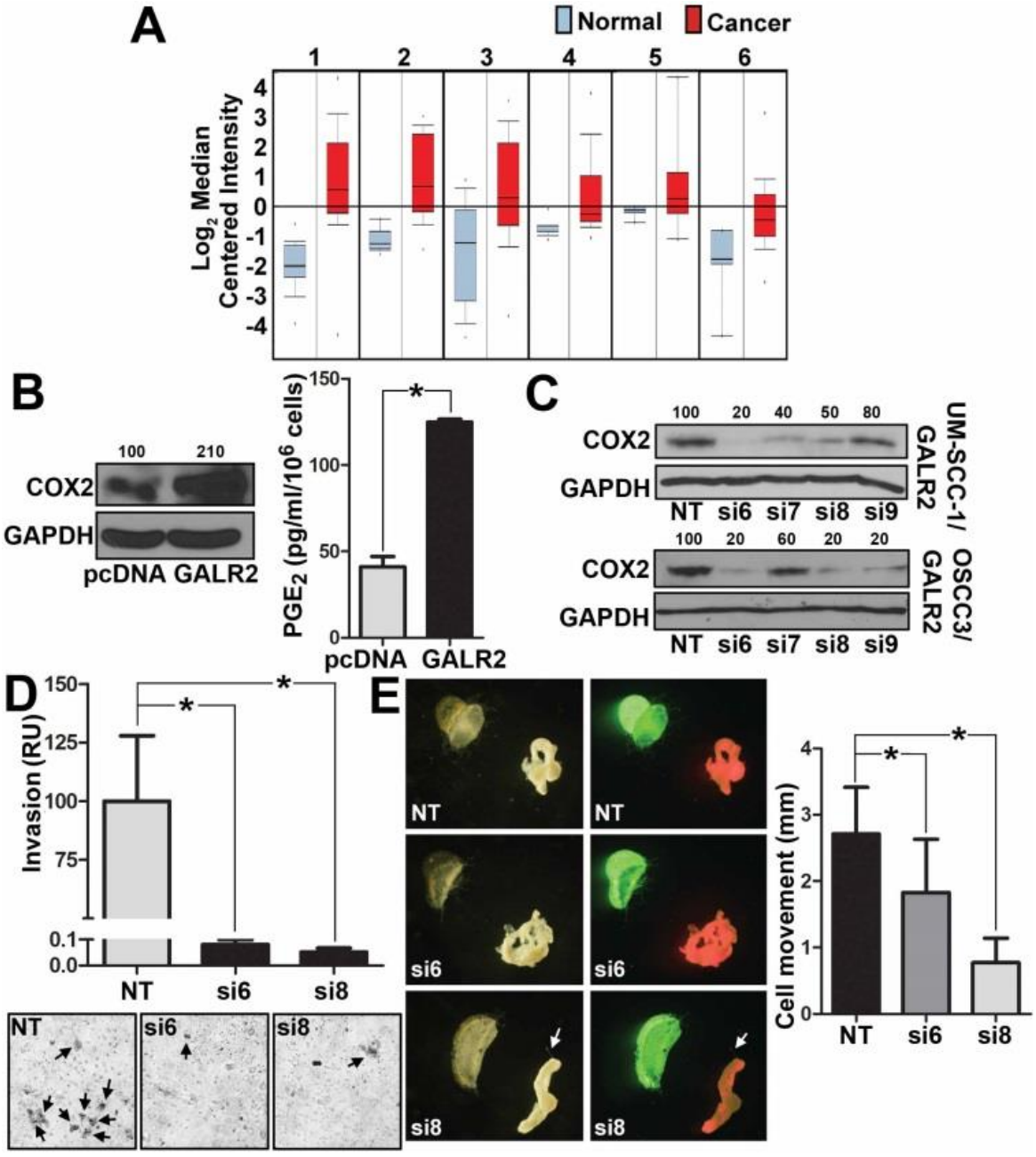

Figure III.10: COX2 is highly expressed in HNSCC and mediates invasion via GALR2. A. A meta-analysis of HNSCC studies on Oncomine™ shows that COX2 is highly expressed in cancer versus normal samples ($P < 0.01$). **B.** OSCC3-GALR2 cells express more COX2 and secrete more PGE_2 than control cells (left, immunoblot of whole cell lysates; right, ELISA of CM). **C.** Four individual siRNA were tested in UM-SCC-1-GALR2 and OSCC3-GALR2 cells; si6 and si8 were selected. Downregulation of COX2 in OSCC3-GALR2 cells using siRNA decreases invasion on a Boyden chamber assay (**D**) and also decreases invasion of cells toward nerves in co-culture (**E**). In vitro and nerve explant data are representative of 3 independent experiments run with triplicate samples. *$P <$ 0.05 (1-sided *t*-test); data are represented by the mean + SD.

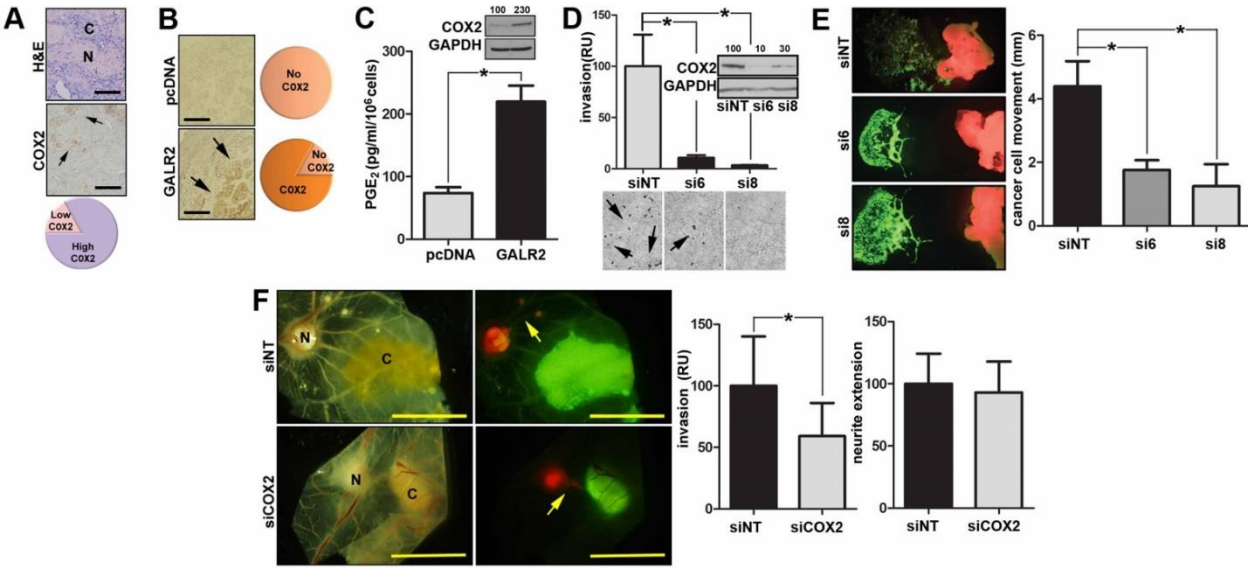

Figure III.11: COX2 regulates HNSCC progression but not neural-tumor crosstalk. **A.** Most human tumors with PNI express high COX2 adjacent to nerves (arrows, bar=100µm). **B.** Most murine tumors with high GALR2 express COX2 at the invasive front (arrows, bar=100µm), but COX2 is not highly expressed by control tumors. **C.** UM-SCC-1-GALR2 cells express more COX2 (immunoblot) and secrete more PGE_2 (ELISA) than controls. **D.** siRNA-mediated downregulation of COX2 in UM-SCC-1-GALR2 cells decreases invasion (arrows label invasive cells, immunoblot verifies knockdown). **E.** Downregulation of COX2 decreases invasion of UM-SCC-1-GALR2 cells toward DRG in co-culture. **F.** siRNA-mediated COX2 downregulation in UM-SCC-1-GALR2 tumors on a CAM blocks cancer cell invasion (left graph), but does not affect the extension of DRG toward tumors (right graph, bar=100µm). For CAM experiments, n=6 for both, and in vitro and DRG explant data are representative of 3 independent experiments run with 3 samples. *$P < 0.05$ (1-sided *t*-test); data represented by mean + SD.

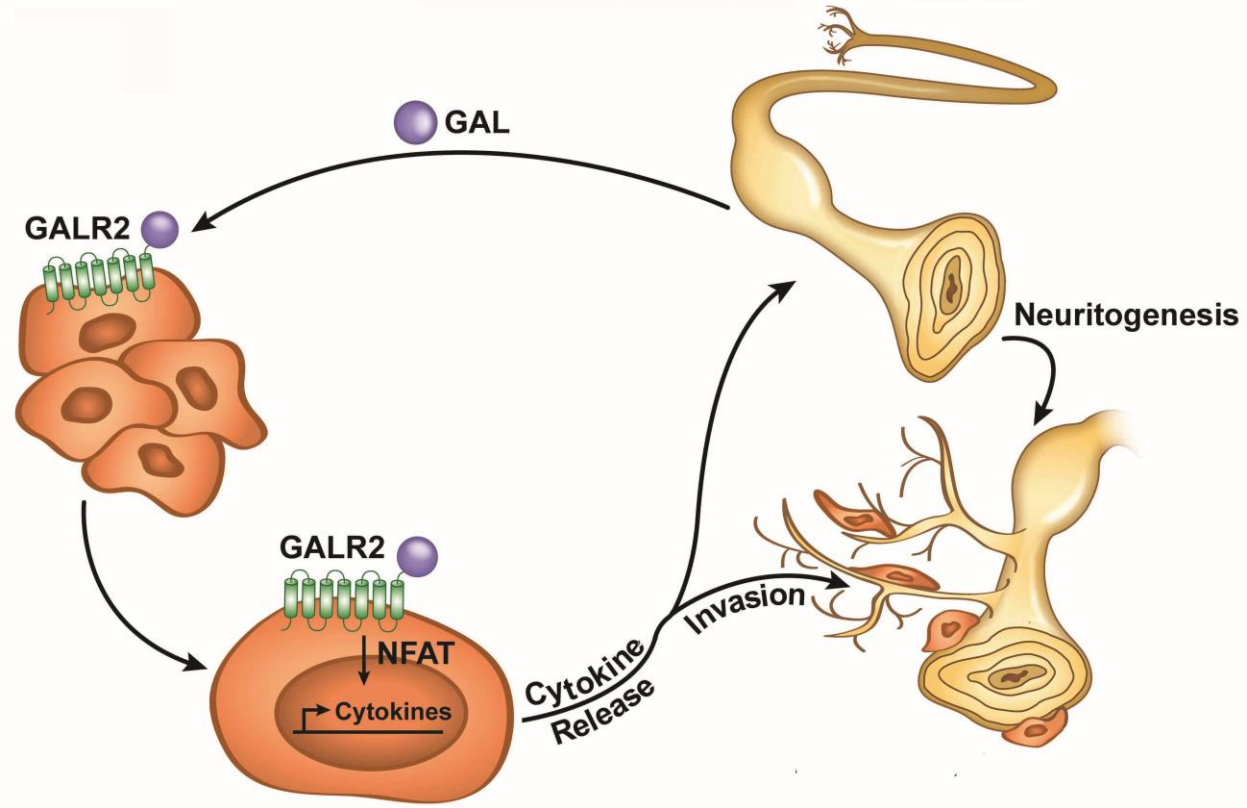

Figure III.12: A model of neural-tumor crosstalk mediated by the neuropeptide GAL. Neurons release GAL following injury or inflammation and activate tumor-expressed GALR2. GALR2 activation leads to NFATC2-mediated transcription and secretion of COX2/PGE_2, thereby promoting PNI. Targeting GALR2 or GAL blocks PNI by disrupting neural-tumor crosstalk.

***NFATC2* (NFATC2)**	si7 – GCUUAGAAACGCCGACAUU si8 – AGACGGAGCCCACGGAUGA si9 – GCAGAAUCGUCUCUUUACA si10 – GAACCUCGCCAAUAAUGUC sh1 – 5’ TATCTTCTCATAGCTGGTG 3’ sh2 – 5’ TTTGCTGTCCATCTGTGGT 3’
***PTGS2* (COX2)**	si6 – GGACUUAUGGGUAAUGUUA si7 – GAUAAUUGAUGGAGAGAUG si8 – GUGAAACUCUGGCUAGACA si9 – CGAAAUGCAAUUAUGAGUU

Table III.1: siRNA and shRNA target sequences.

***PTGS* (COX2)**	F1, 5’-GAATTTACCTTTCCCGCCTCTC-3’ R1, 5’-AAGCCCGGTGGGGGCAGGGTTT-3’ F2, 5’-GAAGCCAAGTGTCCTTCTGC-3’ R2, 5’-GGAGAGGGAGGGATCAGAC-3’ F3, 5’-AAGGCATACGTTTTGGACATTTAGC-’3 R3, 5’-CTTTATATTGGTGACCCGTGGAGCT-3’
***GAL* (GAL)**	F1, 5'-TTCGGGATTAGGGTCTCTCC-3' R1, 5'-GGTCCTCTGGGCCATCATAG-3' F2, 5'-CTATGATGGCCCAGAGGACC-3' R2, 5'-GGCGCCAGTAGTACCTTGAG-3' F3, 5'-CTATGATGGCCCAGAGGACC-3' R3, 5'-ATATGCGGCGCACCCGGGAGCC-3'

Table III.2: Chromatin immunoprecipitation (ChIP) primer pair sequences.

Database Reference	Accession Number
(150)	GenBank Series GSE2379
(151)	GenBank Series GSE13601
(152)	Data referenced in manuscript
(153)	GenBank Series GSE2280
(154)	GenBank Series GSE25099, GSE25103
(155)	GenBank Series GSE20939
(156)	GenBank Series GSE6791
(157)	ArrayExpress E-TABM-302
(158)	ArrayExpress A-UMCU-3
(159)	GenBank Series GSE12452
(160)	GenBank Series GSE3292
(161)	Data referenced in manuscript
The Cancer Genome Atlas (National Cancer Institute)	Microarray data available through TCGA Data Portal: https://tcga-data.nci.nih.gov/tcga/
(162)	GenBank Series GSE3524
(163)	GenBank Series GSE9844

Table III.3: Accession numbers for microarray databases used for meta-analyses.

Full Name (Gene)	N (Significant/Non-Significant Studies)	t-test (df)	*P*
Galanin (GAL)	17 (6/11)	2.536 (16)	0.011
Brain-derived neurotrophic factor (BDNF)	17 (5/12)	2.143 (16)	0.024
Neural growth factor (NGF)	17 (3/14)	1.327 (16)	0.1015
Glial cell line-derived neurotrophic factor (GDNF)	13 (2/11)	0.997 (12)	0.169
Neurotrophin-3 (NTF3)	17 (2/15)	0.84 (16)	0.2065
Neuropeptide Y (NPY)	17 (2/15)	0.84 (16)	0.2065
Peptide YY (PYY)	17 (1/16)	0.15 (16)	0.4415
Vasoactive Intestinal Peptide (VIP)	17 (1/16)	0.15 (16)	0.4415

Table III.4: Meta-analyses of neuronal proteins. Meta-analyses were completed to compare expression of 10 neuropeptides and neurotrophins for normal versus HNSCC samples using the Oncomine™ database. GAL and BDNF were both significantly overexpressed in HNSCC. Tachykinin-3 (TAC3), Neurotrophin-4 (NTF4) and Calcitonin-related polypeptide (CALCB) did not significantly differ in expression in any studies.

Sex	
Male	8
Female	4
Age	
<50 years	1
50 years – 70 years	8
>70 years	3
Location(s)	
Tongue	7
Lateral	5
Ventral	2
Dorsal	1
Inferior	1
Floor of the mouth	3
Buccal mucosa	2
Palate	1
Diagnoses	
Well differentiated	10
Moderately differentiated	1
Poorly differentiated	1

Table III.5: Clinical data. The clinical data associated with human biopsy specimens with PNI is provided.

CHAPTER IV

The Impact of the Nerve on Metastasis

INTRODUCTION

Metastasis remains a major problem in cancer treatment and directly contributes to 90% of cancer-related deaths (164). Tumors discovered at an early stage can often be treated successfully with surgery or irradiation, but after metastasis, treatments are far less successful (165). Tumor cells that metastasize not only re-seed at distant sites, but can metastasize from the re-seeded tumors to a recurrent tumor at the original site, or to additional tertiary sites (166). Therefore, development of novel anti-metastasis treatments should be a priority for cancer biologists as these treatments would likely improve the survival of patients.

Epithelial-mesenchymal transition (EMT) contributes to early metastasis of tumor cells. Tumor cells that leave the primary tumor must resist anoikis, or apoptosis resulting from the loss of cell-cell contact (166). Following this step, also known as detachment, metastasizing cells must enter blood vessels (intravasation), survive in circulation, arrest in target organ tissue, leave the circulation (extravasation), and then seed at target tissue to survive and proliferate (164). After invading, cancer cells transition back to an

epithelial morphology (mesenchymal-epithelial transition or MET) to proliferate and generate metastasized tumors.

Metastasizing cells face several survival challenges and must cross multiple tissue barriers and evade the host immune response (167). Once metastatic cells reach target organs, they must regain a blood supply and adapt to a new microenvironment (166). Due to the intense survival challenges faced by metastasizing cells, it is believed that only a few cells that enter the circulation will actually seed distant metastases (165).

Over a century ago it was realized that tumor cells do not randomly distribute to distant sites throughout the body, but instead favor certain metastatic sites such as the liver or lung. Stephan Paget, an English surgeon, observed that the relative blood supply was related to the frequency of metastases to these sites. He published the “seed and soil” hypothesis in 1889, proposing that metastasis can only occur when the seed, or metastatic cell, is compatible to the soil, or target organ of metastasis (168).

This hypothesis follows that in order for the outgrowth of a tumor, the tumor must get compatible growth signals from the microenvironment (166). Also, cooperation between the normal host tissue and tumor cells is essential in order for cancer to survive the perilous survival challenges faced in the process of metastasis (164). There is a growing appreciation in the cancer biology community of host-tumor interactions involved in temporal and spatial regulation of metastasis. Early investigations of host-tumor interactions in the early metastatic niche have identified endothelial cells, platelets and leukocytes as some of the host partners regulating metastasis (164).

PNI has been correlated with metastasis in many clinical studies of head and neck squamous cell carcinoma (HNSCC) (6, 169-171). Although host nerves in the tumor microenvironment may play a role in regulating metastasis, the mechanism of this interaction is unknown. An in vivo model that can capture the dynamic interaction between tumor and nerves with an option of quantifying metastases is necessary to understand the role of nerves in metastasis. In this chapter, we propose a CAM-based model to evaluate nerve-tumor interactions in the context of metastasis. Knowledge of nerve-tumor interactions in the context of metastasis may contribute to development of therapies targeting early metastasis.

METHODS

Cell Culture. HNSCC cell line UM-SCC-1 (from Thomas Carey, University of Michigan) was genotyped to verify the cell line at the University of Michigan DNA Sequencing Core prior to studies. Cells were cultured in Dulbecco's Modified Eagle Medium (DMEM, Gibco®) supplemented with 10% fetal bovine serum (FBS, Gibco®) and 1% PenStrep (Gibco®). Cells were transfected with pcDNA™3.1-GALR2 (Missouri S&T cDNA Resource Center).

Data Analysis. GraphPad Prism (GraphPad software) was used for statistics. Student's *t*-test was performed with a *P*-value of <0.05 determined to be statistically significant.

CAM Model. Fertilized Lohmann White Leghorn eggs were obtained from the Michigan State University Department of Animal Sciences Poultry Farm. The eggs were incubated and randomly distributed into treatment groups of 6-8 eggs, and tumor cells were seeded as described (66). Chick embryos that did not develop or eggs that became contaminated during the experiment were excluded from analysis.

CAM Nerve-Tumor Metastasis Assay. DRG were dissected from rats within 1 hour of euthanasia and labeled using CellTracker Red CMTPX (Invitrogen^{TM}). DRGs were seeded on the CAM with fluorescently-labeled HNSCC cells dyed with a lipophilic tracer, DiO (a dialkylcarbocyanine derivative). The CAM was harvested after 3-6 days. A 1 cm^2 portion of the upper CAM was collected from the window used to seed the cells. The shell was cut in half horizontally and a 1 cm^2 portion of the lower CAM was collected from the portion of the CAM directly below the tumor, from an area containing a density of vasculature. The middle portion of the liver was also collected for analysis. Tumor area was imaged using a Leica Stereo microscope and quantified using ImageJ. Additionally, lower CAM tissue was imaged using a Leica Stereo microscope to observe metastatic tumor nodules, and lower CAM and liver tissues were digested and human DNA quantified using qPCR to estimate the number of metastatic cells at each site.

RESULTS

Overview of the CAM Nerve-Tumor Metastasis Model

Figure IV.1 shows a flowchart of the CAM nerve-tumor metastasis model. Briefly, a fertilized chicken egg is opened, and a rat dorsal root ganglion (DRG) is placed on the upper CAM. Subsequently, human HNSCC cells are seeded on the CAM, and the system is incubated for 2-6 days, depending on interest in early or late metastatic events. After incubation, the upper CAM is harvested for imaging and histological analysis. The lower CAM and liver of the developing chick are also collected for qualitative and quantitative analysis of metastases. The lower CAM can be imaged to view metastatic tumors, and both the tissue from the lower CAM and liver are digested and human DNA is quantified.

Nerves Contribute to Increased Tumor Size

We performed a time course experiment to investigate the impact of the nerve on tumor growth. Using the approach outlined in **Figure IV.1**, we seeded tumor cells alone or co-grafted a nerve and tumor on a CAM, and collected the upper CAM from the eggs at days 13, 14 and 15 of development. Stereo microscopy images of the tumors are shown in **Figure IV.2A**. The area of the tumors was quantified for each day of the timecourse and compared. Although the tumors with or without nerves did not differ in size at the initiation of the timecourse, by day 15 the tumors with nerves were significantly larger than tumors without nerves (**Figure IV.2B**).

Nerves Contribute to Increased Tumor Metastases

After determining that the nerve enhances tumor size, we investigated the impact of the nerve on metastasis of the tumors. If a nerve enhances metastasis, it may do so by enhancing tumor cell proliferation or survival. Therefore, we evaluated metastasis at day 13, a timepoint before there was a difference in tumor size between tumors with and without nerve. The lower CAM was imaged using a Stereo microscope, and metastatic tumor nodules were observed embedded in lacey vascular structure in tumors seeded with nerve. However, tumors seeded without nerve did not have obvious metastases (**Figure IV.3A**). Additionally, the lower CAM tissues were digested and human DNA quantified. There were about 2.5 times as many metastatic tumor cells present in lower CAM tissue from tumors seeded with nerves compared to tumors without nerves (**Figure IV.3B**). We also attempted to quantify DNA in tissues from livers of the chick embryos but we did not see a difference in metastatic cells between the 2 groups. This is likely in part because liver metastases would be a later metastatic event in this system, which would require additional days of incubation, and also because at such an early timepoint the livers of the chicks are underdeveloped and may not support metastases.

DISCUSSION

Using the CAM nerve-tumor metastasis system, we were able to confirm that the interaction of nerves with tumor contributed to the growth and metastatic potential of HNSCC tumors. This system allows us to both quantitatively and qualitatively observe interactions of nerves with tumors and the resulting metastatic tumors to the lower CAM

of the chick eggs. Several advantages, as well some limitations of the model are listed in **Table IV.1**.

In vivo model systems of metastases generally fall into 2 groups: xenograft transplantable models, which like our model, contain tissues from different species, and syngeneic models, which include tissues from the same species or carcinogen-induced or spontaneous tumors (166). Our system is a xenograft system since it contains tissues from human, rat and chicken species. Syngeneic models are useful since they can be adapted to an immunocompetent animal, however due to inbreeding, tumors lack the genetic complexity usually observed in human tumors. In contrast, xenograft tumors can be readily adapted to include human cells, but must use immunodeficient animals which limits the ability to observe the role of the immune system in tumor progression (166).

Using either a xenograft or syngeneic transplantable model approach, the next choice when developing a model is to use an experimental metastasis system (where tumors are injected directly into the circulatory system, such as in a lateral tail vein injection), or a spontaneous metastasis system. Experimental metastasis models are rapid, and tight control over the entry point of cells into the circulation has led to some valuable observations of the metastatic process (172). However, with experimental metastasis models, the initial steps of invasion are bypassed and therefore the location of the resulting metastatic tumors may depend mostly on the blood circulation from the site of the injection. For example, metastases from a lateral tail vein injection develop in the lung, whereas metastases from a portal vein injection develop in the liver. Ultimately however, artificial injection of tumor cells does not replicate true metastasis; tumors may be inadvertently seeded into the circulation system, or alternatively the mechanical

disruption of host tissue may actually suppress metastasis (173). Spontaneous metastasis models may be harder to control and more time consuming, however the initial steps of invasion are preserved, which can lead to different mechanisms of metastases produced through experimental and spontaneous systems, such as differences in expression of matrix metalloproteinases, which are essential for invasion (174).

The CAM tumor-nerve metastasis model described depends on spontaneous metastasis, and therefore the early invasive events are preserved. Spontaneous metastasis models may involve orthotopic seeding of tumor cells (for example injection of HNSCC tumor cells into the oral mucosa, a site at which the primary tumor occurs), or heterotopic seeding, or seeding of tumor cells at a site different from the origin of the tumor. For example, subcutaneous injection of HNSCC cells onto the backs of mice is heterotopic seeding. The seed-soil hypothesis correctly predicts that tumors are more suitably supported at the site of origin (i.e. a site containing the correct soil to support a particular type of tumor), and therefore more metastases are generally seen from tumors seeded at orthotopic sites than heterotrophic sites (166).

The CAM system does not have oral mucosa, and therefore orthotopic seeding of HNSCC tumors is not possible. However, we carefully selected the CAM model for our metastasis system because of the distinct similarities between the CAM and oral mucosa, including a basement membrane and rich blood supply seen in both types of tissue. We have observed that HNSCC cells readily grow and metastasize in the CAM system, thereby suggesting that the CAM mimics several important characteristics of oral mucosa. Tumor size and angiogenesis are readily quantified within the first 2 days after the tumor cells are seeded. Invasion is observed by 2 days post-seeding, and metastasis is

observed within 3-10 days. The process of tumor growth, invasion and metastasis is similar to the sequence of clinical progression of HNSCC, and replicates the progression from early non-invasive pre-cancerous lesions to invasive lesions that breach the basement membrane. An important difference between the CAM and oral mucosa is that the CAM does not have a rich supply of nerves. This is a great benefit to our CAM-nerve model since the impact of neural tissue on tumor progression can be evaluated by addition of DRG. Due to the simplicity of the CAM structure, it may be possible to adapt this model to study the importance of other stromal elements in host-tumor interactions regulating metastasis.

While the initial steps of metastasis including intravasation and arrest may only take a few minutes, the later steps may take hours or days to complete (164). Due to the short timeframe of early metastatic steps, these steps have been historically overlooked as potential therapeutic targets, and the focus of therapy has been on controlling the bulk of the tumor. EMT cells and stem cells likely evade tumor cytolytic therapies, and therefore therapies that target invasion and metastasis are essential to improve patient outcomes (164). Anti-metastatic therapies will be useful to prevent metastases for patients presenting with tumors that have a high likelihood of metastasis, and to prevent re-seeding of tumors at primary sites (recurrence) from metastases at tertiary sites (175).

In order to develop effective anti-metastatic therapies, we must develop a greater understanding of specific host-tumor interactions contributing to metastasis. Our CAM nerve-tumor model can be adapted to observe interactions of multiple host tissues within tumors. Also, it is possible to use pharmaceuticals in the CAM model system to attempt to disrupt mechanisms of metastasis. In the future, we intend to use this model to further

investigate the mechanism by which tumor-nerve interactions promote metastasis and PNI. Also, we are using the CAM nerve-tumor model to develop a mathematical model of tumor progression (176).

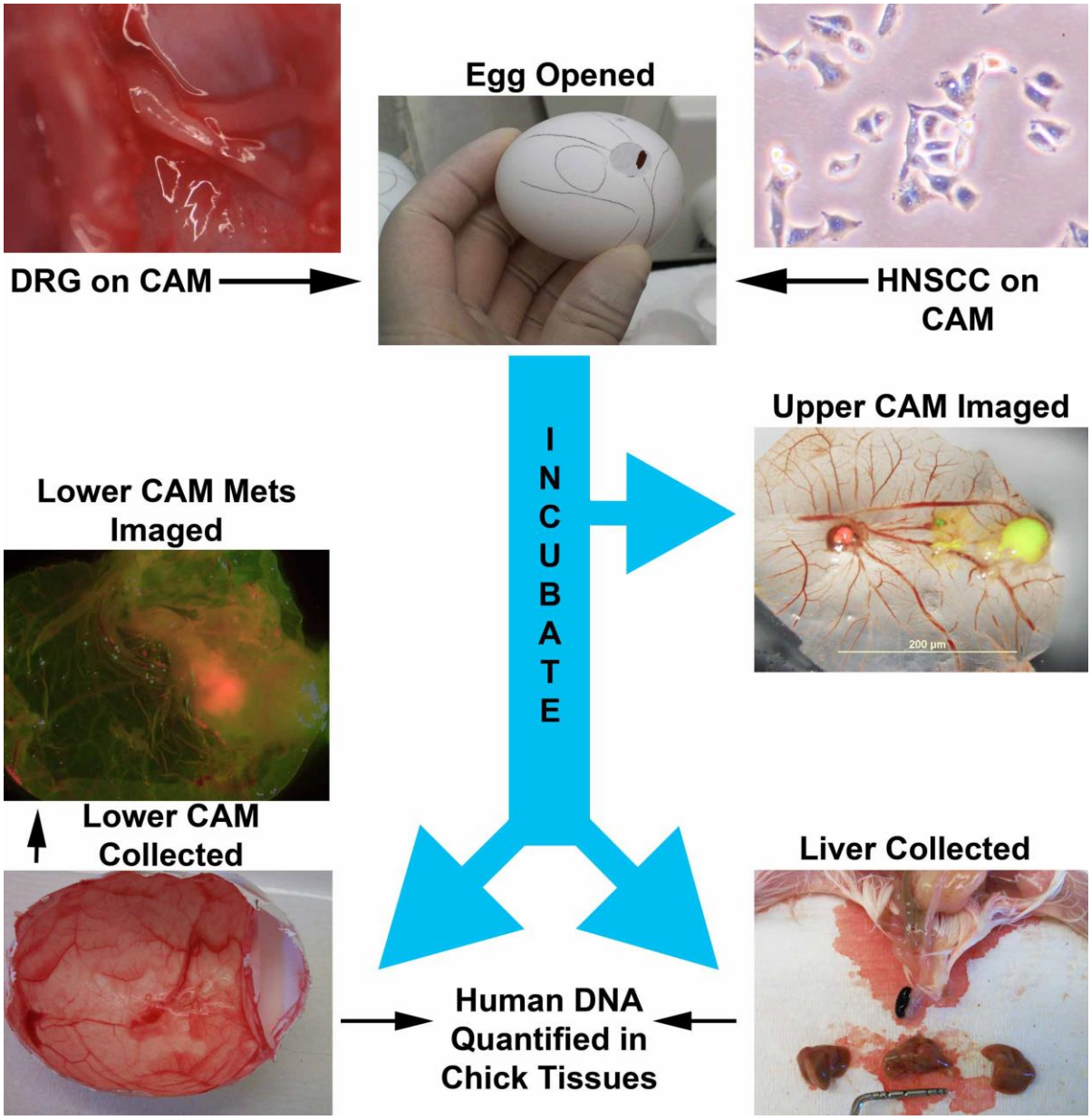

Figure IV.1: A timeline showing the CAM-PNI cancer progression model. A rat DRG and human HNSCC cells are co-grafted onto a fertilized chicken egg, and then incubated. After several days, the upper CAM is collected and imaged, and the lower CAM and liver of the developing chicken embryo are collected for metastasis studies.

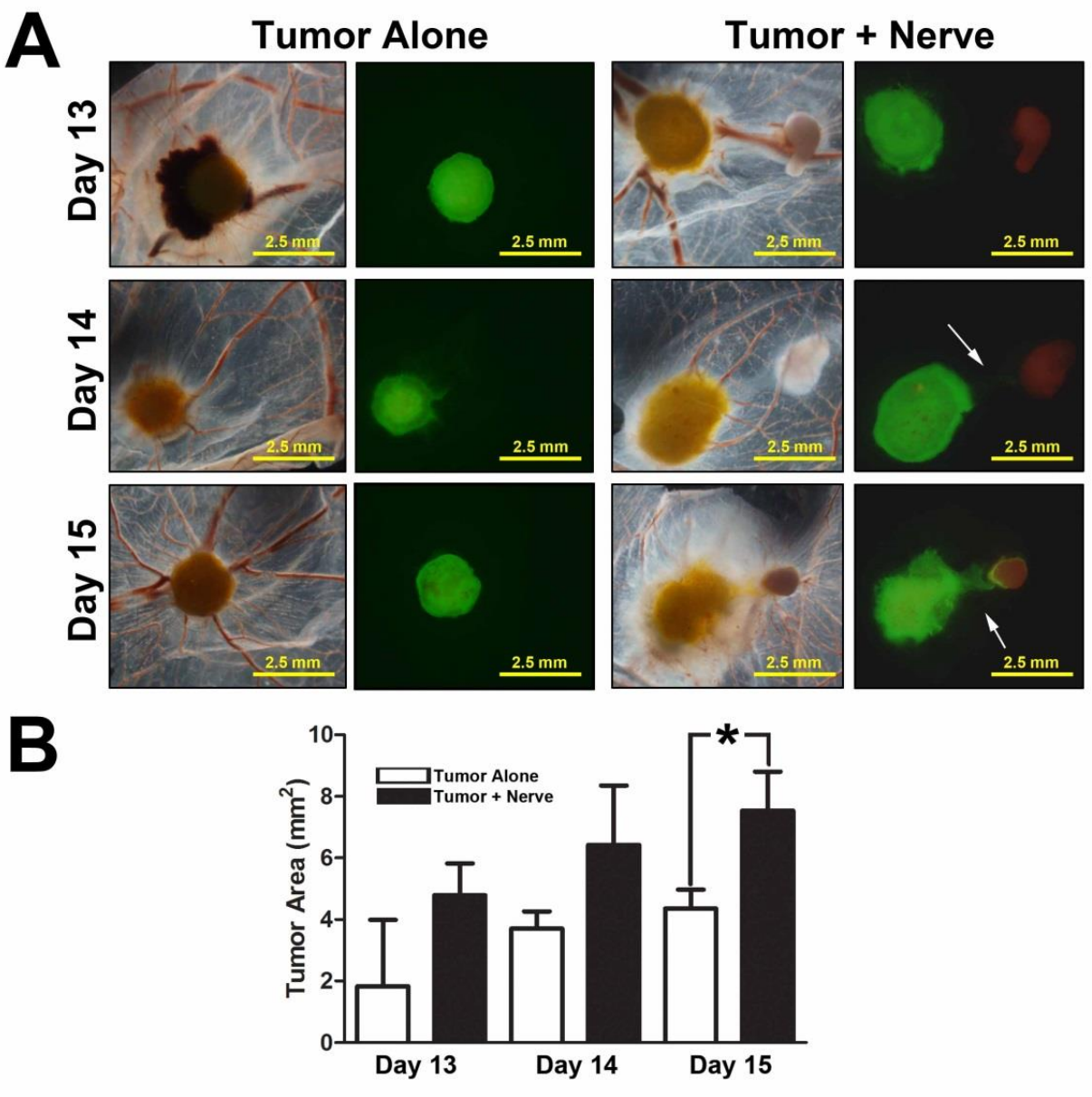

Figure IV.2: Time course of HNSCC tumors grown in absence or presence of a nerve. HNSCC tumors grown in presence of absence of a nerve (A, arrows highlight frank PNI that becomes increasingly apparent through over the 3 timepoints). B. By day 15, tumors grown with nerve are significantly larger than tumors grown in absence of a nerve.

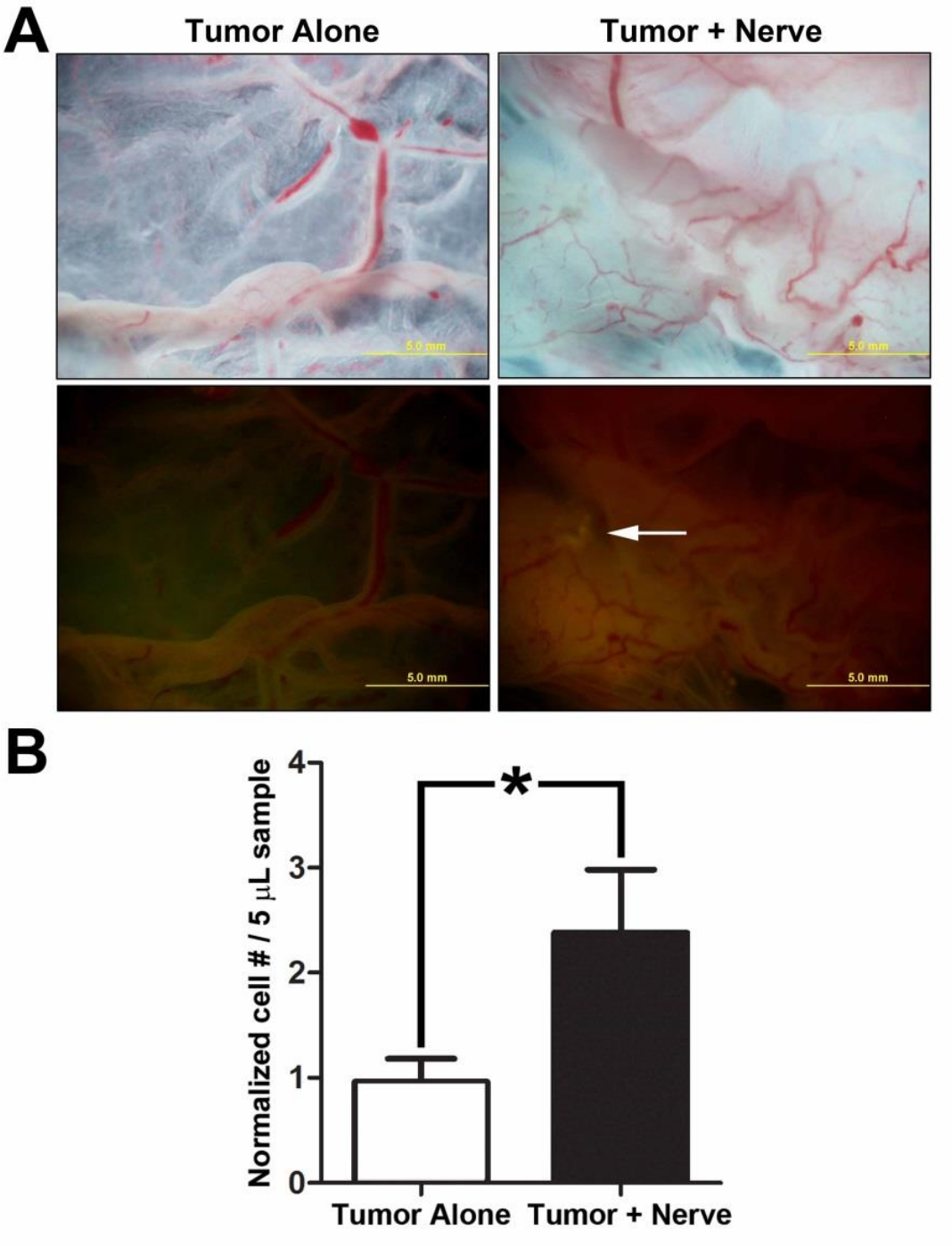

Figure IV.3: Metastases quantified in presence or absence of nerve. **A.** Metastatic nodules noted in lower CAM tissue (arrow) for tumor grown in presence of a nerve. **B.** When human DNA in lower CAM tissue is quantified with qPCR, tumors grown in the presence of a nerve have significantly more metastatic cells in lower CAM tissue than tumors grown in the absence of nerves.

Advantages	Disadvantages
• Short time duration • Can observe metastasis qualitatively and quantitatively • Can use human cells • Can adapt to study interactions with other types of tissues • Can observe metastases across many timepoints, including very early timepoints • Can use pharmacological agents • Inexpensive, can use with large sample number • Can adapt to in vivo microscopy techniques	• Lack of immune interactions • Host tissue differs genetically from human tissue • Limited by development of immune system in developing chicken • Technically demanding

Table IV.1: Advantages and disadvantages of CAM-nerve metastasis model.

CHAPTER V

Conclusion and Future Directions

Conclusion

Invasion is the critical phenotype of tumor progression that distinguishes pre-cancer from HNSCC. Understanding the molecular mediators of invasion will lead to diagnostic and prognostic biomarkers and potential novel treatment targets. EMT and tumor-stromal interactions contributing to invasion are areas of increasing interest in cancer biology. Nerve-tumor interactions contribute to aggressive tumor progression, however the mediators of these interactions are poorly understood due to the lack of appropriate research models. In this thesis, we present in vitro and novel in vivo methods to investigate invasion and specifically, PNI. Using our CAM-based in vivo approach, we demonstrate that nerve-derived GAL initiates crosstalk between nerves and cancer cells by activating GALR2 in tumors. Activated GALR2 then induces NFATC2-mediated secretion of pro-inflammatory mediators and neuropeptides from tumor cells, leading to invasion towards nerves and neuritogenesis. We demonstrate that GALR2-mediated PGE_2 secretion is required for invasion, and GALR2-mediated GAL secretion induces neurite outgrowth towards the tumor, thereby completing a feedback loop. Our findings clearly establish that reciprocal communication between nerves and cancer cells occurs during PNI (**Figure V.1**). Our model is the first in vivo approach that allows reciprocal interaction of tumor and nerve. Additionally, we adapt the CAM-PNI model to study the

impact of the nerve on growth and metastasis of HNSCC. Our studies show that the presence of a nerve in the microenvironment of developing HNSCC promotes aggressive tumor growth and metastasis.

Future Directions

Our data indicate that GAL and GALR2 may be viable anti-PNI treatment targets. We show that blocking GAL by using an antibody, or GALR2 by using the protein antagonist M871, block PNI and tumor neuritogenesis. Furthermore, blocking NFATC2 in GALR2-overexpressing HNSCC cells also inhibits PNI in vitro and in vivo. In the future, we will also investigate the impact of Tacrolimus on HNSCC in vitro and in vivo. Tacrolimus is a macrolide immunosuppressant that prevents the dephosphorylation or activation of NFATC2. Tacrolimus and similar macrolides that inhibit NFAT activation have been used extensively in clinic to treat several diseases including oral lichen planus, vitiligo and atopic dermatitis (177). Additional in vivo validation using these potential anti-PNI therapies is necessary to determine if they may be useful therapeutically in HNSCC.

In addition, it is important to further explore the mechanism of neuron-tumor crosstalk, and especially to understand the soluble mediators of these interactions that are expressed by both the nerve and the tumor. It has been shown that soluble factors secreted by nerves can induce tumor cell migration (136). We hypothesized that neuronally-derived GAL initiates PNI by activating GALR2 on tumor cells. Our data support this hypothesis; if GAL is removed from conditioned medium from nerves, invasion of HNSCC cells is downregulated. Further investigation of how the concentration

gradient of neuropeptides affects the interaction between cancer and nerves, which respond to the same neuropeptides, will facilitate our understanding of PNI. The development of a nerve-specific GAL inducible conditional knockout mouse, or HNSCC cell lines with inducible knockout of GAL will facilitate these studies.

Our work highlights the importance of the G protein-coupled receptor (GPCR), GALR2, in promoting PNI and tumor-neuron crosstalk. GPCRs have been implicated as potential treatment targets of tumor-neuron interactions (137, 178). GPCRs are often overexpressed in a variety of cancer cells and the ligands of GPCRs regulate several phenotypes, including proliferation, migration and survival, of both cancer and nerves (178). Importantly, GPCRs play a role in promoting and maintaining a microenvironment that favors tumor growth (179). GPCRs and their ligands may mediate a neural-tumor synapse that leads to active cross-talk between the 2 tissue types, facilitating growth and survival of nerves and HNSCC, as well as cancer-associated pain. Although mutations of GPCRs have not been specifically linked to PNI, it is possible that future investigations of tumor-driving GPCR mutations will reveal their importance in promoting tumor-neuronal crosstalk and PNI.

Given the grave clinical significance of PNI, it is essential to highlight the importance of nerve-tumor interactions in promoting aggressive tumors to the clinical community. Our hope is that our work highlighting PNI will eventually lead to a prognostic model that will encourage clinicians to adopt more rigorous and standardized methods to identify and treat PNI appropriately. Histopathologic detection of PNI is very challenging due to the complex microanatomy of peripheral nerves, particularly with subtle microscopic presentations (12). Currently used terminology to describe PNI is confusing;

there is a lack of standardization of definitions and quantification schemes to describe PNI, which can lead to delayed recognition of PNI and mistreatment. The terms small nerve or incidental, and large nerve or clinical PNI are used interchangeably but carry different prognostic significances (6). In the absence of staining for neuronal markers, pathologic detection of PNI may be missed at tumor margins and in tangential sections of nerves. Shortfalls in clinical detection, reporting and researching PNI have resulted in a gap of understanding of this deadly pathologic process. Ultimately due to our lack of understanding of the disease, anti-PNI therapeutics have not been developed. When PNI is detected, clinicians often opt for aggressive adjuvant therapies for lesions that may be treated more effectively and conservatively with anti-PNI therapy. Ultimately improved understanding of the molecular biology of PNI, including markers of perineural involvement in genetic profiling of tumors, will assist clinicians and scientists in the effort to develop and adapt personalized medicine strategies to treat patients.

The general future directions of this work are to develop methodology in detecting, reporting and researching PNI. We intend for our work to address specific deficiencies in clinical and basic science research that are holding back progress in this important research area. This will accelerate development of life-saving treatment protocols that effectively manage tumors that exhibit PNI. A diagnosis of PNI has long been informative to clinicians in treatment planning, but the molecular fingerprint and mechanism must be elucidated. Personalized medicine is a promising treatment planning strategy that relies upon molecular profiling to determine the optimal treatment strategy for each patient (**Appendix E**). PNI mechanisms have not been determined previously, and therefore there are no prognostic markers of PNI (6). Since PNI is known to be associated with

aggressive tumors, it is critical to identify and understand molecular mediators of neural-tumor interactions to include them in these molecular profiles.

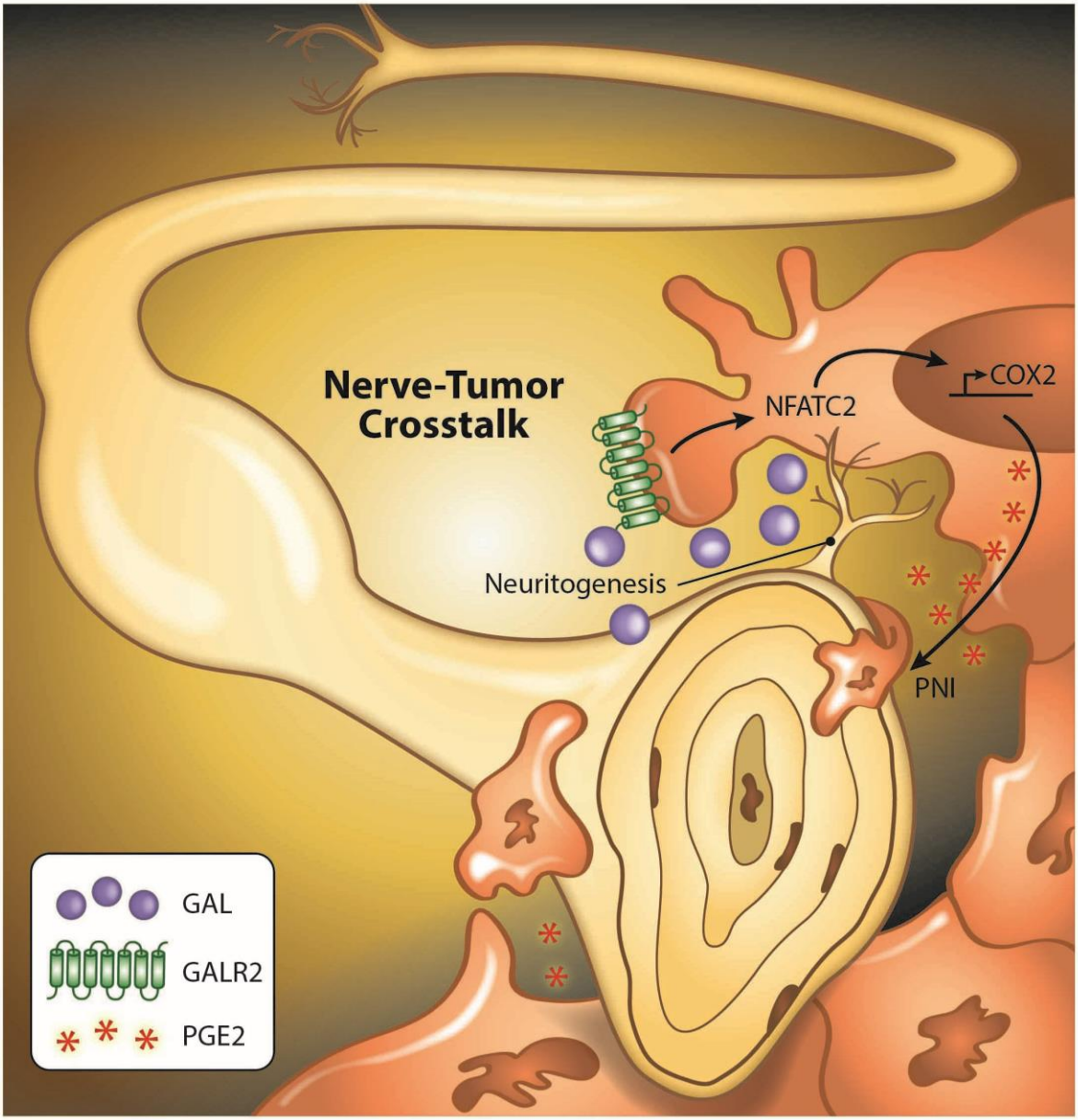

Figure V.1: Summary of proposed mechanism of action.

APPENDICES

APPENDIX A

Biomarkers of Epithelial-Mesenchymal Transition in Squamous Cell Carcinoma

Appendix A is adapted from a published manuscript (79).

Introduction

Understanding the process by which tumor cells destroy the basement membrane of the surface epithelium, invade and metastasize is essential to developing novel treatment of HNSCC. In recent years, there has been increased interest in the role of epithelial-mesenchymal transition (EMT) in facilitating invasion. EMT describes the development of motile cells from non-motile parent epithelial cells (**Figure A.1**). EMT, which occurs in embryonic development, wound healing, and cancer (**Figure A.2**), is classified into 3 subtypes (180). Type 1 occurs in gastrulation and in migration of neural crest cells; some of the migrated cells undergo mesenchymal to epithelial transition (MET) to become epithelial cells in organs produced by the mesoderm and endoderm. This embryological EMT occurs in the orofacial region during palatogenesis. Type 2 occurs in wound healing and can result in fibrosis when there is persistent inflammation. Cytokines generated by tissue injury induce the fibroblast phenotype from epithelial or endothelial cells. Type 3 occurs in subsets of invasive cancer cells by using some of the Type 2 EMT program for migration and aggregation of epithelial cells in wound healing. After invading,

tumor cells can transition back to the epithelial morphology (MET) to proliferate and generate tumors at distant sites.

The purpose of this chapter is to present the growing evidence that EMT has a significant role in invasion and metastasis of HNSCC. Many protein types, including cell-surface proteins, cytoskeletal proteins, extracellular matrix (ECM) components and transcription factors contribute to EMT (**Figure A.3**, **Table A.1**).

CELL-SURFACE PROTEINS

Cell-surface proteins contributing to EMT in HNSCC include cadherins and integrins.

Cadherins

E-cadherin is the main protein of adherens junctions that anchor oral epithelial cells to each other. It is a calcium-dependent cell surface protein that facilitates adhesion between epithelial cells. E-cadherin is characterized by long cytoplasmic and extracellular domains, which create homophilic interactions between adjacent cells to facilitate adhesion. The expression of E-cadherin is decreased during embryonic development, tumor fibrosis and cancer progression (180). In oral epithelial cells, from which HNSCC develops, surface E-cadherin anchors cells to each other and links to the cytoskeleton via β-catenin. Loss of or sequestration of E-cadherin in the nucleus impairs cell-cell adhesion and releases β-catenin, which translocates to the nucleus to induce transcription of EMT genes, such as *TWIST*.

Several studies show reduced E-cadherin in HNSCC, with lowest E-cadherin levels in poorly differentiated tumors (181). E-cadherin expression is similar between primary tumors and metastases, perhaps due to MET in metastatic tumors. The promoter region of the E-cadherin gene (*CDH1*) is hypermethylated in HNSCC, but hypermethylation is not correlated with advanced stage (182), mortality or second primary tumor (183). Meta-analysis of E-cadherin studies in HNSCC showed that abnormal E-cadherin expression is predictive of diminished disease-specific survival (184).

The use of E-cadherin expression to personalize anti-HNSCC therapy has been explored (185, 186). Higher E-cadherin expression is correlated with better sensitivity toward the EGFR-tyrosine kinase inhibitors. The E-cadherin to N-cadherin switch, which occurs during embryonic development and cancer progression, is used to monitor EMT. E-cadherin is expressed in epithelial cells, and N-cadherin is upregulated by TWIST in type 3 EMT in gastric cancer (187). In HNSCC, high expression of N-cadherin correlated with malignant behaviors such as high grade pattern of invasion and poorly differentiated cancer cells (188). Cadherin switching (high expression of N-cadherin and low expression of E-cadherin) was observed in 30 of the 80 cases and correlated with invasion and lymph node metastasis, as well as EMT features. Thus, cadherin switching may be a critical event in the progression of HNSCC through EMT.

Integrins

EMT facilitates relocation of cells from above the basement membrane into the ECM, which involves a change in expression of integrins (180). Integrins are heterodimeric

adhesion receptors composed of α and β subunits. There are 18 α and 8 β subunits that variably combine into 24 different integrins. Integrins bind to ligands, including collagens, laminins, and fibronectin in the ECM. Ligand-bound integrins induce several signaling cascades that control cell polarity, motility, survival, shape, proliferation and differentiation.

Integrins mediate interactions between cells and the surrounding ECM by making transmembrane connections between the cytoskeleton and the ECM. The interaction between the α5 integrin and fibronectin is necessary for metastasis of a melanoma cell line (189). Blocking the α5 subunit in HNSCC, decreases adhesion to collagen IV and fibronectin (190). α5β1 integrin has been associated with cisplatin resistance and enhanced adhesion to fibronectin, which is abolished when the integrin is blocked by a neutralizing antibody (191). β1 integrin increases invasion of HNSCC cells, which decreases significantly when the integrin is blocked (192).

CYTOSKELETAL MARKERS

Cytoskeletal proteins that contribute to EMT in HNSCC include alpha-smooth muscle actin (α-SMA), vimentin and β-catenin.

α-SMA

Cells expressing α-SMA contribute to EMT in embryogenesis and wound healing in normal epithelial cells (180). In squamous cell carcinoma (SCC), the tumor tissue is

surrounded by reactive stroma, made up mostly of cancer associated fibroblasts (CAFs), also known as myofibroblasts because they acquire characteristics of muscle fibers, including expression of α-SMA. Expression of α-SMA is controlled by growth factors and specialized ECM proteins. α-SMA is incorporated into stress fibers of fibroblasts thereby augmenting their contractile ability, which is critical to tissue remodeling. CAFs are known to potentiate the development and progression of epithelial cancers. Fibroblasts can be distinguished based on the stage of tumor development by differences in α-SMA expression, which is expressed more highly in mature fibroblasts than newly transitioning cells. Fibroblasts from HNSCC tumors grow more slowly compared to normal fibroblasts from the oral cavity (193).

HNSCC characterized by extensive genetic copy number alterations, loss of heterozygosity and inactivation of p53 and p16INK4A had higher α-SMA expression, which correlated with poor prognosis in an independent dataset of HNSCC samples when compared with tumors with less genetic instability (193). However, the mechanistic link between α-SMA expression and EMT and HNSCC is unknown.

Vimentin

Vimentin is an intermediate filament that is used as a marker of mesenchymal cells to distinguish them from epithelial cells (180). Vimentin is expressed at sites of cellular elongation and is associated with a migratory phenotype. Increased vimentin expression is frequently used as an EMT marker in cancer.

In HNSCC cell lines, Chen et al. isolated an ALDH1-rich subpopulation of cells and characterized their invasive potential and EMT phenotype (194). Spheroid-derived cells had increased vimentin when compared to monolayer-derived cells from different cell lines. Furthermore, vimentin expression decreased when cells were grown as a monolayer. Vimentin expression is higher in nodal metastatic cells than in the primary HNSCC tumors, and is enhanced by epidermal growth factor and TGF-β (195). Reducing vimentin levels by RNA-interference decreased the proliferation, migration and invasion of metastatic cells compared to control cells (195). Yoon et al. developed an orthotopic model of HNSCC metastasis and selected HNSCC cells through 4 rounds of serial metastasis to obtain a highly metastatic subpopulation (196). The metastatic population acquired mesenchymal features including increased vimentin and integrin α1 and reduced epithelial expression, including reduced E-cadherin and involucrin. In contrast, non-metastatic parental cells had low vimentin expression.

β-Catenin

The Wnt/β-catenin pathway has a critical role in invasion in HNSCC (197). E-cadherin is anchored to the cytoskeleton via β-catenin, a cytoplasmic plaque protein (198). In loss of cell adhesion, as occurs in invasion, E-cadherin is endocytosed and β-catenin is released. In normal and non-invasive cells, β-catenin is usually localized to cell membranes. In cells undergoing EMT, β-catenin is located in the cytoplasm (reflective of its dissociation from E-cadherin). This cytosolic (free) β-catenin translocates to the nucleus to promote transcription of genes that induce EMT. Nuclear β-catenin is a

transcriptional co-activator with T cell factor (TCF)/Lymphoid enhancer-binding factor (LEF), which controls transcription of SNAIL1 (180).

Nuclear β-catenin is correlated with a poor prognosis in patients with metastasic HNSCC (199). Rap1, a ras-like protein, stabilized β-catenin and increased its nuclear localization; more advanced N-stage lesions were associated with high free β-catenin and high active Rap1 (197).

ECM PROTEINS

The ECM proteins that promote EMT in HNSCC include collagen, fibronectin and laminin.

Collagens

While migration of normal cells is strictly controlled by limited proteolysis of the ECM, in cancer, proteolytic remodeling of the ECM facilitates invasion (200). Collagens are the major structural components of the ECM. There are 28 types of collagen that have a triple helical structure. Collagen I and II are fibrillary collagens, while collagen IV constitutes a sheet-like structure that is the major component of basement membranes. There is increased expression of collagen I (α1) and collagen III (α1) in type 1 and 3 EMT, while collagen IV (α1) is down-regulated in all 3 types of EMT (180).

Collagen type I is the most prevalent form in the interstitial matrix. In HNSCC, collagen type I RNA transcripts are more widely expressed in HNSCC than in pre-cancerous or normal tissue. Collagen I stimulated cytokine secretion in genetically

matched primary and metastatic HNSCC cell lines, but cytokine secretion was significantly upregulated in metastatic cells when seated on collagen I (α1) gel (192). The cytokines released (IL-1α, IL-1β, IL-6, TNF-α and TNF-β) stimulated MMP activity and invasion of the HNSCC cells. IL-6 is overexpressed in HNSCC and is a biomarker of poor disease-specific survival (201). Moreover, collagen I enhanced MMP-2 and MMP-9 secretion in both the primary and metastatic cell lines (192). MMP-9 is a biomarker that contributes to invasion of HNSCC and is correlated with poor disease-specific survival (202).

Collagen III (α1) is an ECM component that promotes cancer progression in ovarian (203) and breast cancers (204). In HNSCC, collagen III (α1) cDNA was found to be highly expressed in a Paclitaxel-resistant cell line (205). Altered collagen IV (α1) was linked to invasion and motility of cancer cells. Laminin in tumor cells binds collagen IV (α1) and then secretes gelatinases that break down collagen IV (α1) to facilitate migration of tumor cells (180). Surprisingly, Chen *et al.* found that collagen IV RNA is increased in HNSCC surgical specimens compared to dysplastic and normal tissues (206). Further investigation is necessary to determine the role of collagen IV in invasion of HNSCC.

Fibronectin

Fibronectin is a glycoprotein scaffold for fibrillar ECM (180). It is composed of a dimer of similar subunits of repetitive sequences covalently linked by 2 disulfide bonds at their C-termini. In normal cells, fibronectin mediates cellular interactions with the ECM and is important in migration, differentiation, growth and adhesion of cells. Although fibronectin

is up-regulated in all 3 types of EMT, its use as an EMT biomarker is limited because it is produced by many cell types such as epithelial cells, fibroblasts and mononuclear cells, (187). Fibronectin can be up-regulated by SNAIL and TWIST in type 3 EMT.

In HNSCC, there are contradictory reports with respect to expression of fibronectin. Dooley et al. showed that fibronectin and its receptor are strongly upregulated with α5β6 integrin in SCC cell lines and tissues (207). Three fibronectin isoforms (extra domain A, extra domain B, and IIICS) are generated via alternative splicing depending on cytokine and pH conditions. Fibronectin fragment ED-B is not expressed in normal tissues (except those undergoing wound healing) but expression is correlated with HNSCC and tumor cell aggressiveness (208). The ED-A and IIICS isoforms are expressed in blood plasma of HNSCC patients, suggesting that hydrolytic enzyme-aided invasion leads to degradation of EMC components (209).

Laminin

Similar to collagen, laminin is a major component of the basement membrane. Laminins are glycoproteins made up of one α chain, one β chain and one γ chain. There are 15 known heterotrimers of laminin. Laminin 1 (α1β1γ1) is the laminin of greatest interest in EMT types I and II, where it is downregulated or disrupted. Laminin 5 (α3β3γ2) has been linked to EMT in metaplastic carcinoma of the breast and hepatocarcinoma (180).

The role of laminin 5 in HNSCC is clearly significant. Laminin 5 has been shown to be a major component of the ECM, and laminin 5 expression correlated with invasion and

patient prognosis. Interestingly, the laminin 332 G4 domain, a proteolytic product of laminin 5, promotes laminin 5 deposition, and may have a role in wound healing and SCC formation (210). In a study comparing HNSCC, pre-cancer and normal tissues, overexpression of transcripts of LAMC2 encoding laminin-γ2 chain and COL4A1 collagen IV α1, distinguished HNSCC from pre-cancerous and normal tissues that had lower LAMC2 (206). In another study, high LAMC2 predicted poor HNSCC-specific survival (211).

TRANSCRIPTION FACTORS

The transcription factors that promote EMT in HNSCC include SNAIL, TWIST and LEF-1.

SNAIL Family

SNAIL proteins regulate various aspects of the EMT phenotype, including overexpression of mesenchymal markers fibronectin and vitronectin, and suppression of epithelial markers, including E-cadherin, (180). In addition, SNAIL blocks cell cycle progression and contributes to cell movement and survival. Other targets of SNAIL proteins, include genes regulating cell polarity and apoptosis. SNAIL family proteins are evolutionarily conserved in vertebrates where they have a conserved role in embryonic mesoderm formation.

There are 3 transcription factors in the SNAIL family, of which SNAIL1 and SNAIL2 are functionally equivalent (180). SNAIL1 is important in mediating invasion and inflammation through transcriptional regulation of cytokines, and also in preventing terminal differentiation of HNSCC cells (212). EMT phenotypes and invasion in HNSCC are reduced with siRNA-mediated knockdown of SNAIL1 (213). SNAIL1 expression in primary tumors of HNSCC patients is correlated with metastasis and poor prognosis. SNAIL1 expression correlates with histopathologic grade and depth of invasion in HNSCC (214) and is correlated with poor differentiation of the tumors, lymphovascular invasion and regional metastasis (215). Knockdown of SNAIL1 in HNSCC cell lines attenuated cisplatin resistance by facilitating DNA excision repair by stabilizing ERCC1, which is necessary for nucleotide excision repair (216). Lysyl Oxidase–Like 2, a marker of poor prognosis in SCC, regulates EMT in part by stabilizing SNAIL1 to facilitate tumor progression (217).

Hypoxia contributes to tumor metastasis by initiating EMT through activation of SNAIL2 in HNSCC. SNAIL2 is critical for the induction of MT4-MMP in a hypoxic environment (218). Overall, there is strong evidence to suggest that SNAIL proteins play a role in EMT in HNSCC.

TWIST

TWIST is a basic helix-loop-helix protein that modulates many target genes through E-box responsive elements. There are 2 TWIST genes (TWIST1 and TWIST2) which are well-conserved in vertebrates. TWIST is activated in all 3 types of EMT and is up-

regulated in cancer metastases (180). While mesoderm formation is controlled by SNAIL family proteins, TWIST1 is important in mesoderm differentiation. TWIST proteins can either act as transcriptional repressors (e.g. E-cadherin) or activators (e.g. N-cadherin and fibronectin).

In HNSCC, TWIST expression is positively correlated with lymph node metastasis and clinical stage (219). Hypoxia-inducible factor-1α (HIF-1α) promotes EMT and metastatic phenotypes in HNSCC via upregulation of TWIST expression. Repression of TWIST reverses the EMT and metastatic phenotypes. BMI1, a polycomb-group protein frequently overexpressed in cancers, is regulated by TWIST in HNSCC (220). BMI1 and TWIST expression lead to down-regulation of E-cadherin, which is associated with poor prognosis (220). In a study of 109 HNSCC patients, negative SNAIL1 and TWIST immunostaining was significantly correlated with improved 5-year disease-specific survival (221).

LEF-1

LEF-1, a cotranscriptional activator with TCF, mediates WNT signaling. Through this regulation, LEF-1 plays a role in deciding the fate of cells in normal embryonic development (180). In EMT, the β-catenin/LEF-1 complex is localized to the nucleus where it controls SNAIL gene expression, along with other markers associated with EMT. LEF-1 functions with β-catenin to promote cell survival and proliferation during mammary gland development and in breast cancer (222). LEF-1 and β-catenin are upregulated and translocate to the nucleus in Akt-transfromed keratinocytes (223).

FUTURE DIRECTIONS

In addition to proteins that have a role in HNSCC progression or a correlation with HNSCC, there are several potential biomarkers that should be explored in HNSCC. These proteins have been shown to have a role in EMT in other cancers, but to our knowledge have not been investigated in HNSCC.

Forkhead box protein c2 (FOXC2) is a transcription factor that is expressed in type I EMT and is important in angiogenesis, musculogenesis and the development of the heart, kidney and urinary tract. FOXC2 is expressed in ductal breast cancers and metastatic breast cancer (180). Overexpression of EMT transcription factors such as SNAIL and TWIST increase FOXC2 expression. Furthermore, the overexpression of FOXC2 can induce EMT, which suggests that FOXC2 may play a role in type 3 EMT.

Expression of zona-occludens 1 (ZO-1) occurs in all 3 types of EMT (180). ZO-1 is a tight junction protein that is usually located at cell-cell adhesion membrane complexes in normal epithelial cells. During EMT, ZO-1 relocates from the adhesion membrane complexes to the cytoplasm and then to the nucleus, depending on the degree of differentiation and migration of the cell (224). ZO-1 is involved in the EMT process in colorectal and bile duct cancers, but has not yet been linked to EMT in HNSCC (225, 226).

Zinc finger E-box binding homeobox 1 (ZEB1) is an E-cadherin transcriptional repressor that is downregulated by miR-200 microRNAs in cancer cells that display an EMT phenotype (180). ZEB1 has been investigated in prostate cancer, non-small cell

lung carcinoma and invasive ductal breast cancer, but has not been investigated in HNSCC (227-229).

Osteoblast cadherin (OB-cadherin) is a definitive marker for activated fibroblasts (180). While in cancer and embryonic development, an E-cadherin to N-cadherin switch is used to monitor EMT progression, an E-cadherin to OB-cadherin switch may indicate EMT progression in type II EMT specifically. In cancer, OB-cadherin has an association with prostate and breast cancer where it is hypothesized to be involved in metastasis; its expression in HNSCC is unknown (230).

Cancer stem cells (CSC) are a small population of tumor cells that can both initiate a tumor and repopulate a tumor following treatment, contributing to treatment resistance. In HNSCC, a sub-population of CD44+ cancer stem cells display a phenotypic switch to become either proliferative or migratory (231). The migratory population, designated $CD44^{high}ESA^{low}$, displays reduced E-cadherin and increased vimentin, TWIST, SNAIL1 and SNAIL2, features of EMT cells. Given the striking similarities between EMT and this subpopulation of CSCs, it is likely that future research will elucidate the role of EMT in maintaining the CSC population.

EMT progression involves many signaling pathways that may be targeted in the clinical setting (232, 233). **Figure A.4** summarizes some of the pathways and anti-EMT therapies. The mechanistic role of the EMT markers associated with HNSCC should be clearly defined in order to develop new anti-HNSCC therapies to block HNSCC progression. Understanding the role of EMT in HNSCC will allow clinicians to personalize

treatment for patients with particularly aggressive tumors, and improve treatment outcomes.

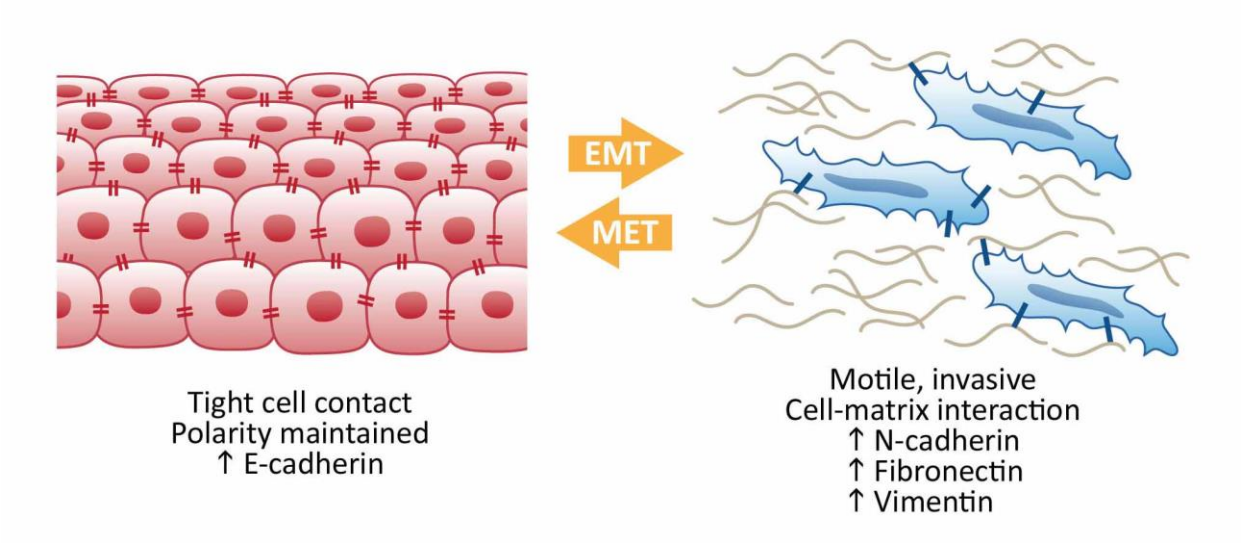

Figure A.1: EMT to MET. Epithelial-like cells display tight cell-cell contacts and maintain polarity, whereas mesenchymal-like cells are more motile and display more contact with the extracellular matrix. Proteins associated with the epithelial-like or the mesenchymal-like states are referred to as biomarkers. As cell progress through EMT and MET, the levels of proteins associated with each state are altered, reflecting the phenotypic switch between the 2 states.

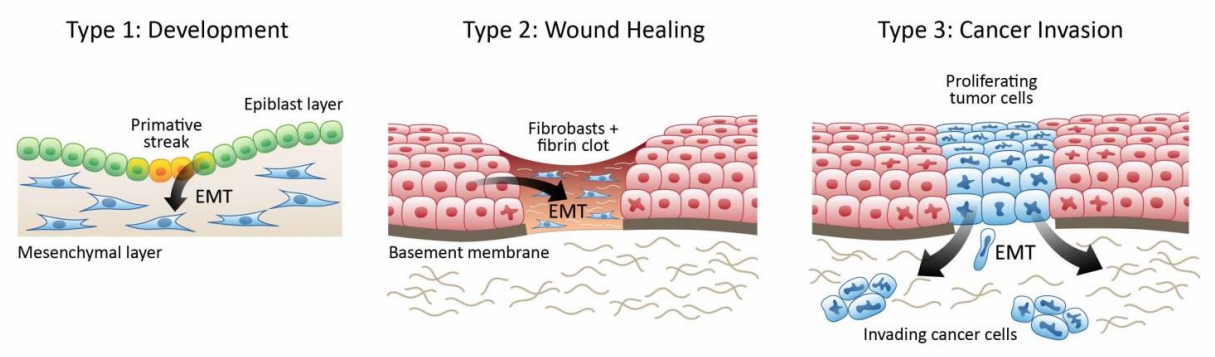

Figure A.2: Three types of EMT. Type 1 EMT occurs in development, for example when in gastrulation epithelial cells transition to motile mesenchymal cells. Type 2 EMT occurs when secondary epithelial or endothelial cells move to interstitial spaces in wound healing or chronic inflammation resulting in fibrosis. Type 3 EMT occurs when epithelial tumor cells migrate beyond a primary tumor and metastasize.

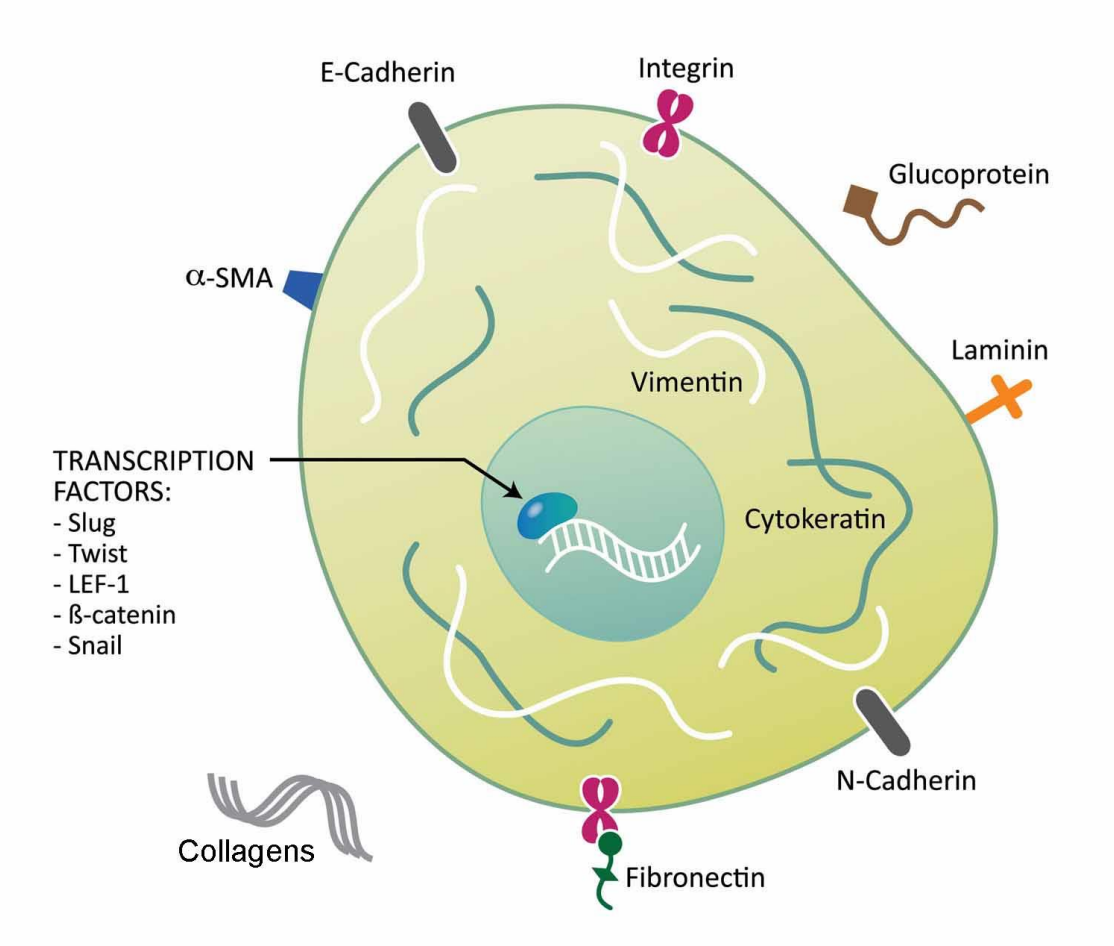

Figure A.3: Proteins involved in EMT. Several proteins have been identified as biomarkers of EMT. These proteins include cell surface proteins, cytoskeletal proteins, extracellular matrix proteins and transcription factors.

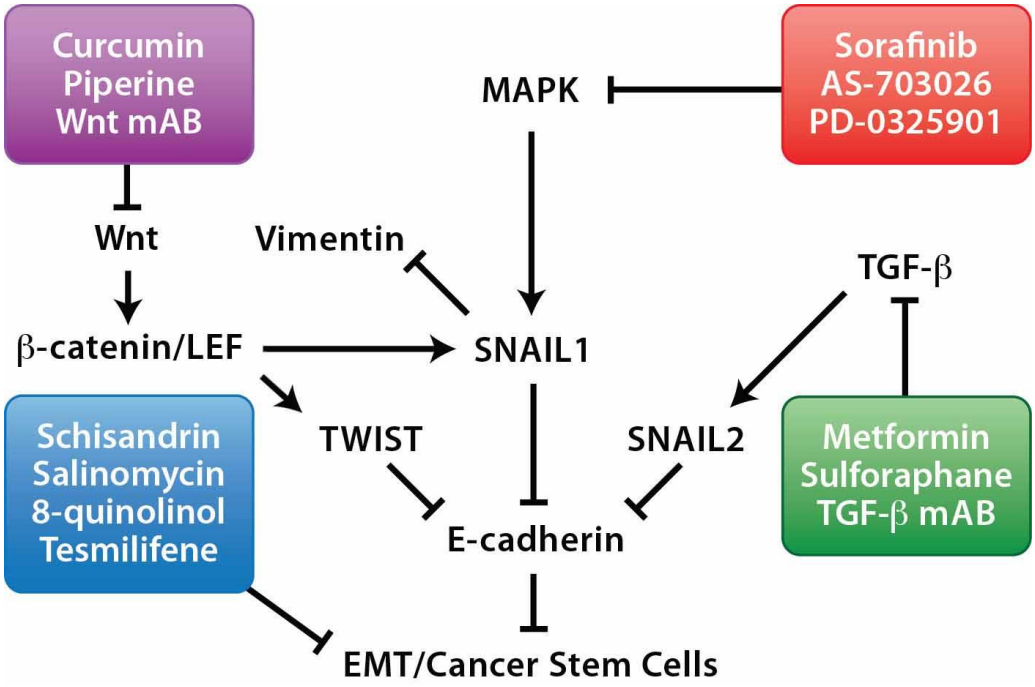

Figure A.4. Targeted therapies against EMT pathways. EMT progression involves many signaling pathways that may be targeted in the clinical setting, which include monoclonal antibodies (mAB) and small molecule inhibitors (boxed).

Biomarker Category	Proteins	References
Cell Surface Proteins	E-Cadherin	(231)
	N-Cadherin	(188)
	Integrins	(190) (191) (234)
Cytoskeletal Proteins	α-SMA	(193)
	Vimentin	(196) (195) (194)
	β-catenin	(235) (199) (197)
Extracellular Matrix Proteins	Collagen (I)	(206) (234)
	Collagen (III)	(204) (203)
	Collagen (IV)	(206)
	Fibronectin	(207) (208) (209)
	Laminin 5	(210) (206) (211)
Transcription Factors	SNAIL1	(213) (212) (214) (216) (215)
	SNAIL2	(218)
	TWIST	(219)
	LEF-1	(223)

Table A.1. Known biomarkers of EMT in HNSCC.

APPENDIX B

CDH11 is a Novel Biomarker of EMT in HNSCC: Discovery and Validation Using an In Silico Approach

Appendix B is adapted from a manuscript that has been submitted for review (236).

INTRODUCTION

Analyses of existing datasets have long informed investigation of potential oncogenes or tumor suppressor genes. Preliminary studies of datasets in the existing literature assisted researchers in designing focused and cost-effective studies. Translational researchers have been especially empowered by clinical datasets. However, previously the availability of datasets to researchers was limited by access to journals and the lack of effective search tools. In recent years, these limitations have been lifted as an increasing number of datasets have become available to researchers through multiple online databases.

The availability of datasets has changed the practice of oncology research, enabling powerful statistical studies that are both used in preliminary searches for molecules to study, and to supplement benchtop studies (237). Modern databases of research outcomes have reinforced the value of statistics in biology (238). The enormous increase in available information has launched the rapidly developing field of

bioinformatics, which focuses on the assembly and utilization of biological databases. The growth of bioinformatics reflects the increasing importance of statistics in biological science, shifting the value of quantitative results over qualitative results.

Easily navigable and increasingly comprehensive in silico studies using databases can suggest whether a gene is involved in a clinical outcome of interest and even hint at possible mechanisms. These databases comprise a new genre of in silico investigation (237). In silico analyses are becoming an increasingly popular mechanism to identify novel molecular targets for study. Moreover, translational researchers use in silico analyses linked to clinical data to complement results generated in the laboratory. Meta-analyses of existing micro-array data demonstrate correlations of markers across many cancer types and clinical conditions.

As in silico analysis becomes a standard of translational research studies, more databases are being assembled for bioinformatics analysis. Available databases include corporate for-fee databases, university-constructed compilations of research outcomes and clinical data, and government-run databases from several countries. Many examples of databases containing data of interest to oncologic researchers are listed and described in **Table B.1**. The Cancer Genome Atlas (TCGA) is an extensive database managed by the National Cancer Institute and the National Human Genome Research Institute that links DNA copy-number variations with multiple cancer types and clinical parameters (239). The database used in the present study is the Oncomine™ database, which currently brings together information from 699 datasets. Studies collected into Oncomine™ report over-expression and under-expression of genes across many studies that include a range of cancer types and sub-types (239).

In this study we demonstrate the value of in silico experiments to nominate and investigate markers of epithelial to mesenchymal transition (EMT) in head and neck squamous cell carcinoma (HNSCC). EMT is a process by which non-motile epithelial cells become motile, and occurs normally in embryonic development and wound healing (180). EMT can also promote invasion and metastasis in cancer (240). Understanding the mechanism of EMT in HNSCC will advance our understanding of tumor progression (79). HNSCC has maintains a dismal 40-50% 5-year survival rate due to lack of effective novel treatment strategies (1). Biomarkers involved in EMT may be attractive treatment targets for HNSCC, and potentially leading to novel personalized medicine strategies. Our results show that multiple EMT markers are highly expressed in HNSCC and correlated with poor clinical outcome, altered sensitivity to chemotherapy and multiple oncogene mutations. In addition, we use in silico analyses to reveal strong correlations between CDH11 (osteoblast-cadherin) and poor clinical outcomes in HNSCC. CDH11 is an emerging EMT marker that is thought to have a role in wound healing and breast cancer progression but little is known about the role of CDH11 in HNSCC (230). CDH11 has been shown to be variably expressed in oral cancer tissues with qPCR (241). Additionally, CDH11 DNA is found to be differentially methylated between primary and metastatic oral tumors (242). In the studies described here, CDH11 expression is validated in multiple HNSCC cell lines and tissues.

METHODS

In silico studies. The Oncomine database (Oncomine™, Compendia Bioscience, Ann Arbor, MI) was used for in silico experiments. Eighteen head and neck cancer datasets

were identified using the search parameters “Cancer Type: Head and neck cancer” and “Analysis Type: Cancer vs Normal Analysis”. Datasets from studies of adenoid cystic carcinoma, thyroid carcinomas or pharyngeal carcinomas were excluded. The following studies were retained: Cromer Head- Neck (150), Estilo Head-Neck (151), Ginos Head-Neck (152), Kuriakose Head-Neck (243), Peng Head-Neck and Peng Head-Neck 2 (154), Pyeon Multi-cancer (156), Talbot Lung (161), Toruner Head-Neck (162), TCGA Head-Neck, Ye Head-Neck (244). Overexpression of EMT markers in HNSCC was demonstrated in multiple datasets. Several filters were used to generate heat maps with corresponding statistical analyses correlating expression of EMT markers with different clinical outcomes, drug responses and oncogene mutations. In addition, a summary of CDH11 overexpression in multiple cancer types was generated, and genes coexpressed with CDH11 in HNSCC were identified.

Statistical Analysis. GraphPad Prism® was used for statistical analyses. HNSCC datasets with mRNA expression data (n=9) were identified in Oncomine. Meta-analyses were performed as described (245). Expression of EMT markers was compared between normal and HNSCC samples by Student’s *t*-test in each HNSCC dataset, and a *P*-value <0.05 was determined to be statistically significant. Each statistically significant study was given an arbitrary value of “1” and non-significant studies were designated a value of “0”. A one-sample *t*-test was performed for each set of values, with a target value of 0.05, and a one-sided *P* value of <0.05 was considered statistically significant.

Immunohistochemistry. Immunostaining was performed on formalin-fixed, paraffin-embedded HNSCC tissue and cell lines, as described (246). The CDH11 affinity purified rabbit polyclonal antibody was from R&D Systems, and rabbit IgG (Dako) was used as a negative control at the same concentration as the primary antibody.

RESULTS

HNSCC Datasets Provide Extensive Data for in silico Studies

The Oncomine database contained 699 datasets and 80915 samples at the time of this study. Of the available datasets, 36 were identified as "Head and Neck Cancer" datasets. **Figure B.1** gives an overview of the content of these datasets. DNA or mRNA expression data is available for the datasets (**Figure B.1A**). While most datasets contain less than 75 samples, 11% contain more than 151 samples (**Figure B.1B**). The data provided comes from a range of sources, including cell panels, tissue panels and TCGA, which was compiled by the National Cancer Institute and National Human Genome Research Institute (**Figure B.1C**). The specimens used to generate the datasets include surgical specimens and samples collected by laser-capture microdissection, manual microdissection and macrodissection (**Figure B.1D**). Several available filters for head and neck cancer dataset analyses are listed in **Table B1**. Expression levels of biomarkers analyzed in the datasets can be linked to many interesting parameters listed including sample site, clinical outcomes, molecular subtypes, pathological subtypes, drug sensitivities and patient demographics.

EMT Biomarkers are Overexpressed in HNSCC

A summary of representative histograms detailing expression levels in the individual studies used to compile the meta-analyses are shown in **Figure B2**. Overexpression of multiple EMT markers in HNSCC is shown, along with a meta-analysis of the expression level in cancer versus normal for the markers across several datasets (**Figure B3**). SNAI2, TGFB1 and CDH11 are significantly overexpressed in HNSCC across 9 datasets.

EMT Biomarkers are Correlated with Aggressive HNSCC

Dataset filters were used to correlate EMT biomarker expression with different HNSCC clinical parameters using the TCGA Head-Neck dataset containing DNA copy-number data. SNAI2 was significantly overexpressed in tumors with positive nodal status (**Figure B.4A**, $P = 0.030$). CDH11 and ACTA2 were both correlated with metastasis (**Figure B.4B**, $P = 1.82 \times 10^{-5}$ and $P = 0.004$, respectively). CDH11 was also significantly correlated with death at 5 years (**Figure B.4C**, $P = 0.02$).

CDH11 is Expressed in HNSCC Cell Lines and Tissue

In silico data suggested that CDH11 is overexpressed in HNSCC, and expression levels correlate with more aggressive tumors. In order to validate our in silico findings, we investigated the expression of CDH11 in HNSCC cell lines and tissues. Using immunohistochemistry, we found that CDH11 is variably expressed across non-malignant and malignant oral epithelial cell lines (**Figure B5**). HOK16B is a transformed human

keratinocyte cell line, which shows low expression of CDH11 compared to HNSCC cell lines. We validated the antibody for immunohistochemistry on paraffin-embedded tissues using colon cancer tissue and associated tumor stroma, which are known to express CDH11 (247). After finding that CDH11 appropriately stained our positive control tissues, we immunostained normal human oral mucosa and pre-neoplastic (epithelial dysplasia) tissues. CDH11 was expressed at low levels in normal human oral tissue (**Figure B.6A**). Next, we immunostained a tissue microarray (TMA) containing human HNSCC tissues and normal oral tissues. CDH11 had low expression in normal tissue, but was variably expressed across HNSCC samples (**Figure B.6B**). HNSCC samples exhibited both higher intensity of staining, and also a higher proportion of cells were stained when compared to normal tissues on the TMA (**Figure B.6B**). These data confirm that CDH11 is expressed in HNSCC tissues at higher levels than normal tissue.

DISCUSSION

Translational researchers are faced with the challenge of making relevant correlations between clinical problems and experimental studies. In silico investigations using multiple datasets provide researchers a practical approach to enhance benchtop investigations with clinically-oriented data or to discover potential new biomarkers. In the present study, we performed meta-analyses of multiple datasets to evaluate expression of EMT markers. Expression of some EMT markers was correlated with common oncogenic mutations. We were able to correlate overexpression of EMT biomarkers with multiple clinical parameters, emphasizing the role of EMT in HNSCC progression.

We identified EMT markers that were differentially associated with sensitivity to a variety of therapeutics. HNSCC has been challenging to treat due to lack of effective novel therapies, and the next era of HNSCC treatment will focus on personalized medicine (248). In silico studies of datasets provide insight into which biomarkers could be used to select the best therapy for patients on a case-by-case basis.

Although in silico studies based on expression of genes are useful, they do not identify all proteins important to tumor progression, specifically those regulated post-translationally. In silico experiments may suggest novel biomarkers, but validation of expression in tissues and cell lines is essential. Since microarrays investigate thousands of genes, false positives are inevitable at any practical *P*-value. We identified CDH11 as a new EMT biomarker in HNSCC in multiple in silico analyses. We then verified that CDH11 is expressed in HNSCC via immunoblot and immunohistochemistry. In contrast, expression of proteins that are activated or inactivated by phosphorylation, such as the tumor suppressor tristetraprolin (TTP), is not as informative as the phosphorylation status of the protein (105).

A molecular concept map may associate expression of a protein with a phenotype of interest, such as cancer recurrence. For example, a molecular concept map revealed that the Myc pathway is associated with breast cancer relapse (249). Pathway analysis is an additional method of analysis that models molecular pathways. Noting gene expression levels along the stages of cancer progression can reveal the mechanism of progression and prognosis associated with pathway activation (250, 251). In addition to gene expression databases, databases of information from electronic health records have been examined in aggregate to identify linkages between health problems. Studies

demonstrating the link between non-insulin-dependent diabetes mellitus with retinopathy and hypertension or the unexpected link between pyloric stenosis and ventricular septal defects demonstrate the utility of bioinformatics even with standard clinical data (252). This technique can be applied to clinical records of cancer patients to potentially identify links between cancer and other health factors or conditions.

The wide range of available databases reflects the rising importance of in silico analyses. These analyses represent an approach to obtain additional, in-depth and up-to-date data on a gene and its function without the additional expense of benchtop studies. As studies are incorporated into readily accessible databases, the application of bioinformatics techniques will become increasingly useful. Furthermore, textual analysis techniques are making it practical to analyze large-scale sets of medical records thereby putting volumes of clinical records into a searchable format. Useful correlations, trends and risk factors can be queried and characterized. Given the value of in silico studies and the improving quality and availability of datasets, the use of bioinformatics techniques may become a standard expectation of any review of clinically relevant biomarkers and may assist in the development of personalized medicine.

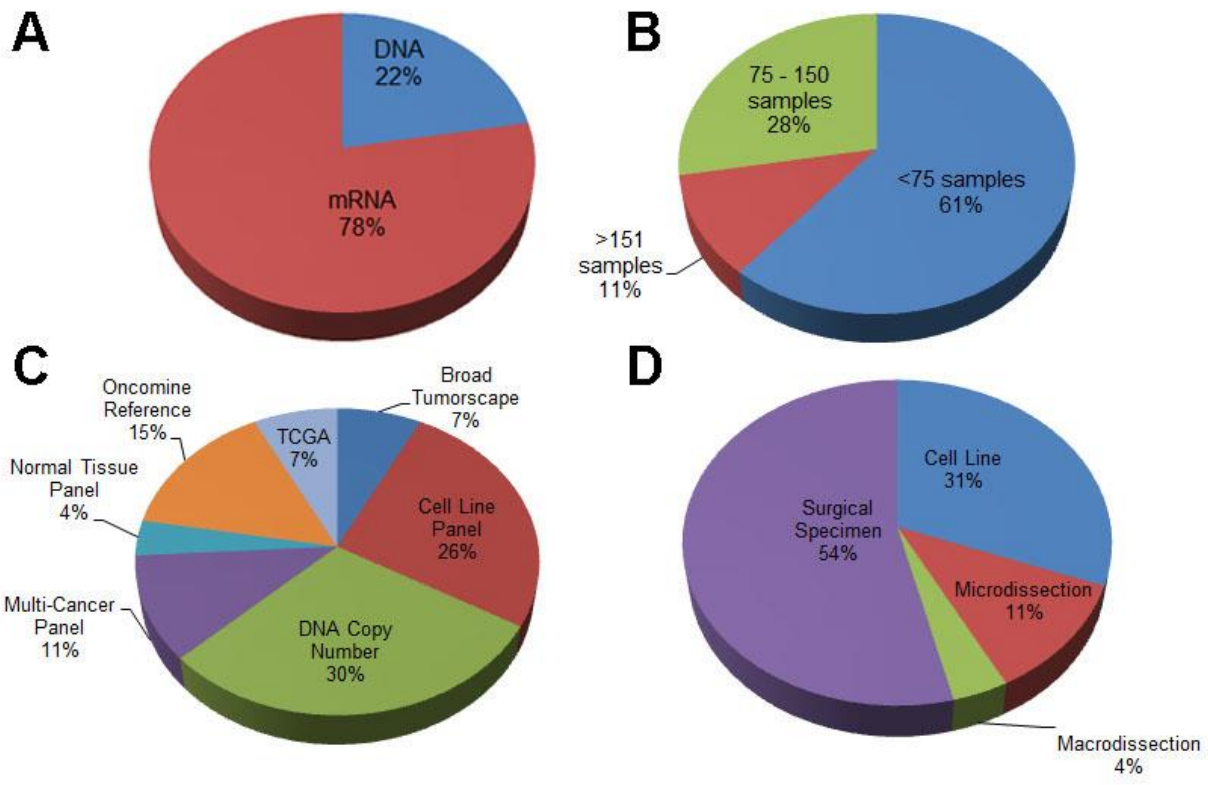

Figure B.1: Details of Head-Neck cancer datasets. A. A larger number of datasets provide mRNA expression (78%) levels than DNA copy-number analyses (22%). **B.** While most of the sample sets have less than 75 samples (61%), 11% contain more than 151 samples. **C.** Data are supplied by a range of sources including cell and tissue and data from sources including The Cancer Genome Atlas (TCGA), which is compiled by the National Cancer Institute and National Human Genome Research Institute. **D.** Samples represent a variety of sources, including cell lines, surgical specimens, and both macro and micro dissections.

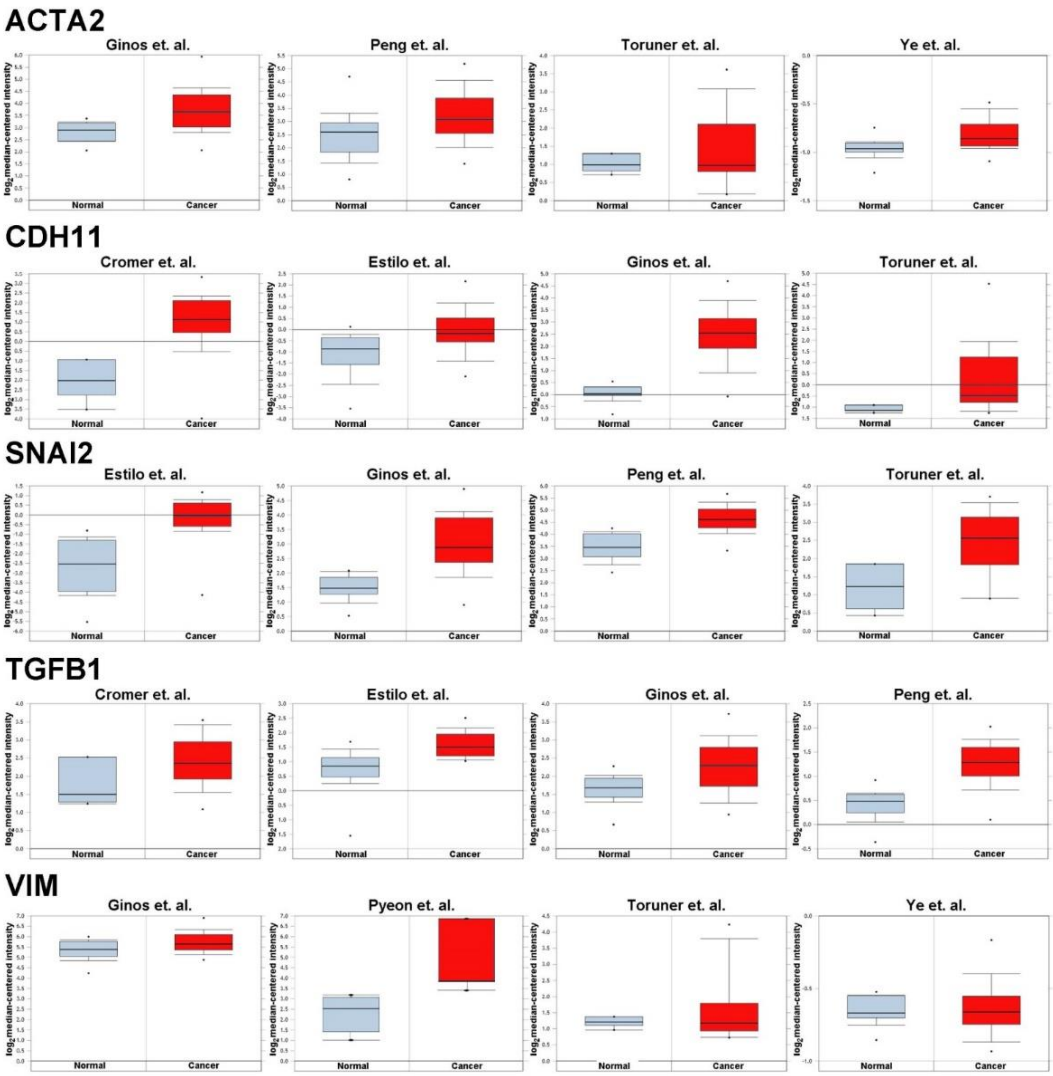

Figure B.2: Expression of EMT biomarkers. Representative histograms for studies of the expression levels of the following EMT biomarkers are shown: ACTA2 (Ginos, $P = 2.48 \times 10^{-6}$; Peng, $P = 0.001$; Toruner, $P = 0.150$; and Ye, $P = 0.002$); CDH11 (Cromer, $P = 0.004$; Estilo, $P = 6.91 \times 10^{-5}$; Ginos, $P = 3.86 \times 10^{-17}$; Toruner, $P = 0.002$); SNAI2 (Estilo, $P = 2.40 \times 10^{-10}$; Ginos, $P = 7.92 \times 10^{-11}$; Peng, $P = 5.04 \times 10^{-11}$; Toruner, $P = 0.018$); GFB1 (Cromer, $P = 0.045$; Estilo, $P = 3.14 \times 10^{-6}$; Ginos, $P = 1.52 \times 10^{-4}$; Peng, $P = 5.09 \times 10^{-15}$); VIM (Ginos, $P = 0.008$; Pyeon, $P = 0.035$; Toruner, $P = 0.131$; Ye, $P = 0.347$).

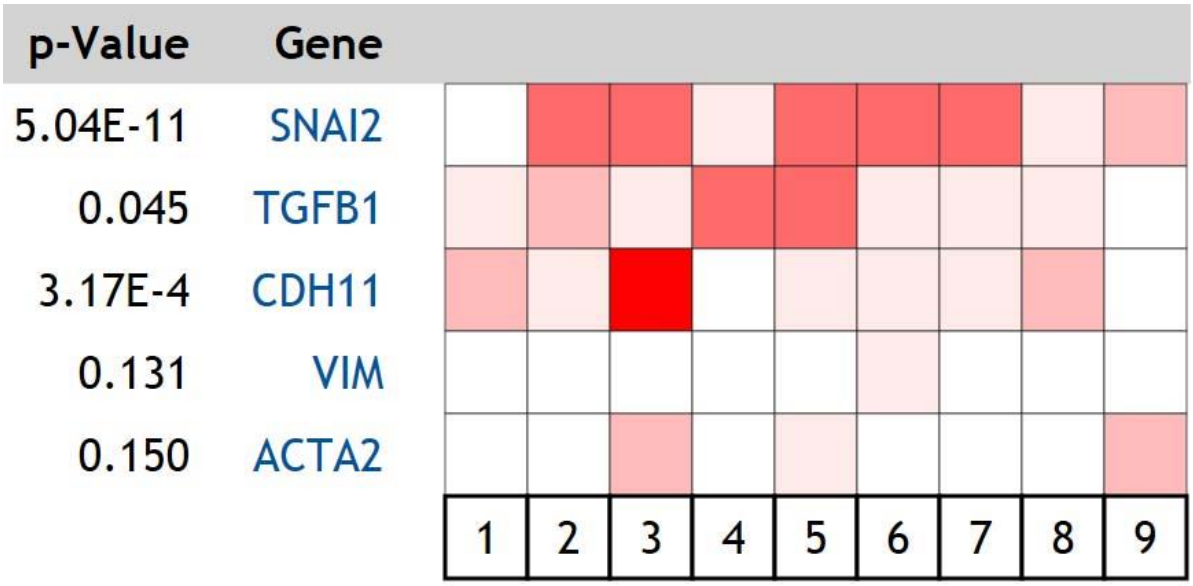

Figure B.3: Overexpression of EMT biomarkers in HNSCC. Overexpression of EMT biomarkers was determined among 9 studies: 1) Cromer Head-Neck (150), 2) Estilo Head-Neck (151), 3) Ginos Head-Neck (152), 4) Kuriakose Head-Neck (243), 5) Peng Head-Neck (154), 6) Pyeon Head-Neck (156), 7) Talbot Lung (161), 8) Toruner Head-Neck (162), 9) Ye Head-Neck (244). SNAI2, TGFB1 and CDH11 were all significantly overexpressed ($P = 5.04 \times 10^{-11}$, $P = 0.045$, and $P = 3.17 \times 10^{-4}$, respectively). Greater red intensity indicates a lower (more significant) *P*-value for comparative overexpression of each marker in cancer tissue versus normal tissue.

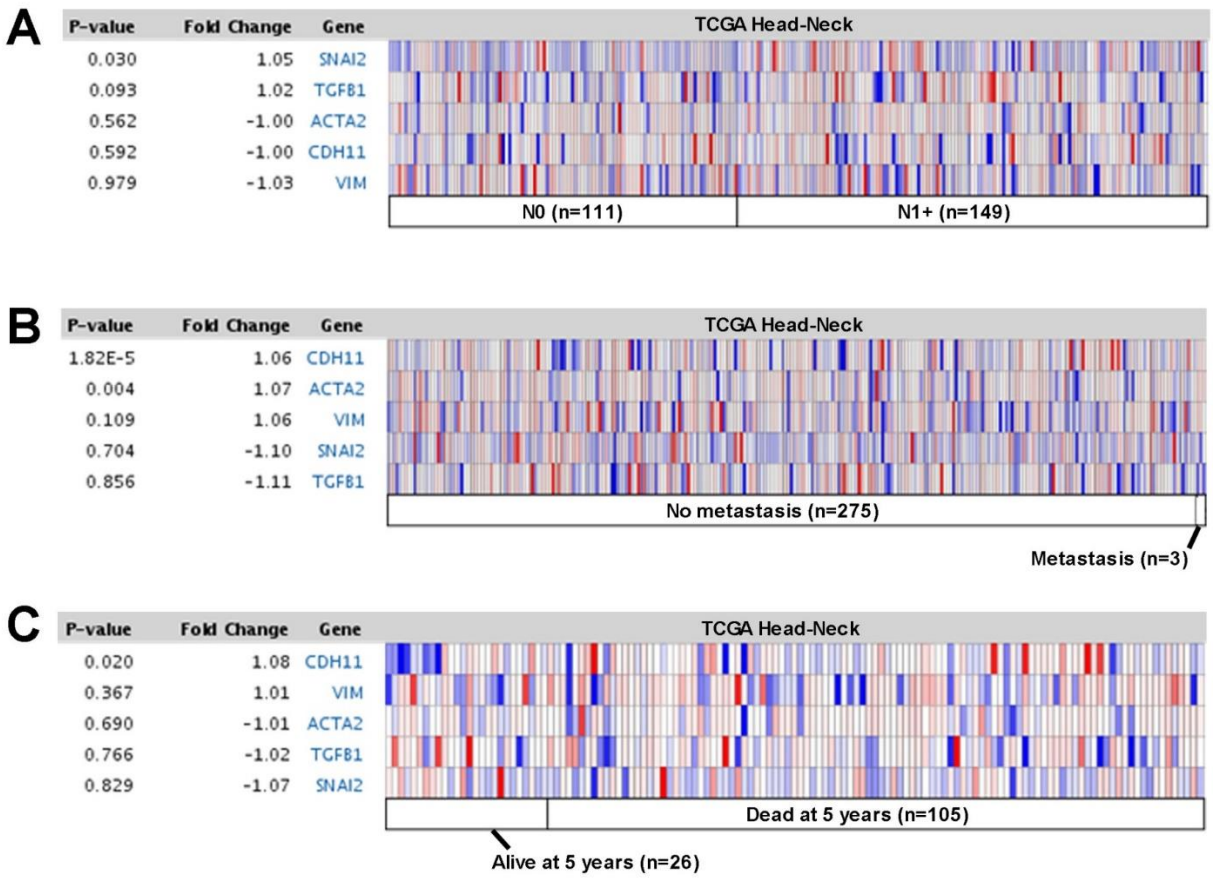

Figure B.4: SNAI2, CDH11 and ACTA2 are correlated with aggressive HNSCC. DNA copy-number of a panel of EMT biomarkers was correlated with HNSCC clinical parameters. **A.** SNAI2 was significantly overexpressed in tumors with positive nodal status ($P = 0.030$). **B.** CDH11 and ACTA2 were both correlated with metastasis ($P = 1.82 \times 10^{-5}$ and $P = 0.004$, respectively). **C.** CDH11 was also significantly correlated with death within 5 years of diagnosis ($P = 0.02$).

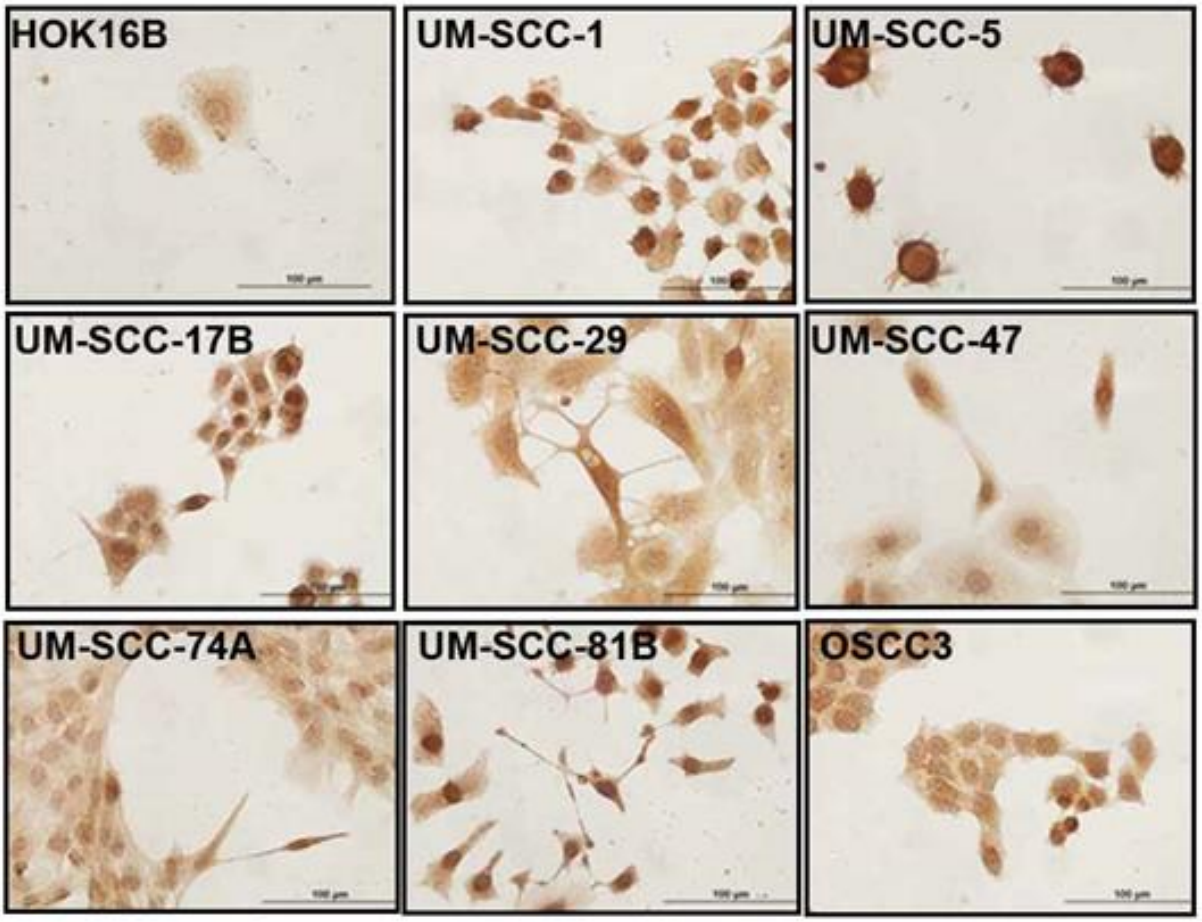

Figure B.5: Validation of CDH11 expression across HNSCC cell lines. CDH11 is variably expressed across several HNSCC cell lines as observed by immunohistochemical detection. HOK16B is a transformed human keratinocyte line that exhibits low staining of CDH11. HNSCC cell lines were incubated with an anti-CDH11 antibody followed by an anti-rabbit secondary antibody. Immunostained cells were photographed under the same conditions at 60x magnification.

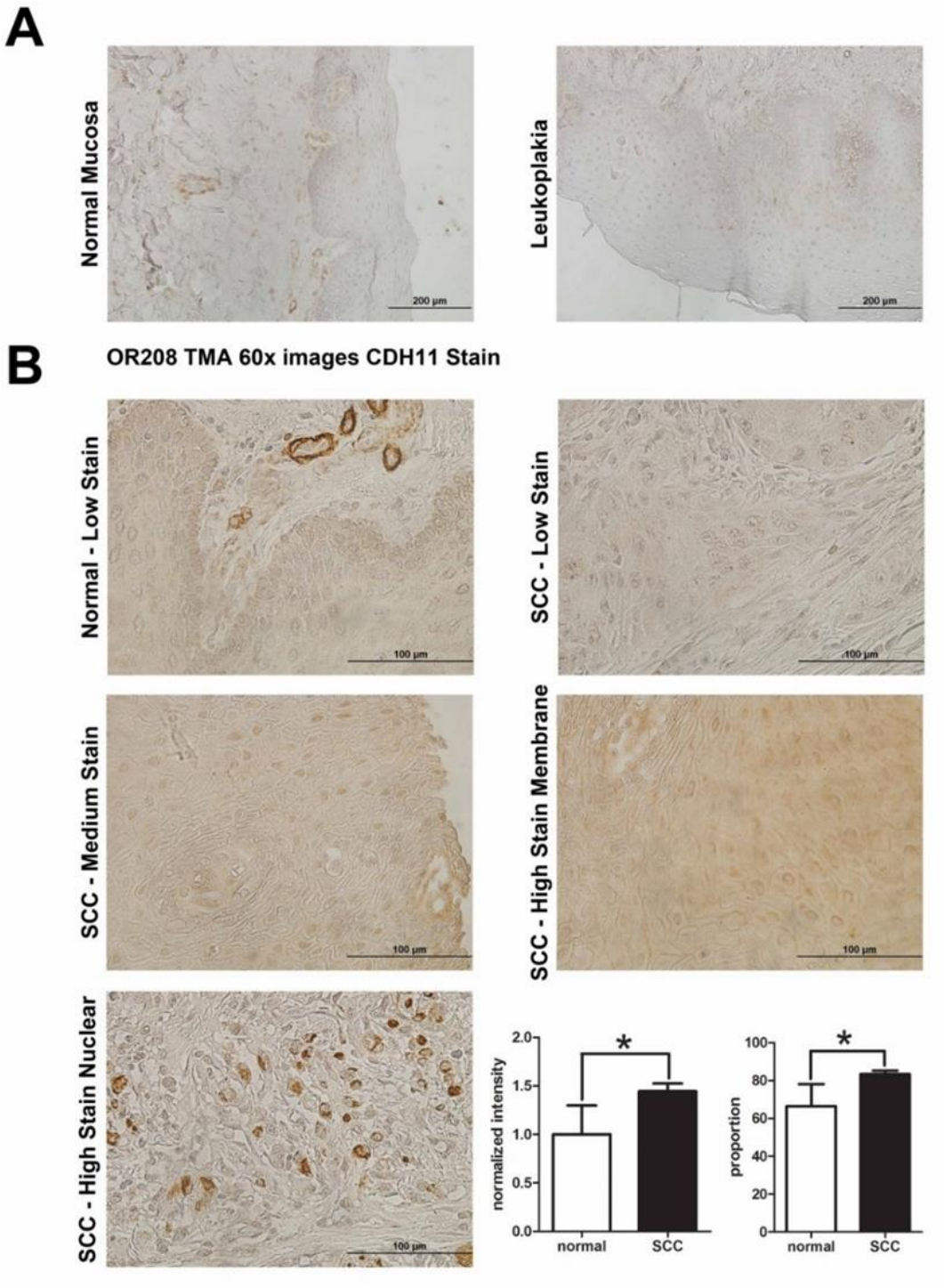

Figure B.6: Validation of CDH11 Expression in HNSCC tumors. A. Normal oral mucosa exhibit low staining of CDH11 in the cytoplasm and some staining in the nucleus. **B.** On a tissue microarray, normal tissue exhibits low staining of CDH11, and CDH11 is variably expressed across HNSCC tissues. When quantified, HNSCC tissues stained with significantly higher intensity, and a higher proportion of each sample stained when compared to normal oral tissue.

Database	Access Information	Description
Cancer Gene Expression Database	http://lifesciencedb.jp/cged/ Freely searchable.	A database of gene expression from studies performed in Japanese institutions.
GENT – Gene Expression Across Normal and Tumor tissue	http://medical-genome.kribb.re.kr/GENT/ Freely searchable.	A database of comparative gene expression across normal and cancer tissues.
KEGG Database (Kyoto Encyclopedia of Genes and Genomes)	http://www.genome.jp/kegg/kegg1.html Freely searchable.	An integrated database of genomic and functional data, links genes to higher-level functions.
Oncomine	https://www.oncomine.org/ Registration available to users from educational, government and non-profit institutions.	A compilation of cancer microarray data, search queries can be narrowly focused.
RefSeq – The Reference Sequence Collection	http://www.ncbi.nlm.nih.gov/RefSeq/ Freely searchable, some content that it links to requires additional access privileges.	The American NIH database of DNA, RNA and protein sequences, provides detailed information on many of these genes and proteins.
The Tumor Gene Family of Databases	http://www.tumor-gene.org/Oral/oral.html Freely searchable.	A set of databases of tumor suppressors, potential oncogenes and cancer-inducing mutations.

Table B.1. Example databases available for in silico oncologic studies.

APPENDIX C

Characterization of Squamous Cell Carcinoma in an Organotypic Culture via Sub-surface Nonlinear Optical Molecular Imaging

Appendix C is adapted from a published manuscript (70).

INTRODUCTION

Head and neck cancer is the sixth most common cancer globally, affecting about 600,000 individuals per year (1). Over 90% of these lesions are HNSCC. New treatments are required since current regimens have not improved survival in over 5 decades. Due to the complexity of the many structures and tissues involved in HNSCC progression, researchers struggle to accurately replicate the disease process in an in vitro setting. Development of models that more closely simulate human HNSCC will enhance translation of pre-clinical studies into successful novel targeted therapies.

Invasion of transformed epithelial cells beyond the basement membrane and into the connective tissue is the defining event that differentiates pre-cancerous oral lesions from HNSCC. The basement membrane separates epithelial cells from the underlying connective tissue and is identified histologically by expression of collagen IV (5). Destruction of the basement membrane and invasion with subsequent regional spread

and distant metastases contribute to the lethality of HNSCC. Since invasion is the key event of tumor progression, a sophisticated model that replicates the basement membrane and connective tissue stroma is necessary to study invasion in HNSCC and many other cancers.

To address the limitations of existing in vitro models of invasion, our laboratory developed the Oral Cancer Equivalent (OCE) model using human HNSCC cells and human connective tissue. Recent advances in tissue engineering have provided xenografts or autologous grafts for humans based on stratification of keratinocytes on human decellularized cadaveric dermis (253). To facilitate studies on the invasive phenotype of HNSCC, we adapted the procedure for creating normal oral tissue grafts to generate the OCE. In the adapted protocol, decellularized human dermal tissue is coated with collagen IV and seeded with human HNSCC cells, which are allowed to stratify and invade. This novel in vitro model simulates invasion of human HNSCC including the complexity of connective tissue and the histopathology. **Figure C.1A** shows a HNSCC lesion that presented as a leukoplakia (white patch) on the lateral surface of the tongue. **Figure C.1B** shows a similar “clinical” appearance of the OCE construct. In both **Figure C.1C** and **Figure C.1D**, arrows indicate invading cells and arrowheads highlight the location of the basement membrane on tissue sections of a HNSCC tumor and an OCE construct. The pattern of rete ridge formation and islands of invasive cells in HNSCC (**Figure C.1C**) are closely simulated by invasion of HNSCC cells in the connective tissue stroma of the OCE (**Figure C.1D**).

In a recent publication describing the role of the RNA binding protein tristetraprolin (TTP) in HNSCC progression, our lab used the OCE model to quantify HNSCC invasion

(105). The OCE method allowed us to quantitatively compare invasion of cells with short-hairpin RNA-mediated knockdown of TTP (shTTP) with control cells (treated with scrambled shRNA, shSCR) on fixed tissue sections. Our initial data showed that cells with TTP-knockdown were more invasive than control cells. The analysis in our previous study was limited to quantification of invasive cells in fixed tissue sections at a single timepoint.

In the present study, we demonstrate the feasibility of using nonlinear optical molecular imaging to image sub-surface live cells on the OCE constructs. With this method, green fluorescent protein (GFP)-tagged cells are used for the OCE constructs, and invasion can be traced at multiple timepoints and at multiple locations on the constructs. In addition, decay of the collagen matrix by the cancer cells can be quantified through obtaining a second harmonic generation (SHG) signal from the connective tissue matrix. We used shTTP-treated cells that we previously showed to be more invasive compared to shSCR-treated control cells to validate and optimize the novel imaging method presented in this manuscript (105). We also compared our live cell imaging results with histological data of fixed tissue sections at multiple time points. Overall, sub-surface nonlinear optical molecular imaging of the OCE confirmed histological quantification of invasion of fixed tissue sections from OCE constructs. The live cell imaging method provided additional levels of analysis by providing a 3D view of cells interacting with the connective tissue matrix in addition to quantification of collagen decay on the OCE constructs.

METHODS

Overview of the OCE Method. The overview of the OCE protocol is shown (**Figure C.2**). Circular fragments of decellularized human dermis were hydrated and coated with human collagen IV. Cells expressing green fluorescent protein (GFP) were seeded on the tissue and allowed to stratify over several days. Invasion of cancer cells and decay of connective tissue matrix were observed and quantified using sub-surface nonlinear optical microscopic molecular imaging over 2 days, after which the constructs were fixed for histopathological studies.

Cell Culture. The HNSCC cell line UM-SCC-1 (from T. Carey) was used for these studies. HNSCC cells were transduced with short hairpin RNA (shRNA) constructs with a vesicular stomatitis virus glycoprotein (VSVG) backbone and a GFP tag in lentiviral particles. A scrambled shRNA (designated shVSVG) was used for the control and shTTP was used for TTP knockdown (Open Biosystems, Catalog No. RHS4430-99139230, Sequence 5'TATTAGAATAAATAAAGTC 3'). UM-SCC-1 cells (35×10^4) were transduced with 1000 multiplicity of infection of control and TTP knockdown vectors in serum-free medium for 3 hours prior to adding 10% FBS. Puromycin (10 ug/ml) was used to establish stable cell lines over 4 weeks. Protein knockdown was confirmed by immunoblot analysis.

Preparation of Human Dermal Tissue. Decellularized dermal tissue (AlloDerm®, LifeCell Corporation) was cut into disks that fit into the individual wells of a 48-well plate. Dermal tissue was placed in a 100 mm cell culture dish and rehydrated with 15 mL

Dulbecco's phosphate-buffered saline (DPBS, Invitrogen), which was changed every 15 minutes for 90 minutes. Forceps were used to aseptically remove the dermal tissue from its commercial packaging. The tissue was gently rinsed with DPBS to determine orientation of the tissue (DPBS added to the epidermal side with the basement membrane easily drains off of the tissue, whereas DPBS added to the dermal side is retained). The dermal tissue was transferred, epidermal side facing up, into a well of the 48-well microplate. The tissue was gently pressed into the microwell plate to ensure there were no bubbles beneath the tissue. One hundred microliters of DPBS was added to each of the wells with tissue. Five microliters of human collagen IV (Fluka, 5 µg/µl suspended in acetic acid) was added to the middle of the DPBS covering the dermal tissue. Human collagen IV was added to enhance HNSCC cell attachment to the decellularized dermal tissue (254, 255). The plate was sealed with Parafilm (BioExpress) and refrigerated overnight at 4°C.

Seeding and Cultivating Cancer Cells on Hydrated Dermal Tissue (day 0). UM-SCC-1 cells transduced with shVSVG or shTTP were grown to 60% confluence. The 48-well microplate containing hydrated dermal tissue coated with collagen IV was warmed in a cell culture incubator (37°C, 5% CO_2) for 30 minutes. Five hundred microliters of complete Dulbecco's Modified Eagle Medium (DMEM) culture media containing 10% fetal bovine serum (FBS) and 1% PenStrep (10,000 Units/mL Penicillin and 10,000 µg/mL Streptomycin) was added to the wells of the 48-well microplate containing the prepared dermal tissue. The complete media provided the nutrients for the HNSCC cells. The HNSCC cells were seeded onto dermal tissue at a density of 5 x 10^5 cells in 100 µl of

DMEM. Cells were incubated in a cell culture incubator at 37°C and 5% CO_2 for 4 days, and the medium was changed every 2 days.

Transfering the OCE to the Air-Liquid Interface (day 5). Transwell carrier inserts (3.0 µm pore size, Costar, Corning Inc.) were placed in a 6-well cell culture dish, and 500 µL of complete DMEM culture medium with 10% FBS and 1% PenStrep was pipetted below the insert. Using sterile forceps, the OCE constructs were lifted by the edge of the dermal tissue and transferred with the epidermal side facing up onto one of the inserts. The constructs were incubated at 37°C in a 5% CO_2 incubator for 2-3 days, and the medium in the lower chamber was changed every day.

Nonlinear Optical Microscopic Molecular Imaging (days 7 and 8)

Instrumentation and Data Acquisition. Nonlinear optical microscopic molecular imaging was performed on a Leica TCS SP5 microscope in epi-illumination mode. The images were collected with a 25x water immersion objective lens (0.95 NA, 2.5 mm working distance). A tunable Ti:sapphire laser (Mai Tai, Spectra-Physics), providing excitation wavelengths ranging from 690 to 1040 nm, was employed to deliver 100 fs pulses with a 80 MHz repetition rate. A 900 nm excitation wavelength was employed to simultaneously excite GFP fluorescence and collagen SHG. For GFP detection, the emitted fluorescence was coupled through a band pass filter from 475 to 575 nm, and collected with a non-descanned photomultiplier tube positioned in close proximity to the sample to increase collection efficiency. For SHG detection, an internal tunable

photomultiplier was tuned with a narrow bandwidth, 440-460 nm, to selectively collect collagen SHG emission. *En-face* images were acquired with raster scanning in the lateral plane and cross-sectional images were acquired with line scanning in the transverse plane. The scanning speed was 200 lines per second, for a total image acquisition time of approximately 40 seconds for the entire field-of-view. To reduce background noise, each line was acquired 8 times, and averaged. The microscope, laser, and image capture were under computer control.

Specimen Preparation. OCE specimens were placed on a glass-bottom 35 mm Petri dish, and wet with a few drops of DPBS to preserve cell viability during the imaging procedure. The Petri dish was placed on the microscope, and *en-face* images were taken at incremental z-steps of either 3 µm, 5 µm, or 10 µm at 4 sites of the TTP-knockdown assay, and 3 sites of the control assay. Vertical cross-section images were taken at 1 site for each of the TTP-knockdown constructs and for the control OCE. All measurements were made in less than 1 hour after removing specimens from incubation conditions.

Image Analysis. Two-photon excited fluorescence images of GFP-expressing cells and SHG images of collagen from the Alloderm® scaffold were pseudo-colored green and blue, respectively, and then merged in 8-bit RGB color format using NIH ImageJ software.

Data Analysis. Cell invasion was assessed by using MATLAB software to analyze z-stack *en-face* SHG channel images to count the number of pixels with intensity values above a certain threshold over the entire field-of-view. The intensity threshold, $I_{threshold}$, is defined to be $I_{threshold} = \mu_{ROI}$, where μ_{ROI} is the mean of the intensity of all non-zero pixels in the region of interest. A decreased number of SHG pixels exceeding the threshold indicated the presence of cancer cells decaying the collagen matrix at the given depth below the surface, which was then plotted as a function of depth to assess cell decay of the collagen matrix by the cancer cells. The mean of the pixel counts was calculated over each *en-face* image of 3 TTP-knockdown assays and 2 control assays, both imaged on day 8 post-seeding, with error bars of one standard deviation of the mean.

Histopathological Studies. OCE constructs were fixed overnight in phosphate buffered formalin (Fisher Scientific). Hematoxylin and eosin staining was performed on tissue sections prepared from fixed OCE constructs, and invasive areas were identified.

RESULTS

Enhanced Invasion of HNSCC Cells with TTP Knockdown is Observed with Both Sub-surface Imaging and Analysis of Fixed Samples

Pro-inflammatory mediators, including cytokines and matrix metalloproteinases, contribute to progression of HNSCC (197, 202, 256). TTP is an RNA-binding protein that induces decay of multiple pro-inflammatory mediators (257). We previously showed that

downregulation of TTP leads to increased production of pro-inflammatory mediators and increased invasion of cancer cells (201). In data presented, HNSCC cells were stably transduced with a short-hairpin RNA (shRNA) construct to downregulate TTP (shTTP) and a control construct (shVSVG). These cells were used to investigate the sub-surface nonlinear optical molecular imaging method to monitor invasion on the OCE constructs and compare the results to parallel histopathological analysis.

HNSCC cells stratified to 2-4 layers, similarly to normal keratinocytes, and developed rete ridges (**Figure C.1D**). Invasive islands beyond the basement membrane were observed on hematoxylin and eosin-stained tissue sections. The increased invasion of cells with downregulated TTP was visualized by hematoxylin and eosin staining of paraffin embedded tissues (**Figure C.3**) and cross-sectional nonlinear optical microscopic molecular imaging of live cells. Control cells formed a generally uniform layer that sits on the OCE scaffold (**Figure C.3A**), whereas TTP-knockdown cells invaded below the OCE scaffold, forming nests of GFP-expressing cells beneath the surface of the OCE (**Figure C.3B**, arrowheads).

Two-photon excited fluorescence images of GFP-expressing cells and SHG images of collagen from the OCE scaffold were pseudo-colored green and blue, respectively, and then merged in 8-bit RGB color format using NIH Image J software. GFP channel images taken near the surface of the assay show a high number of cells in cell lines with or without downregulation of TTP. At 24 μm control cells are no longer visible while TTP-knockdown cells are still visualized, suggesting increased deeper invasion of the TTP-knockdown cells below the surface of the OCE scaffold. A montage

of *en-face* images of the TTP-knockdown OCE from depth 0 μm to 24 μm revealed islands of GFP-expressing cells invading below the specimen surface, visualized as circular rings apparent deep under the surface of the OCE up to 24 μm (**Figure C.4**).

Enhanced Invasion and Basement Membrane Destruction by HNSCC Cells with TTP Knockdown is Quantified with Sub-surface Imaging

Nonlinear optical microscopic *en-face* images of control and TTP-knockdown assays, imaged on day 7 post-seeding, are shown (**Figure C.5A**). The white arrow highlights a cell of interest that appears at depth 24 μm in the TTP-knockdown OCE, but is not present in the same region of the OCE at depth 9 μm. By contrast, in the control OCE many GFP-expressing cells are present in the superficial layers, but GFP fluorescence rapidly decreases with increasing depth below the specimen surface, and no cancer cells are observed in the deep layers.

Figure C.5B shows the number of SHG pixel counts over the entire field-of-view of the *en-face* images, as a function of depth below the surface. The pixel counts are averaged at each depth for 3 TTP-knockdown data cubes and 2 control data cubes, acquired on day 8 post-seeding, and error bars are equal to one standard deviation of the mean. More SHG is present in the top 20 μm of the TTP-knockdown OCE assays than the control assays. From 20-40μm below the surface, SHG levels in the TTP-knockdown assays drop below that of the control assays, and SHG rapidly decreases in the TTP-knockdown assays deeper than 40 μm below the surface. This indicates the increased decay of the collagen matrix by TTP-knockdown cancer cells compared to control cells. Furthermore, the higher level of SHG in the superficial layers of TTP-knockdown assays

suggests increased cell invasion, compared to controls assays where a thick layer of cancer cells stack on the surface of the OCE.

DISCUSSION

Comparison of the OCE with Other Methods

Both two-dimensional (2D) and 3D approaches have been utilized to investigate cancer progression in vivo. An example of a 2D migration model is the scratch assay, where cancer cells growing in a tissue culture dish migrate into an area devoid of cells (201). Cancer cells in 2D culture lack cell-matrix interactions that influence the phenotype and protein expression of these cells, and therefore 3D approaches are preferred to study invasion (258).

Some 3D culture approaches use a collagen matrix composed of proteins derived from an extracellular matrix to create a structure to simulate invasion. In addition, an in vitro cell-layering approach to development of 3D tissues has been described (259). Synthetic matrix-based invasion assays are useful in vitro for preliminary studies to evaluate changes in the invasive phenotype after manipulating proteins of interest in cells, but have significant limitations including the absence of a basement membrane structure and lack of the structural complexity of the connective tissue. In addition to the inadequacy of many in vitro approaches, most mouse models of human HNSCC are also inadequate to investigate invasion because tumor cells are injected directly into the connective tissue, thereby bypassing the basement membrane of the surface epithelium.

Some 3D cancer models emphasize the aggregation of cells and have a variety of advantages and disadvantages (260). A number of models depend on spontaneous aggregation of cells (261), but can only be adapted to study a limited array of cancer types. Microcarrier beads are inexpensive and support 3D structures grown in cell culture (262), but the spheroids generated are mostly made up of beads. Engineered scaffolds are expensive and difficult to use in culture, but are biodegradable and can be used in both in vivo and in vitro settings (263).

The OCE model is advantageous because the commercially available human-derived dermal matrix is used. As demonstrated, live imaging and histopathological studies are feasible with the OCE model. A heterogeneous population of cells can be introduced in the OCE system. The system can be adapted to a wide variety of cell types, and AlloDerm® grafts can be used for both in vivo and in vitro studies.

Potential Applications of the OCE Method

The OCE model described in this protocol provides an exciting opportunity to evaluate the invasive phenotypes of individual cancer cell lines in a 3D assay and to evaluate the impact of altered protein expression on invasion. Virtual histopathology of live cells on an OCE construct can be derived through sub-surface nonlinear optical microscopy to observe and quantify invasion of cancer cells (264, 265). Subsequently the constructs can be fixed for light microscopy, including immunohistochemistry studies. The OCE model can be adapted to study the progression of many tumor types by altering the cell lines and culture conditions used.

Three dimensional culture systems that preserve cell-matrix interactions are indicated for regenerative tissue applications because they preserve stem cell phenotypes (266) and facilitate epithelial-mesenchymal transition (EMT) (267), which has been shown to mediate invasion of HNSCC cells (79). Application of this imaging technique will be useful to optimize previously described protocols that generate 3D constructs to replicate normal tissue, such as normal oral (268) and airway (269) mucosa. In addition, adaptation of the imaging methodology described in this protocol may be an interesting application to view cellular changes in a recently published protocol describing viral infection of human tissue explants (270).

Limitations of the OCE Method

The main advantages of the OCE method over other in vitro methodologies include the invasion of cancer cells in the connective tissue stroma after disruption of the basement membrane, thereby simulating intraoral HNSCC. In addition, the procedure allows for stratification of cultured cells and growth of the cells in a 3D setting with complex cell-cell and cell-matrix interactions. However, the OCE model has some limitations. HNSCC involves multiple epithelial-stromal interactions, including interactions between cancer cells and fibroblasts, blood vessels, immune cells and nerves. Although the OCE construct described here does not contain other cell types involved in the disease process, the model can be modified to add different cell types. Because the OCE method takes several days, it is necessary to transfect cells with a GFP tag rather than use a fluorescent dye, which will degrade over the duration of the experiment. The model also requires significant optimization. The number of cells, cell culture conditions,

concentration of chemoattractant used, and the time of harvesting all must be determined during optimization studies. Sub-surface imaging on sequential days helps to determine optimal timepoints for harvesting the OCE for histopathological studies.

In summary, the OCE method is a novel approach of preparing an in vitro model of HNSCC using human cancer cell lines and decellularized human cadaveric dermis. Furthermore, the in vivo imaging method described here and the comparison to histology from paraffin-embedded tissue sections will be useful to monitor many types of 3D tissue constructs.

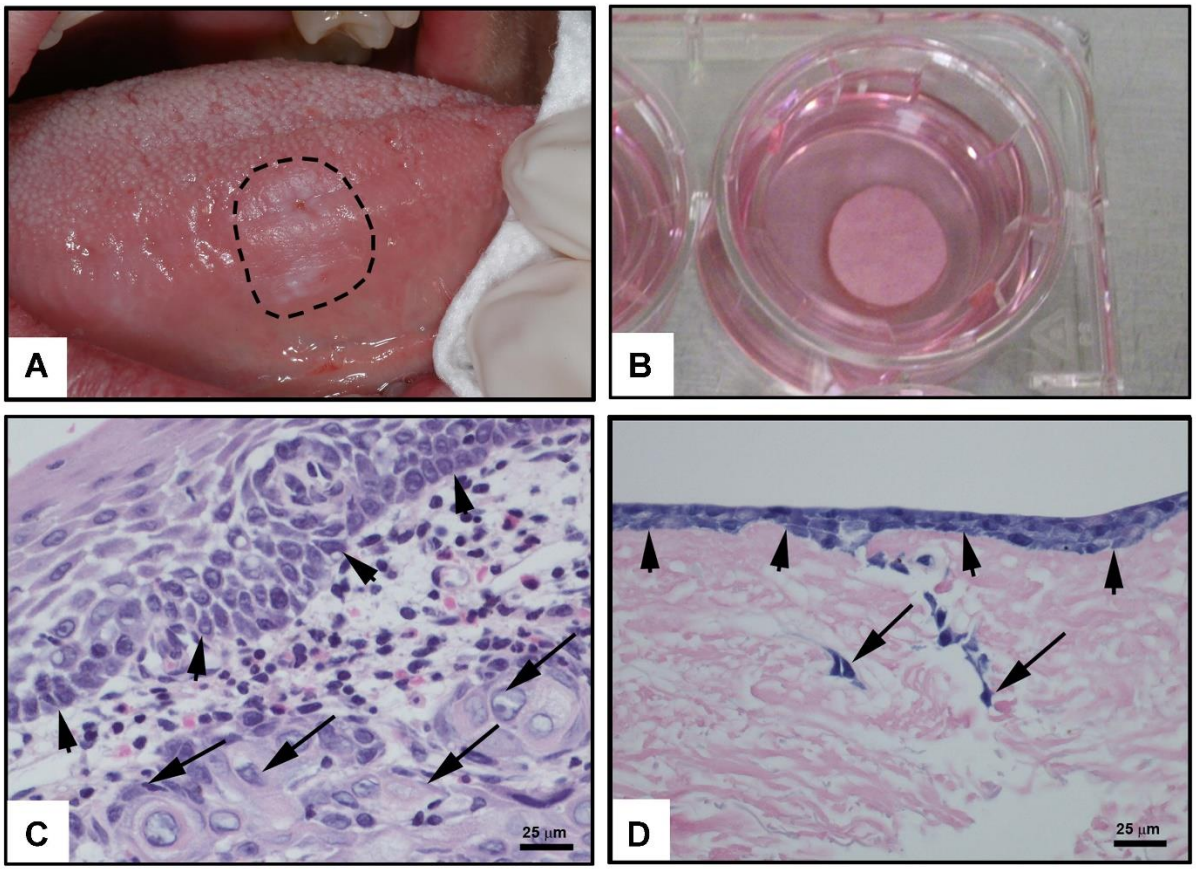

Figure C.1: Histological comparison of HNSCC and OCE model. A. A lesion that presented clinically as a leukoplakia was subsequently diagnosed as HNSCC. **B.** Formalin-fixed OCE and OCE tissues in culture are shown. Histology of human HNSCC (**C**) and of an OCE (**D**) shows invasion in both specimens. Arrowheads point out the basement membrane and arrows show invading cancer cells.

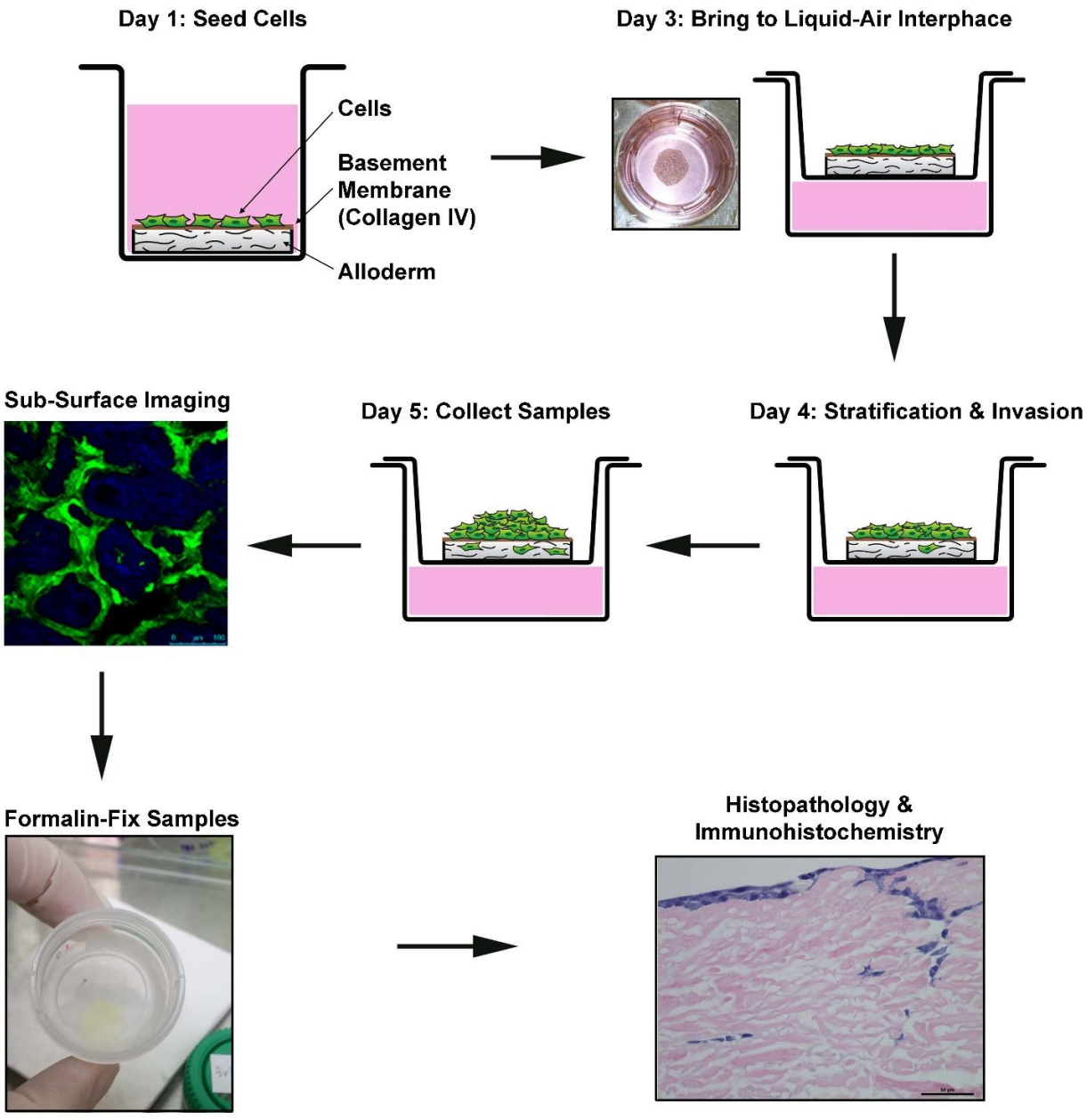

Figure C.2: Overview of OCE protocol. HNSCC cells are plated on hydrated decellularized human cadaveric tissue coated with collagen IV on day 1. On day 3 the OCE is brought to the liquid-air interface and invasion of HNSCC cells occurs through day 5, when sub-surface imaging of live cells is performed. The OCE tissues are then fixed, paraffin-embedded and processed for histopathological and protein expression studies.

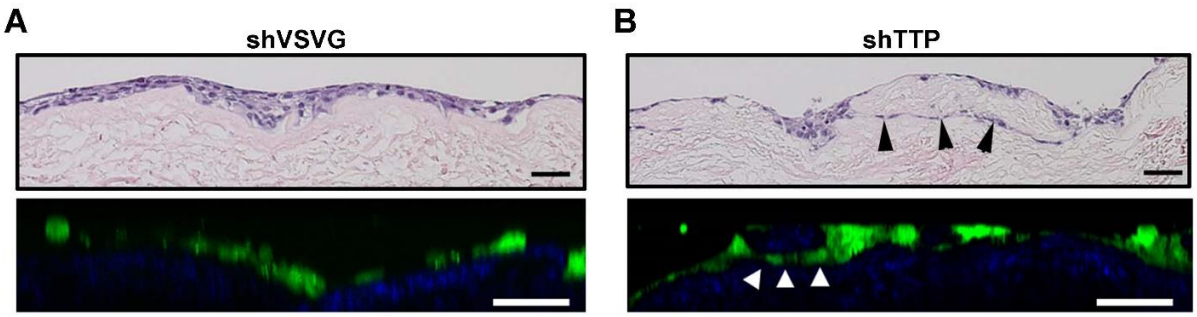

Figure C.3: Comparison of OCE histology produced via hematoxylin-eosin staining and nonlinear optical microscopic molecular imaging. The vertical cross-section image of the OCE with control HNSCC cells (**A**) shows cells forming a layer on top of the tissue scaffold with little invasion below the surface, whereas the OCE with HNSCC cells with downregulated TTP (**B**) shows cells invading below the surface, forming nests of cells within the connective tissue. The quality of vertical cross-section images is degraded as compared to *en-face* images, due to the inherent poorer resolution of non-linear optical microscopy in the axial dimension, and scattering effects when imaging deep below the tissue surface. Bars=50 µm.

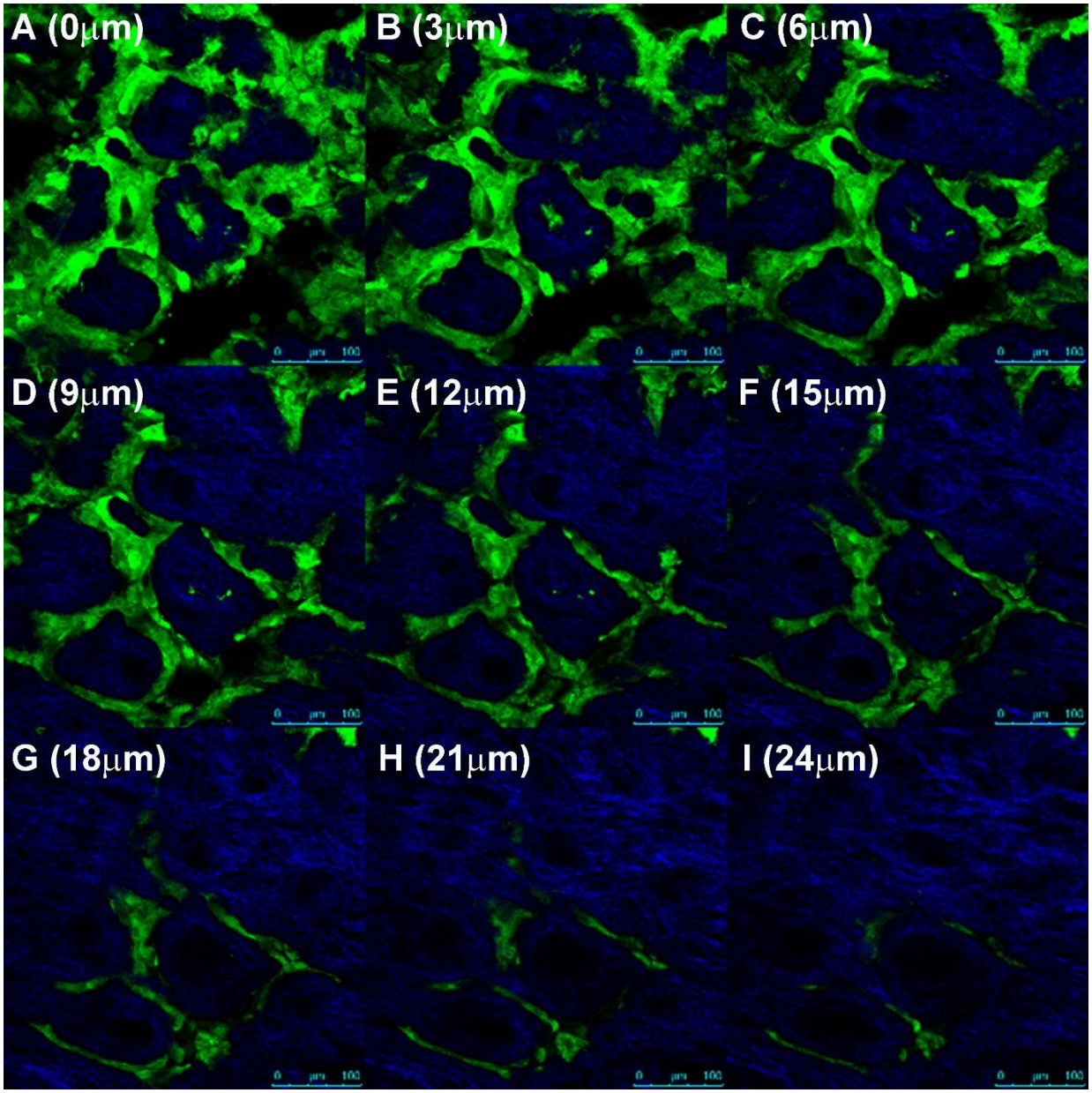

Figure C.4: *En-face* image montage of UM-SCC-1-shTTP cells in the OCE at 3 μm depth increments below the surface of the OCE. GFP-expressing cells form strings of cells invading below the surface of the assay, visualized as green rings that are apparent in all *en-face* images from the surface to a depth of 24 μm. Scale bars = 100 μm.

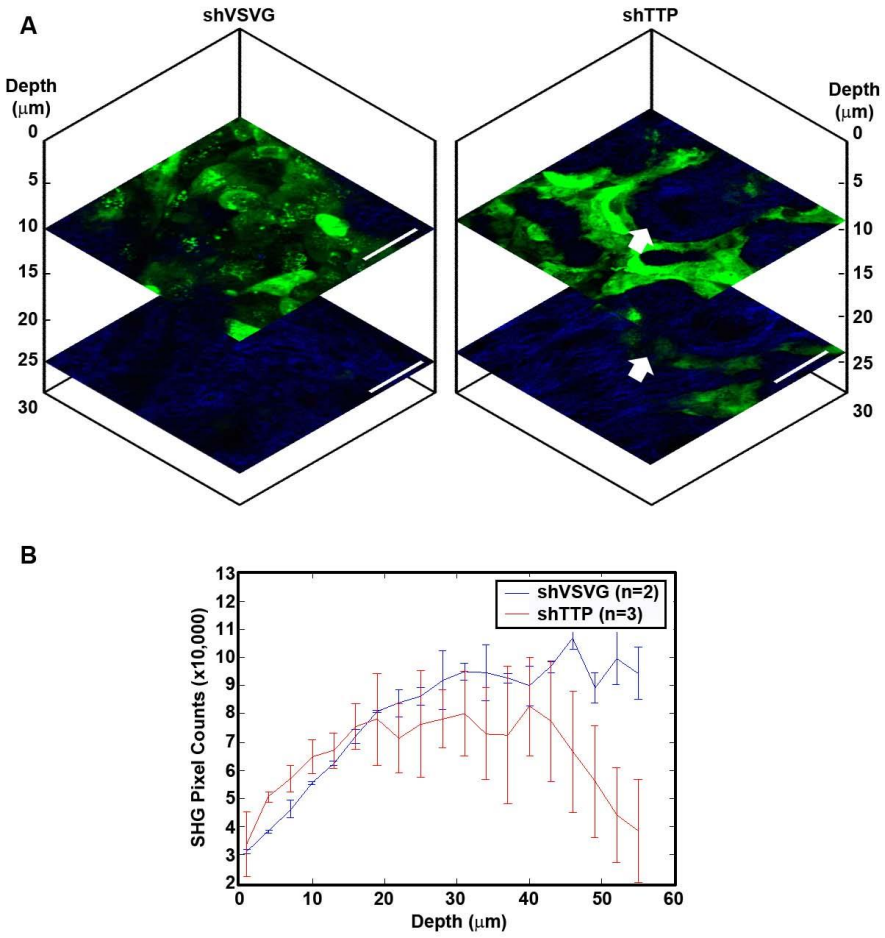

Figure C.5: Vertical stack of depth-resolved *en-face* nonlinear optical microscopic molecular images of OCE immunofluorescence assays, and quantification of SHG pixel counts as a function of depth. Representative data cube of a 3D stack of *en-face* images taken of control and TTP-knockdown OCE assays 7 days post-seeding are shown (**A**). Green indicates 2-photon excited fluorescence from GFP-expressing UM-SCC-1 cells. Blue shows second harmonic generation (SHG) from collagen, in decellularized human cadaveric dermis scaffold of the OCE. Whereas the control cells (left) are no longer visible in the deeper tissues of the dermis, cells with downregulated TTP (right) are still visible at 24 μm below the surface, indicating that these cells are invading through the tissue scaffold. The white arrow highlights a region of interest where an invading cell is present at a depth of 24 μm, but is not present in the same region of the OCE at a depth of 9 μm. Bars=50 μm. The number of SHG pixel counts over the entire field-of-view of the *en-face* images, as a function of depth below the surface, was quantified for 3 TTP-knockdown data cubes and 2 control data cubes of OCE assays imaged 8 days post-seeding (**B**). TTP-knockdown assays have higher SHG content in superficial layers than control assays, but rapidly lose SHG signal in the deeper layers compared with control assays, suggesting decay of the collagen matrix by invading cancer cells.

APPENDIX D

The Chick CAM Assay, a Novel Model of Head and Neck Squamous Cell Carcinoma

Appendix D is adapted from a published manuscript (66).

INTRODUCTION

Although the CAM assay has been in use for many years, the benefits of studying tumor invasion using this model are more recently recognized. The CAM is a highly vascularized membrane that is located directly below the egg shell. This makes the CAM easy to access through a small hole in the egg shell. The CAM is also made up primarily of collagen IV, which simulates the basement membrane of human oral epithelium. The CAM assay has been used to measure invasion of a variety of cell types, including fibroblasts (271) and several types of cancer cells, including melanoma cells (272-274).

We propose that the chick embryo is an excellent model of invasion and metastasis of human HNSCC. The CAM consists of the chorionic epithelium separated from the underlying allantoic membrane by connective tissue. The chorionic epithelium is separated from the connective tissue by an epithelial-derived basement membrane that contains collagen IV (275). The cellular connective tissue contains types I and III collagen and blood vessels. In this model, HNSCC cells are seeded on top of the CAM and allowed to invade. Thus, the CAM recapitulates intraoral human HNSCC progression including disruption of the basement membrane, complexity of the connective tissue,

angiogenesis and metastasis. Even the histopathologic features simulate invasion observed in HNSCC. Destruction of the basement membrane can be easily visualized and tumor growth, invasion into the connective tissue, and metastasis can be accurately quantified, making this a valuable model for investigating progression of HNSCC.

In this study, we describe for the first time the use of the CAM to investigate multiple tumorigenic phenotypes simultaneously, including tumor growth, invasion, metastasis and angiogenesis in HNSCC. Recently, we showed that EZH2 (enhancer of zeste homolog 2), the histone methyltransferase, promotes progression of HNSCC by inducing multiple cancer phenotypes, likely via methylation of multiple tumor suppressor genes (71, 75). In order to develop the CAM model, we investigated the role of EZH2 in tumor growth, angiogenesis, invasion and metastasis in vivo. In addition, we show the role of EZH2 in epithelial-mesenchymal transition (EMT) in mouse tumors, CAM tumors and in HNSCC cell lines. Overall, we are able to establish the CAM model of HNSCC and investigate the role of EZH2 in several hallmarks of tumor progression.

METHODS

CAM in vivo Model of HNSCC Tumor Progression. The University of Michigan Unit for Laboratory Animal Medicine was consulted regarding ethical use of the chicken embryo CAM for experiments.

Dropping the CAM. Fertilized commercial Lohmann White Leghorn eggs were obtained from the Michigan State University Department of Animal Sciences Poultry

Farm. Prior to hatching, the eggs were maintained at 24ºC. Eggs were subsequently "hatched" in a humidified incubator (Digital Sportsman Incubator; G.Q.F. Manufacturing) at 38°C with 60% humidity. The initial day of incubation is considered day 0. On day 11, the following structures were labeled on the egg using the ACE light source (Trevigen Inc.): large blood vessel, umbilical cord, air sac, small square window for the artificial air sac generation and a large window area for seeding cancer cells. Using a Dremel 1100-N/25 7.2- Volt Stylus Lithium-Ion Cordless Rota (Robert Bosch Tool Company), a 1 cm^2 window was drilled on the top of the egg shell, maintaining the outer egg shell membrane. A pinpoint hole was prepared on the side of the egg at the location of the airsac. Twenty five microliters of HBSS (Invitrogen, Life Technologies) was added on top of the 1 cm^2 window at the top of the egg. Then, using a 30½ gauge needle, the outer eggshell membrane was punctured at the location of the window so that the buffer separates the outer eggshell membrane from the CAM. The small pinpoint hole was vacuumed using a Pasteur pipet bulb, causing the air bubble to move to the window and allowing the CAM to drop. Then the egg shell was drilled in the large window area and blunt ended forceps were used to peel off the eggshell membrane without disturbing the CAM. The large square hole was covered with parafilm and the egg was place in the incubator without shaking.

Seeding HNSCC Cells. HNSCC cells ($1x10^6$) were resuspended in 5 µl of Hank's Balanced Salt Solution (HBSS). The pipette was used to make a bead of cell and medium that is dropped onto the CAM surface, without allowing the pipette tip to touch

the CAM. The square window on the egg was sealed with Tegaderm HP Transparent Film Dressing. The eggs were incubated without shaking for approximately 3 days.

Harvesting the CAM. Using a needle and syringe, a small amount of 4% paraformaldehyde was injected onto the surface of the CAM. Dissecting scissors were used to cut open the large window to visualize the CAM and the tumor. Using scissors and a pair of forceps, each CAM was lifted and cut around the tumor. The tumors and surrounding CAM were transferred to a 6-well dish containing 4% paraformaldehyde and incubated at 4°C for 4 hours. The CAMs were transferred to cold 30% sucrose and stored overnight at 4°C. The next day, the CAMs were embedded in Optimal Cutting Temperature Compound (Tissue-Tek) and frozen at -80°C until sectioning and staining. 8-10 µm tissue sections were fixed in 4% paraformaldehyde for 5 minutes followed by staining with hematoxylin and eosin.

Endpoint Assays. For tumor growth and angiogenesis studies, suspensions of $5x10^5$ HNSCC cells with stable knockdown of EZH2 or controls were suspended in 5 µl HBSS and plated on the upper CAM. The window on the egg shell was resealed with adhesive tape and eggs were returned to the incubator for 48 hours before harvesting the tumor (n=5 chick embryos per experimental group). Surface area of the tumors was quantified using ImageJ software and statistically compared between control tumors and tumors with stable EZH2 knockdown. Angiogenesis was also quantified using red color density within 200 µm of tumors in images using ImageJ software

(http://rsbweb.nih.gov/ij/) with the Colour Threshold plugin provided through the University of Birmingham School of Dentistry website.

(http://www.dentistry.bham.ac.uk/landinig/software/software.html).

For invasion assays, cells were dyed with the lipophilic tracer, DiO (a dialkylcarbocyanine derivative) prior to experiments. Tumor sections were imaged at 20x and invasive islands were quantified for each image. Statistical analysis to compare the number of invasive islands was performed.

For collagen IV staining, the frozen tissue sections were fixed in methanol, washed in PBS and blocked with 0.1% BSA, 10% NGS in PBS for 30-60 minutes. The collagen IV antibody was diluted 1:1 in 0.1% BSA, 5% NGS and incubated on the tissue sections for 2 hours. The coverslips were mounted with Prolong Gold Antifade reagent with DAPI (Invitrogen, Life Technologies).

For metastasis experiments, HNSCC cells were plated as described for invasion studies at day 8. The lower CAM, liver and lungs were collected at day 16. Human DNA was quantified from DNA extracted from the harvested tissues using alu-PCR to compare metastasis from control and EZH2 knockdown tumors. To generate the standard curve, genomic DNA from human HNSCC cells (each human cell contains 6.6 pg of DNA) was mixed with 1 µg of chicken genomic DNA in logarithmically increasing concentrations as 0.1, 1.0, 10, 100, 1000, and 10000 cells. PCR was performed in triplicate for each of the standards as well as the experimental samples. The absolute number of metastatic human cells in the experimental sample was calculated from the standard curve using linear regression.

Cell Culture. The HNSCC cell line, UM-SCC-29 (from T. Carey), used in this study was validated by genotyping at the University of Michigan DNA Sequencing Core, and cultured as described (202, 246). Cells were maintained in DMEM (Gibco, Life Technologies) supplemented with 10% FBS and 1% PenStrep. EZH2 in HNSCC cells was stably downregulated as described (71); scrambled shRNA (shSCR) was used for control cells and shEZH2 for EZH2 knockdown cells (Open Biosystems). Cells were selected with puromycin (Sigma-Aldrich).

Immunoblot Analysis. Immunoblot analysis was performed as previously described (197). 1% NP40 lysis buffer was used to lyse HNSCC cells. EZH2 (BD Biosciences, San Jose, CA) and GAPDH (Millipore) primary antibodies were used. The secondary antibody used was horseradish peroxidase-conjugated anti-mouse (Jackson Immuno-Research Laboratories). SuperSignal West Pico Chemiluminescent system (Thermo Scientific) was use to visualize immunoreactive proteins and ImageJ software was used to quantify signal intensity (http://rsbweb.nih.gov/ij/).

Immunohistochemistry. Immunohistochemistry of tissue sections was performed as described (246). The primary antibodies used were vimentin (Proteintech) and E-cadherin (BD Biosciences) and biotinylated goat anti-rabbit and biotinylated goat anti-mouse secondary antibodies were used (Biocare Medical). Imaging of cells was performed at the Microscopy and Image Analysis Core at the University of Michigan on an Olympus BX-51 microscope. Representative fields were imaged at 20x.

Murine Model of HNSCC Using Subcutaneous Injection. Athymic nude mice were used as described (276). UM-SCC-29 cells (1 x 10^6) were stably transduced with shSCR or shEZH2 and injected subcutaneously to assess tumor growth (272). Histopathologic analysis of these tumors is shown in the present study.

Immunofluorescence Detection of Vimentin and E-cadherin. Cells were labeled with vimentin (Proteintech) and E-cadherin (BD Scientific) primary antibodies diluted in 0.3% triton X-100 overnight at 4ºC, washed, and incubated for 2 hours at room temperature in an appropriate conjugated secondary antibody, washed and incubated in DAPI (1:3000) for 3 minutes. Imaging of cells was performed at the Microscopy and Image Analysis Core at the University of Michigan on an Olympus BX-51 microscope. Representative fields were imaged at 100x.

Data Analysis. Statistical analysis was performed using Student's *t*-test using GraphPad Prism (GraphPad Software). A *P*-value of <0.05 was accepted as statistically significant.

RESULTS

EZH2 Enhances HNSCC Tumor Size on the CAM

Using the CAM in vivo model, we investigated the impact of EZH2 on tumor growth in HNSCC. EZH2 is a master regulatory gene in HNSCC that inhibits expression of tumor suppressor genes (71). UM-SCC-29 cells with stable knockdown of EZH2 (UM-SCC-29-shEZH2) and corresponding control cells with empty vector (UM-SCC-29-shSCR) were seeded on the CAM (n = 5 for each group). After 48 hours, the upper CAM was harvested

from each chick embryo and the surface area of the tumors was quantified (**Figure D.1A**). shRNA-mediated EZH2 knockdown was confirmed by immunoblot (**Figure D.1B**). UM-SCC-29-shEZH2 cells produced tumors that were significantly smaller than tumors generated by control cells (P = 0.0460, **Figures D.1A**, dashed lines and **Figure D.1C**). Although the difference in size between control and EZH2-deficient tumors is significant, the variability in tumor size led to a higher p-value than anticipated. A larger sample size may have provided a lower p-value to better reflect the difference in tumor size between the groups. Additionally, because since some tumors appear to be more bulky than others, 3D analysis of tumor size may provide a more consistent estimation of tumor size.

EZH2 Promotes Angiogenesis of HNSCC Tumors on the CAM

To investigate the impact of EZH2 on tumor-associated angiogenesis, the area of blood vessels within 200 μm of the tumors were quantified. shEZH2 tumors had decreased blood vessel area adjacent to tumors compared to controls, indicating decreased angiogenesis of the tumors (P = 0.0348, **Figures D.1A**, arrows and **Figure D.1D**).

EZH2 Enhances Basement Membrane Disruption and Invasion of HNSCC Tumors on the CAM

Tumors produced by UM-SCC-29-shSCR and –shEZH2 were harvested and sectioned. Collagen IV staining was performed on the section to visualize disruption of the basement membrane on the upper CAM. Tumors produced with UM-SCC-29-shSCR control cells showed more disruption of the basement membrane than tumors with stable

knockdown of EZH2 (**Figure D.2A**). This correlated with an increased number of invasive tumor islands in UM-SCC-29-shSCR tumors than in tumors from cells with downregulation of EZH2 (**Figure D.2B**, $P = 0.0053$).

EZH2 Promotes a Mesenchymal Phenotype of HNSCC In Vitro and of Murine and CAM Tumors

Previously, we established that downregulation of EZH2 inhibited tumor growth in mice (71). Control tumors, expressing high EZH2, exhibited an aggressive phenotype including cells, with large nuclei, little cytoplasm, and spindled morphology (arrows), invading skeletal muscle (arrowheads) (**Figure D.3A**, upper panel). In contrast, tumors with EZH2 knockdown (**Figure D.3A**, lower panel) exhibited well differentiated epithelial cells (keratin formation; arrowheads) with increased cytoplasm (arrows), a less aggressive, more epithelioid phenotype. To verify the impact of EZH2 on epithelial-mesenchymal transition, UM-SCC-29-shEZH2 and -shSCR cells were plated at 60% confluence and fixed. Immunofluorescence labeling of vimentin and E-cadherin were performed, and 5 representative fields were imaged at 100x (**Figure D.3B**). Intensity of fluorescence was quantified and normalized to the average intensity of shSCR cells. Control cells have a more mesenchymal phenotype with increased vimentin ($P < 0.001$) and decreased E-cadherin (p=0.0342) compared to cells with EZH2 knockdown (**Figure D.3B**). These findings are consistent with EZH2 inducing an EMT phenotype. In addition, immunohistochemistry was performed for vimentin and E-cadherin expression on CAM tumor sections from shSCR and shEZH2 treated cells (**Figure D.3C**). Tumors with EZH2

knockdown had decreased vimentin expression (arrows) and higher E-cadherin staining (arrows) than control tumors.

EZH2 Promotes Metastasis of HNSCC Tumor Cells on the CAM

The invasive phenotype of tumor cells facilitates extension into the surrounding structures and spread to distant sites (metastasis) via the blood vessels. In the CAM model, metastasis requires invasion of cells through the basement membrane of the surface epithelium and into the blood vessels. Since EZH2 promotes invasion, we also investigated its effect on metastasis using the CAM model. UM-SCC-29-shSCR and shEZH2 cells were incubated on the CAM of day 7 chick embryos. The eggs were incubated until day 15, when the lower CAM and liver of the developing chick were harvested. The metastasized human cells in the chicken background were quantified as described by qPCR for amplification of human Alu sequences (85, 277), which eliminates cross-reactivity with chicken DNA. When using control UM-SCC-29 cells, metastases were detected in all lower CAM specimens and 4/5 of the livers of the developing chicks. However, when using cells with reduced EZH2 expression, no metastases were detected in either the lower CAM or liver in any samples (**Figures D.3D** and **Figure D.3E**, P = 0.0151).

DISCUSSION

Over the past decade, the histone methyltransferase EZH2 has emerged as a key player in tumor progression in many cancer types, including HNSCC (71) breast (278, 279), bronchial (280), lung (281) and prostate (282). Overexpression of EZH2 is often

linked to poor prognosis and advanced disease (283). EZH2 expression is also correlated to increased angiogenesis in tumors (284), in part due to paracrine signaling between tumor cells and associated vasculature (285). EZH2 has also been shown to have a role in cancer stem cell maintenance (286).

Our laboratory recently showed that EZH2 contributes to HNSCC progression by hypermethylating the promoter region of the tumor suppressor Rap1GAP (71, 75). We found that EZH2 is upregulated in HNSCC cell lines compared to normal keratinocytes, and that EZH2 promotes tumor growth in vitro and in vivo in the mouse model. In our previous study we also evaluated the role of EZH2 in invasion using in vitro assays, and found that EZH2 expression is highly correlated with HNSCC cell invasion (71). However, we were unable to evaluate the impact of EZH2 on early invasive phenotypes i.e. destruction of the basement membrane of surface epithelium since in the mouse model, tumor cells are injected directly into the connective tissue. Invasion beyond the basement membrane is required for transformation of a pre-cancerous lesion (epithelial dysplasia) to HNSCC (287).

In our current study, we chose the CAM in vivo model of tumor progression to validate our previous in vitro findings about the role of EZH2 in tumor invasion. In this study, which is to our knowledge the first study to describe the use of the CAM model to investigate tumor progression of HNSCC, we show that downregulation of EZH2 in HNSCC cells inhibits destruction of the basement membrane and decreases invasion in vivo. In addition, we show that EZH2 mediates angiogenesis, growth and metastasis of HNSCC.

There are many benefits of using the CAM to study tumor progression (288). The CAM assay is completed in a short time period and is relatively inexpensive compared to most in vivo models. The lack of a mature immune system at the time the assay is performed allows for use of different cell types, and cells from different species. Because the chicken embryo has been used scientifically for centuries, the system is well described in the literature. Limitations of the assay include the extensive optimization and the large number of eggs that are required to obtain consistent results. As in other in vivo systems, tumors produced on the CAM exhibit some variability. Therefore, it is appropriate to use a sample size of at least 5 eggs per group to characterize differences.

In addition to establishing the CAM model of HNSCC tumor progression, we also evaluated the role of EZH2 expression on the histopathological presentation of HNSCC tumors and on the expression of the EMT markers vimentin and E-cadherin. EMT is a process by which non-motile cells lose contact with neighboring cells and become more motile (180). EMT has been shown to promote HNSCC invasion, metastasis and tumor stemness (287). While control cells produced aggressive, mesenchymal-like tumors in vivo, tumors produced from HNSCC cells with reduced EZH2 expression had a more epithelial-like appearance, consistent with a less aggressive tumor. In addition, knockdown of EZH2 leads to decreased vimentin and increased E-cadherin expression in HNSCC cells and CAM tumors. These findings indicate that EZH2 plays a role in mediating EMT in the HNSCC cell line UM-SCC-29. We have previously shown that EZH2-mediated invasion is not dependent on E-cadherin alteration in the E-cadherin deficient cell line, OSCC3. Therefore, other factors that are still under investigation have a role in EZH2-mediated EMT, independent of E-cadherin (75).

Our study investigating the role of EZH2 in tumor progression is the first to describe the use of the CAM model to study progression of HNSCC. The CAM model can be used to investigate tumor size, angiogenesis, invasion and metastasis of HNSCC. In addition, we show that knockdown of EZH2 expression in HNSCC cells leads to less aggressive tumors with a more epithelial-like phenotype. Together, these studies highlight the emerging role of EZH2 in HNSCC progression. Future studies will elucidate the mechanistic role of EZH2 in EMT. In addition, the role of EZH2 inhibitors should be explored as a therapeutic option for HNSCC treatment.

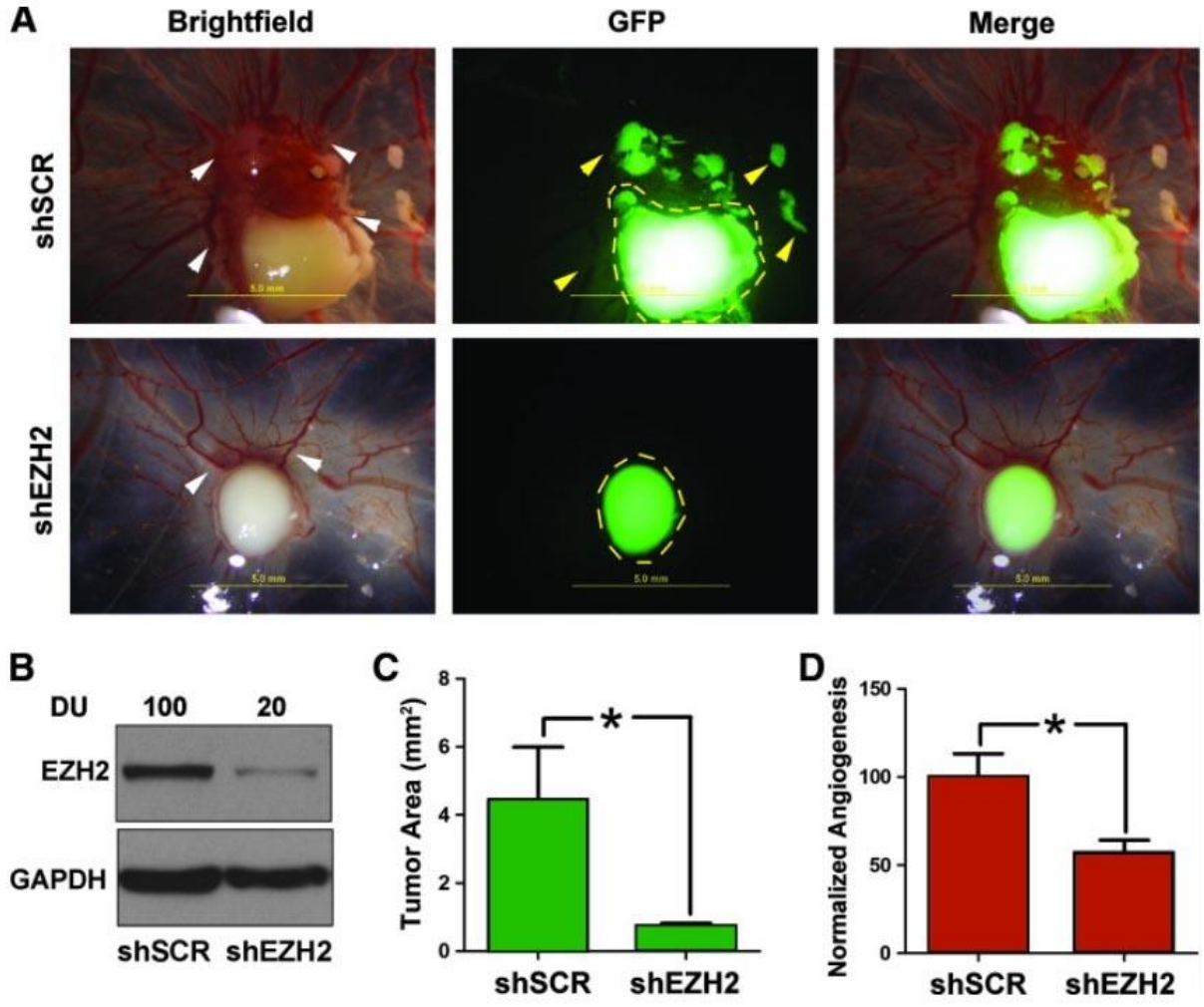

Figure D.1: EZH2 promotes tumor growth and angiogenesis. Fluorescently-labeled UM-SCC-29-SCR and –shEZH2 cells were seeded on the CAM. The upper CAM and tumors were collected 2 days later to analyze tumor growth and angiogenesis. White arrowheads show blood vessel growth approximating tumor (**A**, brightfield images). Dashed lines outline tumor generated from HNSCC cells on CAM (**A**, GFP images). Yellow arrowheads identify tumor islands migrating from primary tumor (**A**, GFP images). shRNA-mediated EZH2 knockdown was confirmed by immunoblot (**B**). The average tumor growth and blood vessel density was calculated for both shSCR and shEZH2 tumors (n=5 for each group). Tumor size (**C**) and angiogenesis (**D**) were significantly decreased for shEZH2 tumors compared to control tumors.

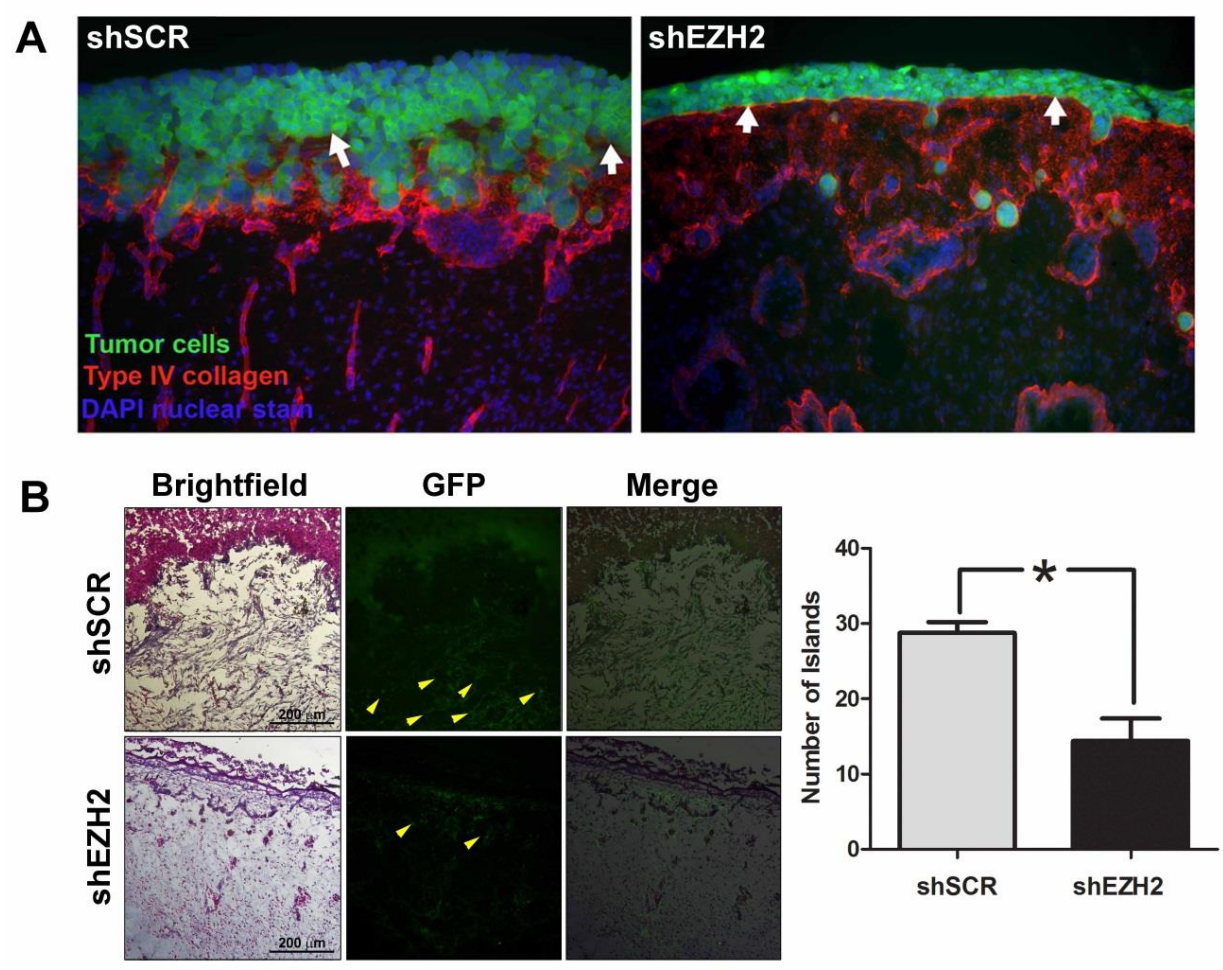

Figure D.2: EZH2 promotes destruction of the basement membrane and invasion. Arrows (**A**) identify the basement membrane structure and tumor cells are labeled green. shSCR tumor cells are highly proliferative and invasive, and destroy the basement membrane structure, but shEZH2 cells do not disrupt the basement membrane. Fewer invasive tumor islands (**B**) are observed on the histology of shEZH2 tumors than control tumors.

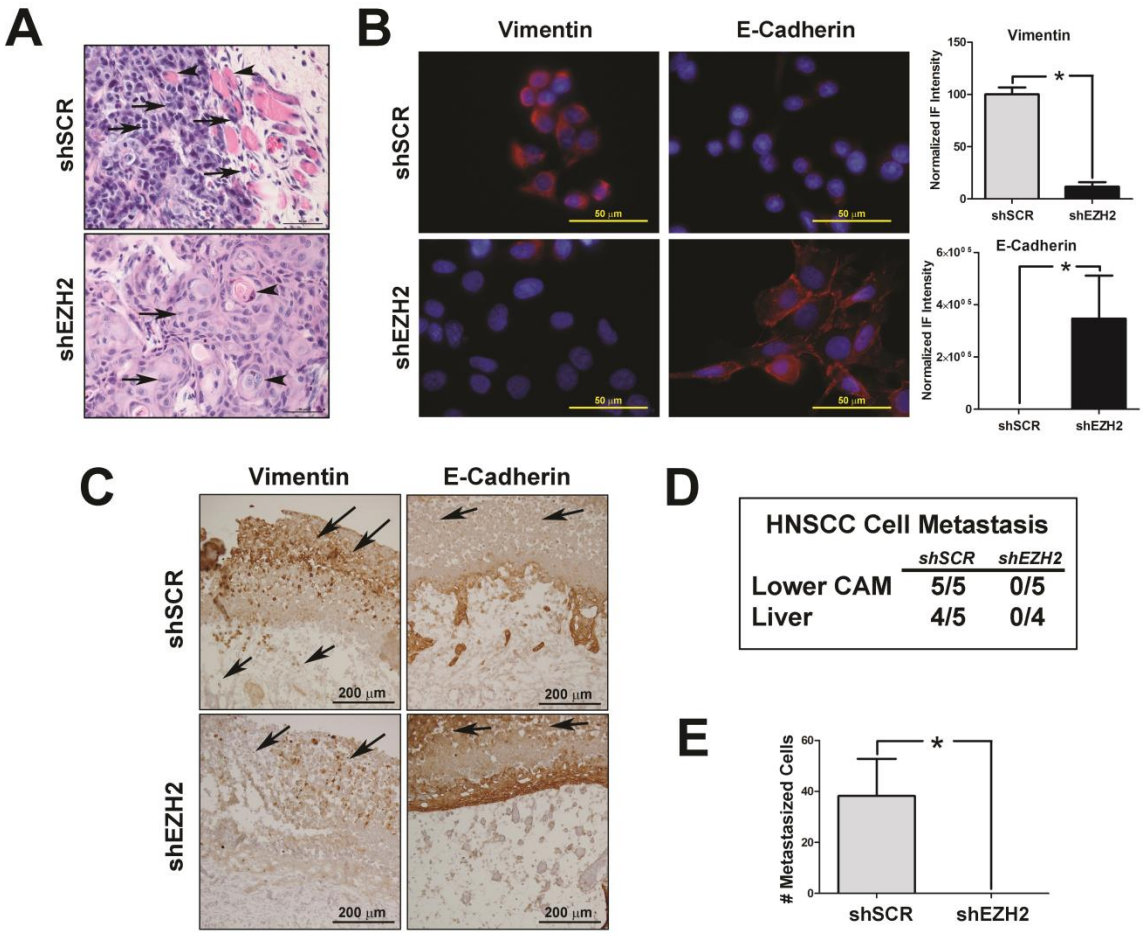

Figure D.3: EZH2 promotes EMT and metastasis of HNSCC. **A**. Histopathologic appearance of HNSCC tumors induced by UM-SCC-29-shSCR and -shEZH2 cells in mice. Control tumors (upper panel) exhibit an aggressive and mesenchymal phenotype with large nuclei, little cytoplasm and spindled morphology (arrows) and invasion into skeletal muscle (arrowheads). Knockdown of EZH2 (lower panel) leads to more epitheloid, well-differentiated tumors containing cells with increased cytoplasm (arrows) and keratin formation (arrowheads). To verify the impact of EZH2 on epithelial-mesenchymal transition, immunofluorescent labeling of vimentin and E-cadherin were performed and representative fields were imaged at 100x (**B**). Relative fluorescence was measured for 5 representative fields and quantified. Control cells have a more mesenchymal phenotype with increased vimentin ($p<0.001$) and decreased E-cadherin ($P=0.0342$) compared to cells with EZH2 knockdown. HNSCC cells were seeded on the CAM and the lower CAM and liver were collected at day 15. Immunohistochemistry of EMT markers on CAM sections shows decreased vimentin (arrows, **C**) and more intense E-cadherin expression of tumor cells (arrows, **C**) for shEZH2 tumors compared to shSCR tumors. Metastases were observed to both the lower CAM and liver for controls but no metastases were observed for any shEZH2 tumors (**D** and **E**).

APPENDIX E

Personalized Medicine Strategies for Cancer Treatment: Lessons Learned from Tumor Antigens

Appendix E is adapted from a published manuscript (248), which is a commentary of a published research article (289).

HNSCC is among the 10 most common cancers in the world. Nearly half of the 600,000 individuals affected globally will die of the disease within 5 years of diagnosis (1). If HNSCC is detected early, the prognosis is favorable. Due to late detection, most patients are at risk for recurrence and metastasis, which contribute to morbidity (1). To improve patient survival, robust screening tests are necessary to discover HNSCC at an early stage. Moreover, a biomarker-based approach may assist in management of HNSCC to improved treatment outcomes (290).

Tumor antigens are proteins specifically expressed by tumor cells and recognized by the immune system of the host (291). The immune response can be characterized to identify a cancer-specific signature (292). Novel cancer-specific autoantibody signatures can be used as a screening tool for early detection, allowing for effective treatment. Moreover, because cancers are heterogenic diseases, disparities in treatment response,

for example resistance or sensitivity to chemotherapy, are likely linked to a specific tumor antigen repertoire. With the information about the tumor provided by its antigen signature, the most appropriate targeted treatment can be selected. Our laboratory recently explored the immune response to identify a novel antibody signature specific to HNSCC (289). Overall, the major findings of this study were 3-fold. First, we used phage display and a liquid ELISA assay to develop an antibody signature for HNSCC. Next, using an in silico approach, we nominated tumor antigens for functional validation. Finally, we validated L23 as an oncogene through multiple in vivo and in vitro approaches.

Using phage display to enrich the antibody response to tumor antigens, we identified previously undescribed tumor antigens in HNSCC. In the phage display technique, bacteriophage vectors are used to display tumor antigens. Using these phages as bait, antibodies specific for HNSCC were enriched via biopanning. An immunomic array was constructed from the enriched phages and used to screen additional control and HNSCC sera. The clones most specific for HNSCC were validated by the Luminex 200™ system. Ultimately, we identified a HNSCC-specific signature including in-frame proteins, one of which was L23. Finally, using in vitro and in vivo approaches, we validated L23 as an oncogene. An important aspect of the recent study was the use phage libraries from tumors at different sites to detect a HNSCC-specific signature.

The potential of personalized medicine strategies will be harnessed when efficient and reliable methods of tumor detection and treatment selection are developed. Routine screening of patient serum for a cancer signature would facilitate early detection. **Figure E.1** shows an overview of a screening and personalized treatment strategy based on the antibody signature in serum. In the proposed strategy, a “master immunomic array” would

include tumor antigens specific for different cancers. This would detect a cancer-specific antibody signature using serum collected during a routine physical exam. Thus, tumor-specific antibodies present in sera will assist in early detection similarly to prostate-specific antigen (PSA), which has assisted in early diagnosis of prostate cancer (293).

The cancer-antibody signature may also inform treatment selection and predict treatment progression. For example, an autoantibody signature for prostate cancer is apparently a more specific screening tool than PSA, and may assist in guiding treatment strategies (294, 295).

Finally, antibody signatures will help identify novel proteins involved in tumor progression, i.e. which early stage lesions although treated appropriately, will progress aggressively. Identification of these tumors would inform selection of aggressive treatment strategies at an early stage. In our recent study, we validated the role of L23 as an oncogene in HNSCC. The roles that other HNSCC-specific proteins have in tumor progression are unknown. As we strive to achieve personalized medicine based strategies for cancer therapy, it is exciting to consider that some tumor antigens may be novel therapeutic targets. Perhaps through improved screening tools and novel therapeutic approaches based on HNSCC tumor antigens, we will see an improvement in survival from this devastating disease.

Oncomine™ (Compendia Bioscience, Ann Arbor, MI) was used for analysis and visualization.

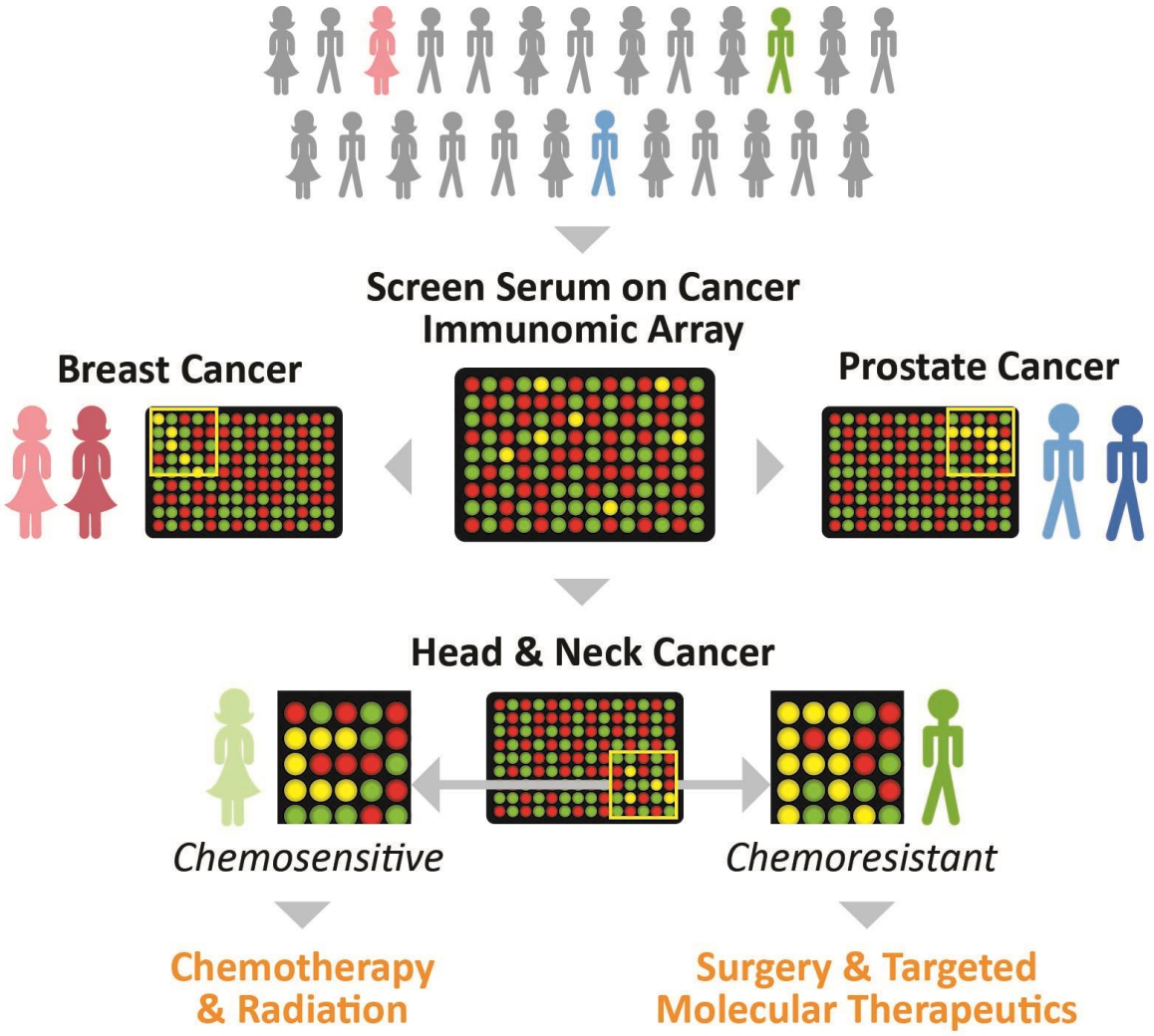

Figure E.1: An immunomics approach for early detection and personalized treatment strategies for cancer. A routine blood draw collected from individuals in an asymptomatic population is screened using a cancer immunomic array. Individuals with different types of cancer are identified at an early stage with a positive serum test. In addition, within each cancer-specific signature, chemosensitive and chemoresistant signatures are identified by the array. These signatures inform healthcare providers of the specific treatment needs of each patient, allowing for a personalized treatment strategy to be developed.

REFERENCES

REFERENCES

1. Leemans CR, Braakhuis BJ, Brakenhoff RH. The molecular biology of head and neck cancer. Nat Rev Cancer. 2011;11(1):9-22.
2. Menzin J, Lines LM, Manning LN. The economics of squamous cell carcinoma of the head and neck. Curr Opin Otolaryngol Head Neck Surg. 2007;15(2):68-73.
3. Lee JM, Turini M, Botteman MF, Stephens JM, Pashos CL. Economic burden of head and neck cancer. A literature review. Eur J Health Econ. 2004;5(1):70-80.
4. Siegel R, Ward E, Brawley O, Jemal A. Cancer statistics, 2011: the impact of eliminating socioeconomic and racial disparities on premature cancer deaths. CA Cancer J Clin. 2011;61(4):212-36.
5. Rowe RG, Weiss SJ. Breaching the basement membrane: who, when and how? Trends in cell biology. 2008;18(11):560-74.
6. Binmadi NO, Basile JR. Perineural invasion in oral squamous cell carcinoma: a discussion of significance and review of the literature. Oral oncology. 2011;47(11):1005-10.
7. Liebig C, Ayala G, Wilks JA, Berger DH, Albo D. Perineural invasion in cancer: a review of the literature. Cancer. 2009;115(15):3379-91.
8. Mendenhall WM, Amdur RJ, Hinerman RW, Werning JW, Malyapa RS, Villaret DB, et al. Skin cancer of the head and neck with perineural invasion. Am J Clin Oncol. 2007;30(1):93-6.
9. Neumann E. Secondare cancroid infiltration des nervus mentalis bei einem. Archiv fur pathologische Anatomie und Physiologie und fur klinische Medicin. 1862;24(1-2):201-2.
10. Mohs FE, Lathrop TG. Modes of spread of cancer of skin. AMA Arch Derm Syphilol. 1952;66(4):427-39.
11. Dunn M, Morgan MB, Beer TW. Perineural invasion: identification, significance, and a standardized definition. Dermatol Surg. 2009;35(2):214-21.
12. Matorin PA, Wagner RF, Jr. Mohs micrographic surgery: technical difficulties posed by perineural invasion. International journal of dermatology. 1992;31(2):83-6.
13. Moonis G, Cunnane MB, Emerick K, Curtin H. Patterns of perineural tumor spread in head and neck cancer. Magn Reson Imaging Clin N Am. 2012;20(3):435-46.
14. Lane JE, Williams MR, Kent DE. Perineural involvement of squamous cell carcinoma presenting with formication. Cutis. 2010;85(3):121-3.
15. Lee EK, Lee EJ, Kim MS, Park HJ, Park NH, Park S, 2nd, et al. Intracranial metastases: spectrum of MR imaging findings. Acta Radiol. 2012;53(10):1173-85.
16. Ballantyne AJ, McCarten AB, Ibanez ML. The Extension of Cancer of the Head and Neck through Peripheral Nerves. Am J Surg. 1963;106:651-67.

17. Lian K, Bharatha A, Aviv RI, Symons SP. Interpretation errors in CT angiography of the head and neck and the benefit of double reading. AJNR Am J Neuroradiol. 2011;32(11):2132-5.
18. Ginsberg LE, Eicher SA. Great auricular nerve: anatomy and imaging in a case of perineural tumor spread. AJNR Am J Neuroradiol. 2000;21(3):568-71.
19. Murakawa K, Tada M, Takada M, Tamoto E, Shindoh G, Teramoto K, et al. Prediction of lymph node metastasis and perineural invasion of biliary tract cancer by selected features from cDNA array data. J Surg Res. 2004;122(2):184-94.
20. Chen TC, Jan YY, Yeh TS. K-ras mutation is strongly associated with perineural invasion and represents an independent prognostic factor of intrahepatic cholangiocarcinoma after hepatectomy. Ann Surg Oncol. 2012;19 Suppl 3:S675-81.
21. Ben QW, Wang JC, Liu J, Zhu Y, Yuan F, Yao WY, et al. Positive expression of L1-CAM is associated with perineural invasion and poor outcome in pancreatic ductal adenocarcinoma. Ann Surg Oncol. 2010;17(8):2213-21.
22. Seki H, Tanaka J, Sato Y, Kato Y, Umezawa A, Koyama K. Neural cell adhesion molecule (NCAM) and perineural invasion in bile duct cancer. J Surg Oncol. 1993;53(2):78-83.
23. Seki H, Koyama K, Tanaka J, Sato Y, Umezawa A. Neural cell adhesion molecule and perineural invasion in gallbladder cancer. J Surg Oncol. 1995;58(2):97-100.
24. Solares CA, Brown I, Boyle GM, Parsons PG, Panizza B. Neural cell adhesion molecule expression: no correlation with perineural invasion in cutaneous squamous cell carcinoma of the head and neck. Head Neck. 2009;31(6):802-6.
25. Kolokythas A, Cox DP, Dekker N, Schmidt BL. Nerve growth factor and tyrosine kinase A receptor in oral squamous cell carcinoma: is there an association with perineural invasion? Journal of oral and maxillofacial surgery : official journal of the American Association of Oral and Maxillofacial Surgeons. 2010;68(6):1290-5.
26. Chen-Tsai CP, Colome-Grimmer M, Wagner RF, Jr. Correlations among neural cell adhesion molecule, nerve growth factor, and its receptors, TrkA, TrkB, TrkC, and p75, in perineural invasion by basal cell and cutaneous squamous cell carcinomas. Dermatol Surg. 2004;30(7):1009-16.
27. Ma J, Jiang Y, Jiang Y, Sun Y, Zhao X. Expression of nerve growth factor and tyrosine kinase receptor A and correlation with perineural invasion in pancreatic cancer. J Gastroenterol Hepatol. 2008;23(12):1852-9.
28. Sakamoto Y, Kitajima Y, Edakuni G, Sasatomi E, Mori M, Kitahara K, et al. Expression of Trk tyrosine kinase receptor is a biologic marker for cell proliferation and perineural invasion of human pancreatic ductal adenocarcinoma. Oncol Rep. 2001;8(3):477-84.
29. Zhu Z, Friess H, diMola FF, Zimmermann A, Graber HU, Korc M, et al. Nerve growth factor expression correlates with perineural invasion and pain in human pancreatic cancer. J Clin Oncol. 1999;17(8):2419-28.
30. Banerjee R, Henson BS, Russo N, Tsodikov A, D'Silva NJ. Rap1 mediates galanin receptor 2-induced proliferation and survival in squamous cell carcinoma. Cell Signal. 2011;23(7):1110-8.

31. Chen W, Dong S, Zhou J, Sun M. Investigation of myoepithelial cell differentiation into Schwann-like cells in salivary adenoid cystic carcinoma associated with perineural invasion. Mol Med Rep. 2012;6(4):755-9.
32. Klose T, Abiatari I, Samkharadze T, De Oliveira T, Jager C, Kiladze M, et al. The actin binding protein destrin is associated with growth and perineural invasion of pancreatic cancer. Pancreatology. 2012;12(4):350-7.
33. He C, Jiang H, Geng S, Sheng H, Shen X, Zhang X, et al. Expression of c-Myc and Fas correlates with perineural invasion of pancreatic cancer. Int J Clin Exp Pathol. 2012;5(4):339-46.
34. Ayala GE, Dai H, Tahir SA, Li R, Timme T, Ittmann M, et al. Stromal antiapoptotic paracrine loop in perineural invasion of prostatic carcinoma. Cancer research. 2006;66(10):5159-64.
35. Zhang S, Qi L, Li M, Zhang D, Xu S, Wang N, et al. Chemokine CXCL12 and its receptor CXCR4 expression are associated with perineural invasion of prostate cancer. J Exp Clin Cancer Res. 2008;27:62.
36. Ayala GE, Dai H, Li R, Ittmann M, Thompson TC, Rowley D, et al. Bystin in perineural invasion of prostate cancer. Prostate. 2006;66(3):266-72.
37. Ambrosio EP, Rosa FE, Domingues MA, Villacis RA, Coudry Rde A, Tagliarini JV, et al. Cortactin is associated with perineural invasion in the deep invasive front area of laryngeal carcinomas. Hum Pathol. 2011;42(9):1221-9.
38. Swanson BJ, McDermott KM, Singh PK, Eggers JP, Crocker PR, Hollingsworth MA. MUC1 is a counter-receptor for myelin-associated glycoprotein (Siglec-4a) and their interaction contributes to adhesion in pancreatic cancer perineural invasion. Cancer research. 2007;67(21):10222-9.
39. Prueitt RL, Yi M, Hudson RS, Wallace TA, Howe TM, Yfantis HG, et al. Expression of microRNAs and protein-coding genes associated with perineural invasion in prostate cancer. Prostate. 2008;68(11):1152-64.
40. Iwahashi N, Nagasaka T, Tezel G, Iwashita T, Asai N, Murakumo Y, et al. Expression of glial cell line-derived neurotrophic factor correlates with perineural invasion of bile duct carcinoma. Cancer. 2002;94(1):167-74.
41. Solares CA, Boyle GM, Brown I, Parsons PG, Panizza B. Reduced alphaB-crystallin staining in perineural invasion of head and neck cutaneous squamous cell carcinoma. Otolaryngol Head Neck Surg. 2010;142(3 Suppl 1):S15-9.
42. Abiatari I, Gillen S, DeOliveira T, Klose T, Bo K, Giese NA, et al. The microtubule-associated protein MAPRE2 is involved in perineural invasion of pancreatic cancer cells. Int J Oncol. 2009;35(5):1111-6.
43. Abiatari I, DeOliveira T, Kerkadze V, Schwager C, Esposito I, Giese NA, et al. Consensus transcriptome signature of perineural invasion in pancreatic carcinoma. Molecular cancer therapeutics. 2009;8(6):1494-504.
44. Duan L, Hu XQ, Feng DY, Lei SY, Hu GH. GPC-1 may serve as a predictor of perineural invasion and a prognosticator of survival in pancreatic cancer. Asian J Surg. 2013;36(1):7-12.
45. De Oliveira T, Abiatari I, Raulefs S, Sauliunaite D, Erkan M, Kong B, et al. Syndecan-2 promotes perineural invasion and cooperates with K-ras to induce an invasive pancreatic cancer cell phenotype. Mol Cancer. 2012;11:19.

46. Ayala GE, Dai H, Ittmann M, Li R, Powell M, Frolov A, et al. Growth and survival mechanisms associated with perineural invasion in prostate cancer. Cancer research. 2004;64(17):6082-90.
47. Yang X, Zhang P, Ma Q, Kong L, Li Y, Liu B, et al. EMMPRIN silencing inhibits proliferation and perineural invasion of human salivary adenoid cystic carcinoma cells in vitro and in vivo. Cancer Biol Ther. 2012;13(2):85-91.
48. Fukuda M, Kusama K, Sakashita H. Cimetidine inhibits salivary gland tumor cell adhesion to neural cells and induces apoptosis by blocking NCAM expression. BMC cancer. 2008;8:376.
49. Chen W, Zhang HL, Jiang YG, Li JH, Liu BL, Sun MY. Inhibition of CD146 gene expression via RNA interference reduces in vitro perineural invasion on ACC-M cell. J Oral Pathol Med. 2009;38(2):198-205.
50. Chen W, Zhang H, Wang J, Cao G, Dong Z, Su H, et al. Lentiviral-mediated gene silencing of Notch-4 inhibits in vitro proliferation and perineural invasion of ACC-M cells. Oncol Rep. 2013;29(5):1797-804.
51. Binmadi NO, Yang YH, Zhou H, Proia P, Lin YL, De Paula AM, et al. Plexin-B1 and semaphorin 4D cooperate to promote perineural invasion in a RhoA/ROK-dependent manner. Am J Pathol. 2012;180(3):1232-42.
52. Bakst RL, Lee N, He S, Chernichenko N, Chen CH, Linkov G, et al. Radiation impairs perineural invasion by modulating the nerve microenvironment. PloS one. 2012;7(6):e39925.
53. Hibi T, Mori T, Fukuma M, Yamazaki K, Hashiguchi A, Yamada T, et al. Synuclein-gamma is closely involved in perineural invasion and distant metastasis in mouse models and is a novel prognostic factor in pancreatic cancer. Clinical cancer research : an official journal of the American Association for Cancer Research. 2009;15(8):2864-71.
54. Liebl F, Demir IE, Rosenberg R, Boldis A, Yildiz E, Kujundzic K, et al. The severity of neural invasion is associated with shortened survival in colon cancer. Clinical cancer research : an official journal of the American Association for Cancer Research. 2013;19(1):50-61.
55. Demir IE, Ceyhan GO, Rauch U, Altintas B, Klotz M, Muller MW, et al. The microenvironment in chronic pancreatitis and pancreatic cancer induces neuronal plasticity. Neurogastroenterol Motil. 2010;22(4):480-90, e112-3.
56. Dai H, Li R, Wheeler T, Ozen M, Ittmann M, Anderson M, et al. Enhanced survival in perineural invasion of pancreatic cancer: an in vitro approach. Hum Pathol. 2007;38(2):299-307.
57. Ayala GE, Wheeler TM, Shine HD, Schmelz M, Frolov A, Chakraborty S, et al. In vitro dorsal root ganglia and human prostate cell line interaction: redefining perineural invasion in prostate cancer. Prostate. 2001;49(3):213-23.
58. Ceyhan GO, Demir IE, Altintas B, Rauch U, Thiel G, Muller MW, et al. Neural invasion in pancreatic cancer: a mutual tropism between neurons and cancer cells. Biochemical and biophysical research communications. 2008;374(3):442-7.
59. Gil Z, Cavel O, Kelly K, Brader P, Rein A, Gao SP, et al. Paracrine regulation of pancreatic cancer cell invasion by peripheral nerves. J Natl Cancer Inst. 2010;102(2):107-18.

60. Gil Z, Kelly KJ, Brader P, Shah JP, Fong Y, Wong RJ. Utility of a herpes oncolytic virus for the detection of neural invasion by cancer. Neoplasia. 2008;10(4):347-53.
61. Guo K, Ma Q, Li J, Wang Z, Shan T, Li W, et al. Interaction of the sympathetic nerve with pancreatic cancer cells promotes perineural invasion through the activation of STAT3 signaling. Molecular cancer therapeutics. 2013;12(3):264-73.
62. Eibl G, Reber HA. A xenograft nude mouse model for perineural invasion and recurrence in pancreatic cancer. Pancreas. 2005;31(3):258-62.
63. Koide N, Yamada T, Shibata R, Mori T, Fukuma M, Yamazaki K, et al. Establishment of perineural invasion models and analysis of gene expression revealed an invariant chain (CD74) as a possible molecule involved in perineural invasion in pancreatic cancer. Clinical cancer research : an official journal of the American Association for Cancer Research. 2006;12(8):2419-26.
64. Imoto A, Mitsunaga S, Inagaki M, Aoyagi K, Sasaki H, Ikeda M, et al. Neural invasion induces cachexia via astrocytic activation of neural route in pancreatic cancer. International journal of cancer Journal international du cancer. 2012;131(12):2795-807.
65. Mitsunaga S, Fujii S, Ishii G, Kinoshita T, Hasebe T, Aoyagi K, et al. Nerve invasion distance is dependent on laminin gamma2 in tumors of pancreatic cancer. International journal of cancer Journal international du cancer. 2010;127(4):805-19.
66. Liu M, Scanlon CS, Banerjee R, Russo N, Inglehart RC, Willis AL, et al. The Histone Methyltransferase EZH2 Mediates Tumor Progression on the Chick Chorioallantoic Membrane Assay, a Novel Model of Head and Neck Squamous Cell Carcinoma. Transl Oncol. 2013;6(3):273-81.
67. Scanlon CS, Inglehart, R.C., D'Silva, N. J. Emerging Value: The chick chorioallantoic membrane (CAM) model in oral carcinogenesis research. Carcinogenesis and Mutagenesis. 2013.
68. Hanahan D, Weinberg RA. Hallmarks of cancer: the next generation. Cell. 2011;144(5):646-74.
69. Van Tubergen EA, Banerjee R, Liu M, Vander Broek R, Light E, Shiuhyang K, et al. Inactivation or loss of TTP promotes invasion in head and neck cancer via transcript stabilization and secretion of MMP9, MMP2 and IL-6. Clin Cancer Res. 2013.
70. Scanlon CS, Van Tubergen EA, Chen LC, Elahi SF, Kuo S, Feinberg S, et al. Characterization of squamous cell carcinoma in an organotypic culture via subsurface non-linear optical molecular imaging. Experimental biology and medicine. 2013;238(11):1233-41.
71. Banerjee R, Mani RS, Russo N, Scanlon CS, Tsodikov A, Jing X, et al. The tumor suppressor gene rap1GAP is silenced by miR-101-mediated EZH2 overexpression in invasive squamous cell carcinoma. Oncogene. 2011;30(42):4339-49.
72. Henson B, Li F, Coatney DD, Carey TE, Mitra RS, Kirkwood KL, et al. An orthotopic floor-of-mouth model for locoregional growth and spread of human squamous cell carcinoma. J Oral Pathol Med. 2007;36(6):363-70.
73. Czerninski R, Amornphimoltham P, Patel V, Molinolo AA, Gutkind JS. Targeting mammalian target of rapamycin by rapamycin prevents tumor progression in an

oral-specific chemical carcinogenesis model. Cancer Prev Res (Phila). 2009;2(1):27-36.
74. Stern CD. The chick; a great model system becomes even greater. Developmental cell. 2005;8(1):9-17.
75. Banerjee R, Russo N, Liu M, Van Tubergen E, D'Silva NJ. Rap1 and its regulatory proteins: the tumor suppressor, oncogene, tumor suppressor gene axis in head and neck cancer. Small GTPases. 2012;3(3):192-7.
76. Murphy JB. Transplantability of Tissues to the Embryo of Foreign Species : Its Bearing on Questions of Tissue Specificity and Tumor Immunity. The Journal of experimental medicine. 1913;17(4):482-93.
77. Auerbach R, Arensman R, Kubai L, Folkman J. Tumor-induced angiogenesis: lack of inhibition by irradiation. International journal of cancer Journal international du cancer. 1975;15(2):241-5.
78. Ossowski L, Reich E. Experimental model for quantitative study of metastasis. Cancer research. 1980;40(7):2300-9.
79. Scanlon CS, Van Tubergen EA, Inglehart RC, D'Silva NJ. Biomarkers of epithelial-mesenchymal transition in squamous cell carcinoma. Journal of dental research. 2013;92(2):114-21.
80. Even-Ram S, Yamada KM. Cell migration in 3D matrix. Curr Opin Cell Biol. 2005;17(5):524-32.
81. Weigelt B, Bissell MJ. Unraveling the microenvironmental influences on the normal mammary gland and breast cancer. Semin Cancer Biol. 2008;18(5):311-21.
82. Gligorijevic B, Condeelis J. Stretching the timescale of intravital imaging in tumors. Cell Adh Migr. 2009;3(4):313-5.
83. Ribatti D. The Chick Embryo Chorioallantoic Membrane in the Study of Angiogenesis and Metastasis. London: Springer; 2010.
84. Bartlett DW, Davis ME. Insights into the kinetics of siRNA-mediated gene silencing from live-cell and live-animal bioluminescent imaging. Nucleic Acids Res. 2006;34(1):322-33.
85. Zijlstra A, Mellor R, Panzarella G, Aimes RT, Hooper JD, Marchenko ND, et al. A quantitative analysis of rate-limiting steps in the metastatic cascade using human-specific real-time polymerase chain reaction. Cancer Res. 2002;62(23):7083-92.
86. Ayala GE, Dai H, Powell M, Li R, Ding Y, Wheeler TM, et al. Cancer-related axonogenesis and neurogenesis in prostate cancer. Clin Cancer Res. 2008;14(23):7593-603.
87. Cavel O, Shomron O, Shabtay A, Vital J, Trejo-Leider L, Weizman N, et al. Endoneurial macrophages induce perineural invasion of pancreatic cancer cells by secretion of GDNF and activation of RET tyrosine kinase receptor. Cancer Res. 2012;72(22):5733-43.
88. Magnon C, Hall SJ, Lin J, Xue X, Gerber L, Freedland SJ, et al. Autonomic nerve development contributes to prostate cancer progression. Science. 2013;341(6142):1236361.
89. Hamburger V, Levi-Montalcini R. Proliferation, differentiation and degeneration in the spinal ganglia of the chick embryo under normal and experimental conditions. J Exp Zool. 1949;111(3):457-501.

90. Cohen S, Levi-Montalcini R, Hamburger V. A Nerve Growth-Stimulating Factor Isolated from Sarcom as 37 and 180. Proc Natl Acad Sci U S A. 1954;40(10):1014-8.
91. Hseu YC, Wu CR, Chang HW, Kumar KJ, Lin MK, Chen CS, et al. Inhibitory effects of Physalis angulata on tumor metastasis and angiogenesis. J Ethnopharmacol. 2011;135(3):762-71.
92. Kim SA, Kwon SM, Kim JA, Kang KW, Yoon JH, Ahn SG. 5'-Nitro-indirubinoxime, an indirubin derivative, suppresses metastatic ability of human head and neck cancer cells through the inhibition of Integrin beta1/FAK/Akt signaling. Cancer Lett. 2011;306(2):197-204.
93. Nagasawa H, Mikamo N, Nakajima Y, Matsumoto H, Uto Y, Hori H. Antiangiogenic hypoxic cytotoxin TX-402 inhibits hypoxia-inducible factor 1 signaling pathway. Anticancer Res. 2003;23(6a):4427-34.
94. Oh SH, Kim WY, Kim JH, Younes MN, El-Naggar AK, Myers JN, et al. Identification of insulin-like growth factor binding protein-3 as a farnesyl transferase inhibitor SCH66336-induced negative regulator of angiogenesis in head and neck squamous cell carcinoma. Clin Cancer Res. 2006;12(2):653-61.
95. Oh SH, Woo JK, Jin Q, Kang HJ, Jeong JW, Kim KW, et al. Identification of novel antiangiogenic anticancer activities of deguelin targeting hypoxia-inducible factor-1 alpha. Int J Cancer. 2008;122(1):5-14.
96. Petruzzelli GJ, Snyderman CH, Johnson JT, Myers EN. Angiogenesis induced by head and neck squamous cell carcinoma xenografts in the chick embryo chorioallantoic membrane model. Ann Otol Rhinol Laryngol. 1993;102(3 Pt 1):215-21.
97. Pisanti S, Borselli C, Oliviero O, Laezza C, Gazzerro P, Bifulco M. Antiangiogenic activity of the endocannabinoid anandamide: correlation to its tumor-suppressor efficacy. J Cell Physiol. 2007;211(2):495-503.
98. Gronau S, Thess B, Riechelmann H, Fischer Y, Schmitt A, Schmitt M. An autologous system for culturing head and neck squamous cell carcinomas for the assessment of cellular therapies on the chorioallantois membrane. Eur Arch Otorhinolaryngol. 2006;263(4):308-12.
99. Nyberg P, Moilanen M, Paju A, Sarin A, Stenman UH, Sorsa T, et al. MMP-9 activation by tumor trypsin-2 enhances in vivo invasion of human tongue carcinoma cells. J Dent Res. 2002;81(12):831-5.
100. Nyberg P, Heikkila P, Sorsa T, Luostarinen J, Heljasvaara R, Stenman UH, et al. Endostatin inhibits human tongue carcinoma cell invasion and intravasation and blocks the activation of matrix metalloprotease-2, -9, and -13. J Biol Chem. 2003;278(25):22404-11.
101. Yang SF, Yang WE, Kuo WH, Chang HR, Chu SC, Hsieh YS. Antimetastatic potentials of flavones on oral cancer cell via an inhibition of matrix-degrading proteases. Arch Oral Biol. 2008;53(3):287-94.
102. Hoppenheit C, Huttenberger D, Foth HJ, Spitzer WJ, Reichert TE, Muller-Richter UD. Pharmacokinetics of the photosensitizers aminolevulinic acid and aminolevulinic acid hexylester in oro-facial tumors embedded in the chorioallantois membrane of a hen's egg. Cancer Biother Radiopharm. 2006;21(6):569-78.

103. Chang HL, Pieretti-Vanmarcke R, Nicolaou F, Li X, Wei X, MacLaughlin DT, et al. Mullerian inhibiting substance inhibits invasion and migration of epithelial cancer cell lines. Gynecol Oncol. 2011;120(1):128-34.
104. Easty DM, Easty GC, Baici A, Carter RL, Cederholm-Williams SA, Felix H, et al. Biological studies of ten human squamous carcinoma cell lines: an overview. Eur J Cancer Clin Oncol. 1986;22(6):617-34.
105. Van Tubergen EA, Banerjee R, Liu M, Vander Broek R, Light E, Kuo S, et al. Inactivation or loss of TTP promotes invasion in head and neck cancer via transcript stabilization and secretion of MMP9, MMP2, and IL-6. Clin Cancer Res. 2013;19(5):1169-79.
106. Huang HZ, Tang HK. [Interaction of vascular endothelial growth factor-C over-expression with tongue squamous cell carcinoma cell line Tca8113 with peri-carcinoma lymphatics]. Zhonghua Kou Qiang Yi Xue Za Zhi. 2005;40(2):126-8.
107. Teruszkin Balassiano I, Alves De Paulo S, Henriques Silva N, Curie Cabral M, da Gloria da Costa Carvalho M. Metastatic potential of MDA435 and Hep2 cell lines in chorioallantoic membrane (CAM) model. Oncol Rep. 2001;8(2):431-3.
108. Bragado P, Estrada Y, Sosa MS, Avivar-Valderas A, Cannan D, Genden E, et al. Analysis of marker-defined HNSCC subpopulations reveals a dynamic regulation of tumor initiating properties. PLoS One. 2012;7(1):e29974.
109. Scanlon CS BR, Inglehart RC, Liu M, Russo N, Hariharan A, Van Tubergen EA, Corson SL, Asangani IA, Mistretta CM, Chinnaiyan AM, D'Silva NJ. Galanin modulates the neural niche to favor perineural invasion in head and neck cancer. (under review). 2014.
110. Bapat AA, Hostetter G, Von Hoff DD, Han H. Perineural invasion and associated pain in pancreatic cancer. Nat Rev Cancer. 2011;11(10):695-707.
111. Johnston M, Yu E, Kim J. Perineural invasion and spread in head and neck cancer. Expert Rev Anticancer Ther. 2012;12(3):359-71.
112. Kaidi A, Qualtrough D, Williams AC, Paraskeva C. Direct transcriptional up-regulation of cyclooxygenase-2 by hypoxia-inducible factor (HIF)-1 promotes colorectal tumor cell survival and enhances HIF-1 transcriptional activity during hypoxia. Cancer research. 2006;66(13):6683-91.
113. Nunez F, Bravo S, Cruzat F, Montecino M, De Ferrari GV. Wnt/beta-catenin signaling enhances cyclooxygenase-2 (COX2) transcriptional activity in gastric cancer cells. PloS one. 2011;6(4):e18562.
114. Henson BS, Neubig RR, Jang I, Ogawa T, Zhang Z, Carey TE, et al. Galanin receptor 1 has anti-proliferative effects in oral squamous cell carcinoma. J Biol Chem. 2005;280(24):22564-71.
115. Siegel GJ, Agranoff, B.W., Albers, R.W., Fisher, S.K., Uhler, M. Basic Neurochemistry: Molecular, Cellular and Medical Aspects. 6 ed: Lippincott Williams & Wilkins; 1999.
116. Sugimoto T, Seki N, Shimizu S, Kikkawa N, Tsukada J, Shimada H, et al. The galanin signaling cascade is a candidate pathway regulating oncogenesis in human squamous cell carcinoma. Genes Chromosomes Cancer. 2009;48(2):132-42.
117. Wynick D, Thompson SW, McMahon SB. The role of galanin as a multi-functional neuropeptide in the nervous system. Curr Opin Pharmacol. 2001;1(1):73-7.

118. Lang R, Gundlach AL, Kofler B. The galanin peptide family: receptor pharmacology, pleiotropic biological actions, and implications in health and disease. Pharmacol Ther. 2007;115(2):177-207.
119. Bollimuntha S, Selvaraj S, Singh BB. Emerging roles of canonical TRP channels in neuronal function. Adv Exp Med Biol. 2011;704:573-93.
120. Muller MR, Rao A. NFAT, immunity and cancer: a transcription factor comes of age. Nat Rev Immunol. 2010;10(9):645-56.
121. Gerlach K, Daniel C, Lehr HA, Nikolaev A, Gerlach T, Atreya R, et al. Transcription factor NFATc2 controls the emergence of colon cancer associated with IL-6-dependent colitis. Cancer Res. 2012;72(17):4340-50.
122. Merati K, said Siadaty M, Andea A, Sarkar F, Ben-Josef E, Mohammad R, et al. Expression of inflammatory modulator COX-2 in pancreatic ductal adenocarcinoma and its relationship to pathologic and clinical parameters. Am J Clin Oncol. 2001;24(5):447-52.
123. Li S, Sun Y, Gao D. Role of the nervous system in cancer metastasis. Oncol Lett. 2013;5(4):1101-11.
124. Zanker KS. The neuro-neoplastic synapse: does it exist? Prog Exp Tumor Res. 2007;39:154-61.
125. Anderson TD, Feldman M, Weber RS, Ziober AF, Ziober BL. Tumor deposition of laminin-5 and the relationship with perineural invasion. Laryngoscope. 2001;111(12):2140-3.
126. Rauch I, Kofler B. The galanin system in cancer. EXS. 2010;102:223-41.
127. O'Meara G, Coumis U, Ma SY, Kehr J, Mahoney S, Bacon A, et al. Galanin regulates the postnatal survival of a subset of basal forebrain cholinergic neurons. Proc Natl Acad Sci U S A. 2000;97(21):11569-74.
128. Alier KA, Chen Y, Sollenberg UE, Langel U, Smith PA. Selective stimulation of GalR1 and GalR2 in rat substantia gelatinosa reveals a cellular basis for the anti- and pro-nociceptive actions of galanin. Pain. 2008;137(1):138-46.
129. Burazin TC, Gundlach AL. Inducible galanin and GalR2 receptor system in motor neuron injury and regeneration. J Neurochem. 1998;71(2):879-82.
130. Kofler B, Berger A, Santic R, Moritz K, Almer D, Tuechler C, et al. Expression of neuropeptide galanin and galanin receptors in human skin. J Invest Dermatol. 2004;122(4):1050-3.
131. Bauer JW, Lang R, Jakab M, Kofler B. Galanin family of peptides in skin function. EXS. 2010;102:51-9.
132. Perumal P, Vrontakis ME. Transgenic mice over-expressing galanin exhibit pituitary adenomas and increased secretion of galanin, prolactin and growth hormone. J Endocrinol. 2003;179(2):145-54.
133. Abbosh C, Lawkowski A, Zaben M, Gray W. GalR2/3 mediates proliferative and trophic effects of galanin on postnatal hippocampal precursors. J Neurochem. 2011;117(3):425-36.
134. Misawa K, Ueda Y, Kanazawa T, Misawa Y, Jang I, Brenner JC, et al. Epigenetic inactivation of galanin receptor 1 in head and neck cancer. Clin Cancer Res. 2008;14(23):7604-13.

135. Takebayashi S, Hickson A, Ogawa T, Jung KY, Mineta H, Ueda Y, et al. Loss of chromosome arm 18q with tumor progression in head and neck squamous cancer. Genes Chromosomes Cancer. 2004;41(2):145-54.
136. Voss MJ, Entschladen F. Tumor interactions with soluble factors and the nervous system. Cell Commun Signal. 2010;8:21.
137. Entschladen F, Drell TLt, Lang K, Joseph J, Zaenker KS. Tumour-cell migration, invasion, and metastasis: navigation by neurotransmitters. Lancet Oncol. 2004;5(4):254-8.
138. Hulse RP, Wynick D, Donaldson LF. Activation of the galanin receptor 2 in the periphery reverses nerve injury-induced allodynia. Mol Pain. 2011;7:26.
139. Lang R, Kofler B. The galanin peptide family in inflammation. Neuropeptides. 2011;45(1):1-8.
140. Hobson SA, Bacon A, Elliot-Hunt CR, Holmes FE, Kerr NC, Pope R, et al. Galanin acts as a trophic factor to the central and peripheral nervous systems. EXS. 2010;102:25-38.
141. Burazin TC, Bathgate RA, Macris M, Layfield S, Gundlach AL, Tregear GW. Restricted, but abundant, expression of the novel rat gene-3 (R3) relaxin in the dorsal tegmental region of brain. J Neurochem. 2002;82(6):1553-7.
142. Marchesi F, Piemonti L, Mantovani A, Allavena P. Molecular mechanisms of perineural invasion, a forgotten pathway of dissemination and metastasis. Cytokine Growth Factor Rev. 2010;21(1):77-82.
143. Chen N, Balasenthil S, Reuther J, Frayna A, Wang Y, Chandler DS, et al. DEAR1 is a chromosome 1p35 tumor suppressor and master regulator of TGF-beta-driven epithelial-mesenchymal transition. Cancer Discov. 2013;3(10):1172-89.
144. Sennino B, Ishiguro-Oonuma T, Wei Y, Naylor RM, Williamson CW, Bhagwandin V, et al. Suppression of tumor invasion and metastasis by concurrent inhibition of c-Met and VEGF signaling in pancreatic neuroendocrine tumors. Cancer Discov. 2012;2(3):270-87.
145. Holmes FE, Mahoney S, King VR, Bacon A, Kerr NC, Pachnis V, et al. Targeted disruption of the galanin gene reduces the number of sensory neurons and their regenerative capacity. Proc Natl Acad Sci U S A. 2000;97(21):11563-8.
146. Gottsch ML, Zeng H, Hohmann JG, Weinshenker D, Clifton DK, Steiner RA. Phenotypic analysis of mice deficient in the type 2 galanin receptor (GALR2). Mol Cell Biol. 2005;25(11):4804-11.
147. Hobson SA, Holmes FE, Kerr NC, Pope RJ, Wynick D. Mice deficient for galanin receptor 2 have decreased neurite outgrowth from adult sensory neurons and impaired pain-like behaviour. J Neurochem. 2006;99(3):1000-10.
148. Mancini M, Toker A. NFAT proteins: emerging roles in cancer progression. Nat Rev Cancer. 2009;9(11):810-20.
149. Tofighi R, Joseph B, Xia S, Xu ZQ, Hamberger B, Hokfelt T, et al. Galanin decreases proliferation of PC12 cells and induces apoptosis via its subtype 2 receptor (GalR2). Proc Natl Acad Sci U S A. 2008;105(7):2717-22.
150. Cromer A, Carles A, Millon R, Ganguli G, Chalmel F, Lemaire F, et al. Identification of genes associated with tumorigenesis and metastatic potential of hypopharyngeal cancer by microarray analysis. Oncogene. 2004;23(14):2484-98.

151. Estilo CL, P Oc, Talbot S, Socci ND, Carlson DL, Ghossein R, et al. Oral tongue cancer gene expression profiling: Identification of novel potential prognosticators by oligonucleotide microarray analysis. BMC cancer. 2009;9:11.
152. Ginos MA, Page GP, Michalowicz BS, Patel KJ, Volker SE, Pambuccian SE, et al. Identification of a gene expression signature associated with recurrent disease in squamous cell carcinoma of the head and neck. Cancer research. 2004;64(1):55-63.
153. O'Donnell RK, Kupferman M, Wei SJ, Singhal S, Weber R, O'Malley B, et al. Gene expression signature predicts lymphatic metastasis in squamous cell carcinoma of the oral cavity. Oncogene. 2005;24(7):1244-51.
154. Peng CH, Liao CT, Peng SC, Chen YJ, Cheng AJ, Juang JL, et al. A novel molecular signature identified by systems genetics approach predicts prognosis in oral squamous cell carcinoma. PloS one. 2011;6(8):e23452.
155. Poage GM, Christensen BC, Houseman EA, McClean MD, Wiencke JK, Posner MR, et al. Genetic and epigenetic somatic alterations in head and neck squamous cell carcinomas are globally coordinated but not locally targeted. PLoS One. 2010;5(3):e9651.
156. Pyeon D, Newton MA, Lambert PF, den Boon JA, Sengupta S, Marsit CJ, et al. Fundamental differences in cell cycle deregulation in human papillomavirus-positive and human papillomavirus-negative head/neck and cervical cancers. Cancer research. 2007;67(10):4605-19.
157. Rickman DS, Millon R, De Reynies A, Thomas E, Wasylyk C, Muller D, et al. Prediction of future metastasis and molecular characterization of head and neck squamous-cell carcinoma based on transcriptome and genome analysis by microarrays. Oncogene. 2008;27(51):6607-22.
158. Roepman P, Wessels LF, Kettelarij N, Kemmeren P, Miles AJ, Lijnzaad P, et al. An expression profile for diagnosis of lymph node metastases from primary head and neck squamous cell carcinomas. Nat Genet. 2005;37(2):182-6.
159. Sengupta S, den Boon JA, Chen IH, Newton MA, Dahl DB, Chen M, et al. Genome-wide expression profiling reveals EBV-associated inhibition of MHC class I expression in nasopharyngeal carcinoma. Cancer Res. 2006;66(16):7999-8006.
160. Slebos RJ, Yi Y, Ely K, Carter J, Evjen A, Zhang X, et al. Gene expression differences associated with human papillomavirus status in head and neck squamous cell carcinoma. Clin Cancer Res. 2006;12(3 Pt 1):701-9.
161. Talbot SG, Estilo C, Maghami E, Sarkaria IS, Pham DK, P Oc, et al. Gene expression profiling allows distinction between primary and metastatic squamous cell carcinomas in the lung. Cancer research. 2005;65(8):3063-71.
162. Toruner GA, Ulger C, Alkan M, Galante AT, Rinaggio J, Wilk R, et al. Association between gene expression profile and tumor invasion in oral squamous cell carcinoma. Cancer genetics and cytogenetics. 2004;154(1):27-35.
163. Ye H, Yu TW, Temam S, Ziober BL, Wang JG, Schwartz JL, et al. Transcriptomic dissection of tongue squamous cell carcinoma. Bmc Genomics. 2008;9.
164. Labelle M, Hynes RO. The initial hours of metastasis: the importance of cooperative host-tumor cell interactions during hematogenous dissemination. Cancer discovery. 2012;2(12):1091-9.

165. Chambers AF, Groom AC, MacDonald IC. Dissemination and growth of cancer cells in metastatic sites. Nature reviews Cancer. 2002;2(8):563-72.
166. Khanna C, Hunter K. Modeling metastasis in vivo. Carcinogenesis. 2005;26(3):513-23.
167. Fidler IJ. The pathogenesis of cancer metastasis: the 'seed and soil' hypothesis revisited. Nature reviews Cancer. 2003;3(6):453-8.
168. Paget S. The distribution of secondary growths in cancer of the breast. 1889. Cancer metastasis reviews. 1989;8(2):98-101.
169. Rahima B, Shingaki S, Nagata M, Saito C. Prognostic significance of perineural invasion in oral and oropharyngeal carcinoma. Oral surgery, oral medicine, oral pathology, oral radiology, and endodontics. 2004;97(4):423-31.
170. Fagan JJ, Collins B, Barnes L, D'Amico F, Myers EN, Johnson JT. Perineural invasion in squamous cell carcinoma of the head and neck. Archives of otolaryngology--head & neck surgery. 1998;124(6):637-40.
171. Tai SK, Li WY, Yang MH, Chu PY, Wang YF. Perineural invasion in T1 oral squamous cell carcinoma indicates the need for aggressive elective neck dissection. The American journal of surgical pathology. 2013;37(8):1164-72.
172. Chambers AF, Naumov GN, Varghese HJ, Nadkarni KV, MacDonald IC, Groom AC. Critical steps in hematogenous metastasis: an overview. Surgical oncology clinics of North America. 2001;10(2):243-55, vii.
173. O'Reilly MS, Holmgren L, Shing Y, Chen C, Rosenthal RA, Moses M, et al. Angiostatin: a novel angiogenesis inhibitor that mediates the suppression of metastases by a Lewis lung carcinoma. Cell. 1994;79(2):315-28.
174. Yamamoto N, Yang M, Jiang P, Xu M, Tsuchiya H, Tomita K, et al. Determination of clonality of metastasis by cell-specific color-coded fluorescent-protein imaging. Cancer research. 2003;63(22):7785-90.
175. Kim MY, Oskarsson T, Acharyya S, Nguyen DX, Zhang XH, Norton L, et al. Tumor self-seeding by circulating cancer cells. Cell. 2009;139(7):1315-26.
176. Jackson TL, Byrne HM. A mechanical model of tumor encapsulation and transcapsular spread. Mathematical biosciences. 2002;180:307-28.
177. Rodriguez-Cerdeira C, Sanchez-Blanco E, Molares-Vila A. Clinical application of development of nonantibiotic macrolides that correct inflammation-driven immune dysfunction in inflammatory skin diseases. Mediators of inflammation. 2012;2012:563709.
178. Muller JM. Potential inhibition of the neuro-neoplastic interactions: the clue of a GPCR-targeted therapy. Progress in experimental tumor research. 2007;39:130-53.
179. O'Hayre M, Degese MS, Gutkind JS. Novel insights into G protein and G protein-coupled receptor signaling in cancer. Current opinion in cell biology. 2014;27C:126-35.
180. Zeisberg M, Neilson EG. Biomarkers for epithelial-mesenchymal transitions. The Journal of clinical investigation. 2009;119(6):1429-37.
181. Wu H, Lotan R, Menter D, Lippman SM, Xu XC. Expression of E-cadherin is associated with squamous differentiation in squamous cell carcinomas. Anticancer Res. 2000;20(3A):1385-90.

182. Calmon MF, Colombo J, Carvalho F, Souza FP, Filho JF, Fukuyama EE, et al. Methylation profile of genes CDKN2A (p14 and p16), DAPK1, CDH1, and ADAM23 in head and neck cancer. Cancer Genet Cytogenet. 2007;173(1):31-7.
183. Dikshit RP, Gillio-Tos A, Brennan P, De Marco L, Fiano V, Martinez-Penuela JM, et al. Hypermethylation, risk factors, clinical characteristics, and survival in 235 patients with laryngeal and hypopharyngeal cancers. Cancer. 2007;110(8):1745-51.
184. Zhao Z, Ge J, Sun Y, Tian L, Lu J, Liu M, et al. Is E-cadherin immunoexpression a prognostic factor for head and neck squamous cell carcinoma (HNSCC)? A systematic review and meta-analysis. Oral Oncol. 2012.
185. Huang DH, Su L, Peng XH, Zhang H, Khuri FR, Shin DM, et al. Quantum dot-based quantification revealed differences in subcellular localization of EGFR and E-cadherin between EGFR-TKI sensitive and insensitive cancer cells. Nanotechnology. 2009;20(22):225102.
186. Eriksen JG, Steiniche T, Overgaard J. The role of epidermal growth factor receptor and E-cadherin for the outcome of reduction in the overall treatment time of radiotherapy of supraglottic larynx squamous cell carcinoma. Acta Oncol. 2005;44(1):50-8.
187. Yang Z, Zhang X, Gang H, Li X, Li Z, Wang T, et al. Up-regulation of gastric cancer cell invasion by Twist is accompanied by N-cadherin and fibronectin expression. Biochem Biophys Res Commun. 2007;358(3):925-30.
188. Nguyen PT, Kudo Y, Yoshida M, Kamata N, Ogawa I, Takata T. N-cadherin expression is involved in malignant behavior of head and neck cancer in relation to epithelial-mesenchymal transition. Histology and histopathology. 2011;26(2):147-56.
189. Qian F, Zhang ZC, Wu XF, Li YP, Xu Q. Interaction between integrin alpha(5) and fibronectin is required for metastasis of B16F10 melanoma cells. Biochem Biophys Res Commun. 2005;333(4):1269-75.
190. Dyce OH, Ziober AF, Weber RS, Miyazaki K, Khariwala SS, Feldman M, et al. Integrins in head and neck squamous cell carcinoma invasion. The Laryngoscope. 2002;112(11):2025-32.
191. Nakahara S, Miyoshi E, Noda K, Ihara S, Gu J, Honke K, et al. Involvement of oligosaccharide changes in alpha5beta1 integrin in a cisplatin-resistant human squamous cell carcinoma cell line. Molecular cancer therapeutics. 2003;2(11):1207-14.
192. Koontongkaew S, Amornphimoltham P, Monthanpisut P, Saensuk T, Leelakriangsak M. Fibroblasts and extracellular matrix differently modulate MMP activation by primary and metastatic head and neck cancer cells. Med Oncol. 2011.
193. Lim KP, Cirillo N, Hassona Y, Wei W, Thurlow JK, Cheong SC, et al. Fibroblast gene expression profile reflects the stage of tumour progression in oral squamous cell carcinoma. The Journal of pathology. 2011;223(4):459-69.
194. Chen C, Wei Y, Hummel M, Hoffmann TK, Gross M, Kaufmann AM, et al. Evidence for epithelial-mesenchymal transition in cancer stem cells of head and neck squamous cell carcinoma. PloS one. 2011;6(1):e16466.
195. Paccione RJ, Miyazaki H, Patel V, Waseem A, Gutkind JS, Zehner ZE, et al. Keratin down-regulation in vimentin-positive cancer cells is reversible by vimentin

RNA interference, which inhibits growth and motility. Molecular cancer therapeutics. 2008;7(9):2894-903.
196. Yoon Y, Liang Z, Zhang X, Choe M, Zhu A, Cho HT, et al. CXC chemokine receptor-4 antagonist blocks both growth of primary tumor and metastasis of head and neck cancer in xenograft mouse models. Cancer research. 2007;67(15):7518-24.
197. Goto M, Mitra RS, Liu M, Lee J, Henson BS, Carey T, et al. Rap1 stabilizes beta-catenin and enhances beta-catenin-dependent transcription and invasion in squamous cell carcinoma of the head and neck. Clin Cancer Res. 2010;16(1):65-76.
198. Wheelock MJ, Johnson KR. Cadherins as modulators of cellular phenotype. Annu Rev Cell Dev Biol. 2003;19:207-35.
199. Tsai YP, Yang MH, Huang CH, Chang SY, Chen PM, Liu CJ, et al. Interaction between HSP60 and beta-catenin promotes metastasis. Carcinogenesis. 2009;30(6):1049-57.
200. Egeblad M, Rasch MG, Weaver VM. Dynamic interplay between the collagen scaffold and tumor evolution. Curr Opin Cell Biol. 2010;22(5):697-706.
201. Van Tubergen E, Broek RV, Lee J, Wolf G, Carey T, Bradford C, et al. Tristetraprolin Regulates Interleukin-6, Which Is Correlated With Tumor Progression in Patients With Head and Neck Squamous Cell Carcinoma. Cancer. 2011;117(12):2677-89.
202. Mitra RS, Goto M, Lee JS, Maldonado D, Taylor JM, Pan Q, et al. Rap1GAP promotes invasion via induction of matrix metalloproteinase 9 secretion, which is associated with poor survival in low N-stage squamous cell carcinoma. Cancer research. 2008;68(10):3959-69.
203. Tapper J, Kettunen E, El-Rifai W, Seppala M, Andersson LC, Knuutila S. Changes in gene expression during progression of ovarian carcinoma. Cancer Genet Cytogenet. 2001;128(1):1-6.
204. Kauppila S, Stenback F, Risteli J, Jukkola A, Risteli L. Aberrant type I and type III collagen gene expression in human breast cancer in vivo. J Pathol. 1998;186(3):262-8.
205. Schmidt M, Schler G, Gruensfelder P, Hoppe F. Differential gene expression in a paclitaxel-resistant clone of a head and neck cancer cell line. Eur Arch Otorhinolaryngol. 2006;263(2):127-34.
206. Chen C, Mendez E, Houck J, Fan W, Lohavanichbutr P, Doody D, et al. Gene expression profiling identifies genes predictive of oral squamous cell carcinoma. Cancer epidemiology, biomarkers & prevention : a publication of the American Association for Cancer Research, cosponsored by the American Society of Preventive Oncology. 2008;17(8):2152-62.
207. Dooley TP, Reddy SP, Wilborn TW, Davis RL. Biomarkers of human cutaneous squamous cell carcinoma from tissues and cell lines identified by DNA microarrays and qRT-PCR. Biochemical and biophysical research communications. 2003;306(4):1026-36.
208. Tijink BM, Neri D, Leemans CR, Budde M, Dinkelborg LM, Stigter-van Walsum M, et al. Radioimmunotherapy of head and neck cancer xenografts using 131I-labeled

antibody L19-SIP for selective targeting of tumor vasculature. Journal of nuclear medicine : official publication, Society of Nuclear Medicine. 2006;47(7):1127-35.
209. Warawdekar UM, Zingde SM, Iyer KS, Jagannath P, Mehta AR, Mehta NG. Elevated levels and fragmented nature of cellular fibronectin in the plasma of gastrointestinal and head and neck cancer patients. Clinica chimica acta; international journal of clinical chemistry. 2006;372(1-2):83-93.
210. Marinkovich MP. Tumour microenvironment: laminin 332 in squamous-cell carcinoma. Nature reviews Cancer. 2007;7(5):370-80.
211. Mendez E, Houck JR, Doody DR, Fan W, Lohavanichbutr P, Rue TC, et al. A genetic expression profile associated with oral cancer identifies a group of patients at high risk of poor survival. Clinical cancer research : an official journal of the American Association for Cancer Research. 2009;15(4):1353-61.
212. Lyons JG, Patel V, Roue NC, Fok SY, Soon LL, Halliday GM, et al. Snail up-regulates proinflammatory mediators and inhibits differentiation in oral keratinocytes. Cancer research. 2008;68(12):4525-30.
213. Yang MH, Chang SY, Chiou SH, Liu CJ, Chi CW, Chen PM, et al. Overexpression of NBS1 induces epithelial-mesenchymal transition and co-expression of NBS1 and Snail predicts metastasis of head and neck cancer. Oncogene. 2007;26(10):1459-67.
214. Hayry V, Makinen LK, Atula T, Sariola H, Makitie A, Leivo I, et al. Bmi-1 expression predicts prognosis in squamous cell carcinoma of the tongue. British journal of cancer. 2010;102(5):892-7.
215. Mendelsohn AH, Lai CK, Shintaku IP, Fishbein MC, Brugman K, Elashoff DA, et al. Snail as a novel marker for regional metastasis in head and neck squamous cell carcinoma. American journal of otolaryngology. 2012;33(1):6-13.
216. Hsu DS, Lan HY, Huang CH, Tai SK, Chang SY, Tsai TL, et al. Regulation of excision repair cross-complementation group 1 by Snail contributes to cisplatin resistance in head and neck cancer. Clinical cancer research : an official journal of the American Association for Cancer Research. 2010;16(18):4561-71.
217. Peinado H, Moreno-Bueno G, Hardisson D, Perez-Gomez E, Santos V, Mendiola M, et al. Lysyl oxidase-like 2 as a new poor prognosis marker of squamous cell carcinomas. Cancer Res. 2008;68(12):4541-50.
218. Huang CH, Yang WH, Chang SY, Tai SK, Tzeng CH, Kao JY, et al. Regulation of membrane-type 4 matrix metalloproteinase by SLUG contributes to hypoxia-mediated metastasis. Neoplasia. 2009;11(12):1371-82.
219. Ou DL, Chien HF, Chen CL, Lin TC, Lin LI. Role of Twist in head and neck carcinoma with lymph node metastasis. Anticancer research. 2008;28(2B):1355-9.
220. Yang MH, Hsu DS, Wang HW, Wang HJ, Lan HY, Yang WH, et al. Bmi1 is essential in Twist1-induced epithelial-mesenchymal transition. Nat Cell Biol. 2010;12(10):982-92.
221. Jouppila-Matto A, Narkio-Makela M, Soini Y, Pukkila M, Sironen R, Tuhkanen H, et al. Twist and snai1 expression in pharyngeal squamous cell carcinoma stroma is related to cancer progression. BMC Cancer. 2011;11:350.
222. Hatsell S, Rowlands T, Hiremath M, Cowin P. Beta-catenin and Tcfs in mammary development and cancer. J Mammary Gland Biol Neoplasia. 2003;8(2):145-58.

223. Segrelles C, Moral M, Lara MF, Ruiz S, Santos M, Leis H, et al. Molecular determinants of Akt-induced keratinocyte transformation. Oncogene. 2006;25(8):1174-85.
224. Polette M, Mestdagt M, Bindels S, Nawrocki-Raby B, Hunziker W, Foidart JM, et al. Beta-catenin and ZO-1: shuttle molecules involved in tumor invasion-associated epithelial-mesenchymal transition processes. Cells Tissues Organs. 2007;185(1-3):61-5.
225. Nemeth Z, Szasz AM, Somoracz A, Tatrai P, Nemeth J, Gyorffy H, et al. Zonula occludens-1, occludin, and E-cadherin protein expression in biliary tract cancers. Pathol Oncol Res. 2009;15(3):533-9.
226. Hirakawa H, Shibata K, Nakayama T. Localization of cortactin is associated with colorectal cancer development. Int J Oncol. 2009;35(6):1271-6.
227. Drake JM, Barnes JM, Madsen JM, Domann FE, Stipp CS, Henry MD. ZEB1 coordinately regulates laminin-332 and {beta}4 integrin expression altering the invasive phenotype of prostate cancer cells. J Biol Chem. 2010;285(44):33940-8.
228. Gemmill RM, Roche J, Potiron VA, Nasarre P, Mitas M, Coldren CD, et al. ZEB1-responsive genes in non-small cell lung cancer. Cancer Lett. 2011;300(1):66-78.
229. Montserrat N, Gallardo A, Escuin D, Catasus L, Prat J, Gutierrez-Avigno FJ, et al. Repression of E-cadherin by SNAIL, ZEB1, and TWIST in invasive ductal carcinomas of the breast: a cooperative effort? Hum Pathol. 2011;42(1):103-10.
230. Farina AK, Bong YS, Feltes CM, Byers SW. Post-transcriptional regulation of cadherin-11 expression by GSK-3 and beta-catenin in prostate and breast cancer cells. PloS one. 2009;4(3):e4797.
231. Biddle A, Liang X, Gammon L, Fazil B, Harper LJ, Emich H, et al. Cancer stem cells in squamous cell carcinoma switch between two distinct phenotypes that are preferentially migratory or proliferative. Cancer research. 2011;71(15):5317-26.
232. Prud'homme GJ. Cancer stem cells and novel targets for antitumor strategies. Curr Pharm Des. 2012;18(19):2838-49.
233. Foroni C, Broggini M, Generali D, Damia G. Epithelial-mesenchymal transition and breast cancer: role, molecular mechanisms and clinical impact. Cancer Treat Rev. 2012;38(6):689-97.
234. Koontongkaew S, Amornphimoltham P, Monthanpisut P, Saensuk T, Leelakriangsak M. Fibroblasts and extracellular matrix differently modulate MMP activation by primary and metastatic head and neck cancer cells. Medical oncology. 2012;29(2):690-703.
235. Chang HW, Roh JL, Jeong EJ, Lee SW, Kim SW, Choi SH, et al. Wnt signaling controls radiosensitivity via cyclooxygenase-2-mediated Ku expression in head and neck cancer. International journal of cancer Journal international du cancer. 2008;122(1):100-7.
236. Scanlon CS IR, Russo N, Banerjee R, Hariharan A, D'Silva NJ. CDH11 is a novel biomarker of EMT in HNSCC: Discovery and validation using an in silico approach. (under review). 2014.
237. Malik A, Singh H, Andrabi M, Husain SA, Ahmad S. Databases and QSAR for cancer research. Cancer informatics. 2006;2:99-111.
238. Arauzo-Bravo M, Ahmad S. Protein Sequence and Structure Databases: A Review. Current Analytical Chemistry. 2005;1(3):355-71.

239. Hanauer DA, Rhodes DR, Sinha-Kumar C, Chinnaiyan AM. Bioinformatics approaches in the study of cancer. Curr Mol Med. 2007;7(1):133-41.
240. Guarino M, Rubino B, Ballabio G. The role of epithelial-mesenchymal transition in cancer pathology. Pathology. 2007;39(3):305-18.
241. Choi P, Jordan CD, Mendez E, Houck J, Yueh B, Farwell DG, et al. Examination of oral cancer biomarkers by tissue microarray analysis. Archives of otolaryngology--head & neck surgery. 2008;134(5):539-46.
242. Carmona FJ, Villanueva A, Vidal A, Munoz C, Puertas S, Penin RM, et al. Epigenetic disruption of cadherin-11 in human cancer metastasis. The Journal of pathology. 2012;228(2):230-40.
243. Kuriakose MA, Chen WT, He ZM, Sikora AG, Zhang P, Zhang ZY, et al. Selection and validation of differentially expressed genes in head and neck cancer. Cellular and molecular life sciences : CMLS. 2004;61(11):1372-83.
244. Ye H, Yu T, Temam S, Ziober BL, Wang J, Schwartz JL, et al. Transcriptomic dissection of tongue squamous cell carcinoma. BMC genomics. 2008;9:69.
245. Russo N, Wang X, Liu M, Banerjee R, Goto M, Scanlon C, et al. A novel approach to biomarker discovery in head and neck cancer using an autoantibody signature. Oncogene. 2013;32(42):5026-37.
246. Mitra RS, Zhang Z, Henson BS, Kurnit DM, Carey TE, D'Silva NJ. Rap1A and rap1B ras-family proteins are prominently expressed in the nucleus of squamous carcinomas: nuclear translocation of GTP-bound active form. Oncogene. 2003;22(40):6243-56.
247. Torres S, Bartolome RA, Mendes M, Barderas R, Fernandez-Acenero MJ, Pelaez-Garcia A, et al. Proteome profiling of cancer-associated fibroblasts identifies novel proinflammatory signatures and prognostic markers for colorectal cancer. Clinical cancer research : an official journal of the American Association for Cancer Research. 2013;19(21):6006-19.
248. Scanlon CS, D'Silva NJ. Personalized medicine for cancer therapy: Lessons learned from tumor-associated antigens. Oncoimmunology. 2013;2(4):e23433.
249. Rhodes DR, Kalyana-Sundaram S, Tomlins SA, Mahavisno V, Kasper N, Varambally R, et al. Molecular concepts analysis links tumors, pathways, mechanisms, and drugs. Neoplasia. 2007;9(5):443-54.
250. Tomlins SA, Mehra R, Rhodes DR, Cao X, Wang L, Dhanasekaran SM, et al. Integrative molecular concept modeling of prostate cancer progression. Nature genetics. 2007;39(1):41-51.
251. Morris DS, Tomlins SA, Rhodes DR, Mehra R, Shah RB, Chinnaiyan AM. Integrating biomedical knowledge to model pathways of prostate cancer progression. Cell cycle. 2007;6(10):1177-87.
252. Hanauer DA, Rhodes DR, Chinnaiyan AM. Exploring clinical associations using '-omics' based enrichment analyses. PloS one. 2009;4(4):e5203.
253. Yoshizawa M, Feinberg SE, Marcelo CL, Elner VM. Ex vivo produced human conjunctiva and oral mucosa equivalents grown in a serum-free culture system. Journal of oral and maxillofacial surgery : official journal of the American Association of Oral and Maxillofacial Surgeons. 2004;62(8):980-8.
254. Izumi K, Takacs G, Terashi H, Feinberg SE. Ex vivo development of a composite human oral mucosal equivalent. Journal of oral and maxillofacial surgery : official

journal of the American Association of Oral and Maxillofacial Surgeons. 1999;57(5):571-7; discussion 7-8.
255. Izumi K, Terashi H, Marcelo CL, Feinberg SE. Development and characterization of a tissue-engineered human oral mucosa equivalent produced in a serum-free culture system. Journal of dental research. 2000;79(3):798-805.
256. Palanisamy V, Jakymiw A, Van Tubergen EA, D'Silva NJ, Kirkwood KL. Control of cytokine mRNA expression by RNA-binding proteins and microRNAs. Journal of dental research. 2012;91(7):651-8.
257. Young LE, Sanduja S, Bemis-Standoli K, Pena EA, Price RL, Dixon DA. The mRNA binding proteins HuR and tristetraprolin regulate cyclooxygenase 2 expression during colon carcinogenesis. Gastroenterology. 2009;136(5):1669-79.
258. Hansson A, Bloor BK, Haig Y, Morgan PR, Ekstrand J, Grafstrom RC. Expression of keratins in normal, immortalized and malignant oral epithelia in organotypic culture. Oral oncology. 2001;37(5):419-30.
259. Haraguchi Y, Shimizu T, Sasagawa T, Sekine H, Sakaguchi K, Kikuchi T, et al. Fabrication of functional three-dimensional tissues by stacking cell sheets in vitro. Nature protocols. 2012;7(5):850-8.
260. Kim JB. Three-dimensional tissue culture models in cancer biology. Seminars in cancer biology. 2005;15(5):365-77.
261. Sutherland RM. Cell and environment interactions in tumor microregions: the multicell spheroid model. Science. 1988;240(4849):177-84.
262. Clark JM, Hirtenstein MD. Optimizing culture conditions for the production of animal cells in microcarrier culture. Annals of the New York Academy of Sciences. 1981;369:33-46.
263. Tan W, Krishnaraj R, Desai TA. Evaluation of nanostructured composite collagen--chitosan matrices for tissue engineering. Tissue engineering. 2001;7(2):203-10.
264. Lloyd WR, Chen L-C, Mycek M-A. Fluorescence Spectroscopy. In: S.P. M, S.J. M, F. R, editors. Optical Techniques in Regenerative Medicine. London, UK: Taylor & Francies Group; 2013, in press.
265. Lloyd WR, Chen L-C, Wilson RH, Mycek M-A. Biophotonics: Clinical Fluorescence Spectroscopy and Imaging. In: D.J. M, J.E. MJ, editors. Biomedical Technology and Devices Handbook. 2 ed. London, UK: Francis & Taylor; 2013, in press.
266. Eiraku M, Sasai Y. Mouse embryonic stem cell culture for generation of three-dimensional retinal and cortical tissues. Nature protocols. 2012;7(1):69-79.
267. Moreno-Bueno G, Peinado H, Molina P, Olmeda D, Cubillo E, Santos V, et al. The morphological and molecular features of the epithelial-to-mesenchymal transition. Nature protocols. 2009;4(11):1591-613.
268. Dongari-Bagtzoglou A, Kashleva H. Development of a highly reproducible three-dimensional organotypic model of the oral mucosa. Nature protocols. 2006;1(4):2012-8.
269. Choe MM, Tomei AA, Swartz MA. Physiological 3D tissue model of the airway wall and mucosa. Nature protocols. 2006;1(1):357-62.
270. Grivel JC, Margolis L. Use of human tissue explants to study human infectious agents. Nature protocols. 2009;4(2):256-69.
271. Levi-Montalcini R. Effects of mouse tumor transplantation on the nervous system. Annals of the New York Academy of Sciences. 1952;55(2):330-44.

272. Kleer CG, Cao Q, Varambally S, Shen R, Ota I, Tomlins SA, et al. EZH2 is a marker of aggressive breast cancer and promotes neoplastic transformation of breast epithelial cells. Proceedings of the National Academy of Sciences of the United States of America. 2003;100(20):11606-11.
273. Ota I, Li XY, Hu Y, Weiss SJ. Induction of a MT1-MMP and MT2-MMP-dependent basement membrane transmigration program in cancer cells by Snail1. Proceedings of the National Academy of Sciences of the United States of America. 2009;106(48):20318-23.
274. Busch C, Krochmann J, Drews U. The chick embryo as an experimental system for melanoma cell invasion. PloS one. 2013;8(1):e53970.
275. Rowe RG, Li XY, Hu Y, Saunders TL, Virtanen I, Garcia de Herreros A, et al. Mesenchymal cells reactivate Snail1 expression to drive three-dimensional invasion programs. The Journal of cell biology. 2009;184(3):399-408.
276. Zhang Z, Mitra RS, Henson BS, Datta NS, McCauley LK, Kumar P, et al. Rap1GAP inhibits tumor growth in oropharyngeal squamous cell carcinoma. Am J Pathol. 2006;168(2):585-96.
277. van der Horst EH, Leupold JH, Schubbert R, Ullrich A, Allgayer H. TaqMan-based quantification of invasive cells in the chick embryo metastasis assay. Biotechniques. 2004;37(6):940-2, 4, 6.
278. Zeidler M, Varambally S, Cao Q, Chinnaiyan AM, Ferguson DO, Merajver SD, et al. The Polycomb group protein EZH2 impairs DNA repair in breast epithelial cells. Neoplasia. 2005;7(11):1011-9.
279. Raaphorst FM, Meijer CJ, Fieret E, Blokzijl T, Mommers E, Buerger H, et al. Poorly differentiated breast carcinoma is associated with increased expression of the human polycomb group EZH2 gene. Neoplasia. 2003;5(6):481-8.
280. Breuer RH, Snijders PJ, Smit EF, Sutedja TG, Sewalt RG, Otte AP, et al. Increased expression of the EZH2 polycomb group gene in BMI-1-positive neoplastic cells during bronchial carcinogenesis. Neoplasia. 2004;6(6):736-43.
281. Cao W, Ribeiro Rde O, Liu D, Saintigny P, Xia R, Xue Y, et al. EZH2 Promotes Malignant Behaviors via Cell Cycle Dysregulation and Its mRNA Level Associates with Prognosis of Patient with Non-Small Cell Lung Cancer. PLoS One. 2012;7(12):e52984.
282. Varambally S, Cao Q, Mani RS, Shankar S, Wang X, Ateeq B, et al. Genomic loss of microRNA-101 leads to overexpression of histone methyltransferase EZH2 in cancer. Science. 2008;322(5908):1695-9.
283. Sauvageau M, Sauvageau G. Polycomb group proteins: multi-faceted regulators of somatic stem cells and cancer. Cell Stem Cell. 2010;7(3):299-313.
284. Crea F, Fornaro L, Bocci G, Sun L, Farrar WL, Falcone A, et al. EZH2 inhibition: targeting the crossroad of tumor invasion and angiogenesis. Cancer Metastasis Rev. 2012;31(3-4):753-61.
285. Lu C, Han HD, Mangala LS, Ali-Fehmi R, Newton CS, Ozbun L, et al. Regulation of tumor angiogenesis by EZH2. Cancer Cell. 2010;18(2):185-97.
286. Chang CJ, Yang JY, Xia W, Chen CT, Xie X, Chao CH, et al. EZH2 promotes expansion of breast tumor initiating cells through activation of RAF1-beta-catenin signaling. Cancer Cell. 2011;19(1):86-100.

287. Scanlon CS, Van Tubergen EA, Inglehart RC, D'Silva NJ. Biomarkers of Epithelial-Mesenchymal Transition in Squamous Cell Carcinoma. J Dent Res. 2012.
288. Lokman NA, Elder AS, Ricciardelli C, Oehler MK. Chick Chorioallantoic Membrane (CAM) Assay as an In Vivo Model to Study the Effect of Newly Identified Molecules on Ovarian Cancer Invasion and Metastasis. Int J Mol Sci. 2012;13(8):9959-70.
289. Russo N, Wang X, Liu M, Banerjee R, Goto M, Scanlon C, et al. A novel approach to biomarker discovery in head and neck cancer using an autoantibody signature. Oncogene. 2012.
290. D'Silva NJ, Ward BB. Tissue biomarkers for diagnosis & management of oral squamous cell carcinoma. The Alpha omegan. 2007;100(4):182-9.
291. Laheru DA, Pardoll DM, Jaffee EM. Genes to vaccines for immunotherapy: how the molecular biology revolution has influenced cancer immunology. Molecular cancer therapeutics. 2005;4(11):1645-52.
292. Stockert E, Jager E, Chen YT, Scanlan MJ, Gout I, Karbach J, et al. A survey of the humoral immune response of cancer patients to a panel of human tumor antigens. The Journal of experimental medicine. 1998;187(8):1349-54.
293. Prensner JR, Rubin MA, Wei JT, Chinnaiyan AM. Beyond PSA: the next generation of prostate cancer biomarkers. Science translational medicine. 2012;4(127):127rv3.
294. Wang X, Yu J, Sreekumar A, Varambally S, Shen R, Giacherio D, et al. Autoantibody signatures in prostate cancer. The New England journal of medicine. 2005;353(12):1224-35.
295. Bradford TJ, Wang X, Chinnaiyan AM. Cancer immunomics: using autoantibody signatures in the early detection of prostate cancer. Urologic oncology. 2006;24(3):237-42.